Revista Brasileira de Ciências Mecânicas

Journal of the Brazilian Society of Mechanical Sciences

2

PUBLICAÇÃO DA ABCM - ASSOCIAÇÃO BRASILEIRA DE CIÊNCIAS MECÂNICAS

VOL. XV - Nº 2 - 1993 ISSN 0100-7386

REVISTA BRASILEIRA DE CIÊNCIAS MECÂNICAS
JOURNAL OF THE BRAZILIAN SOCIETY OF MECHANICAL SCIENCES
Vol. 1. Nº 1 (1979) -
Rio de Janeiro: Associação Brasileira de Ciências Mecânicas
Trimestral
Inclui referências bibliográficas.
1. Mecânica
ISSN-0100-7386

A REVISTA BRASILEIRA DE CIÊNCIAS MECÂNICAS publica trabalhos que cobrem os vários aspectos da ciência e da tecnologia em Engenharia Mecânica, incluindo interfaces com as Engenharias Civil, Elétrica, Química, Naval, Nuclear, Aeroespacial, Alimentos, Agrícola, Petróleo, Materiais, etc., bem como aplicações da Física e da Matemática à Mecânica.

Publicação da /Published by
ASSOCIAÇÃO BRASILEIRA DE CIÊNCIAS MECÂNICAS
THE BRAZILIAN SOCIETY OF MECHANICAL SCIENCES

Secretária da ABCM: Ana Lucia Fróes de Souza
Av. Rio Branco, 124-18º andar - Rio de Janeiro - Brasil
Tel. / Fax (021) 222-7128

REVISTA BRASILEIRA DE CIÊNCIAS MECÂNICAS
JOURNAL OF THE BRAZILIAN SOCIETY OF MECHANICAL SCIENCES

REVISTA FINANCIADA COM RECURSOS DO
Programa de Apoio a Publicações Científicas
MCT CNPq FINEP
FAPESP - Fundação de Amparo a Pesquisa do Estado de São Paulo

RBCM - J. of the Braz. Soc. Mechanical Sciences
Vol. XV - nº 2 - 1993 - pp. 112-123

ISSN 0100-7386
Printed in Brazil

Escolha da Ferramenta no Torneamento de Resina Reforçada com Fibras de Vidro e Carbono

Choice of Tool in Turning of Carbon and Glass Fiber Reinforced Resin

J. R. Ferreira
EFEI - Escola Federal de Engenharia de Itajubá
Departamento de Produção
Cx. Postal 50
37500-000 Itajubá - MG

N. L. Cupini
UNICAMP - Universidade Estadual de Campinas
Departamento de Engenharia de Fabricação
Cx. Postal 6122
13081-970 Campinas - SP

Resumo

Este trabalho consiste na realização de experimentos para analisar o comportamento de ferramentas de diversos materiais no torneamento de compósitos de resina fenólica reforçada com fibras de vidro e carbono. Durante os ensaios foram observados a variação dos desgastes das ferramentas, da rugosidade superficial da peça e da força de avanço. Uma das mais importantes conclusões deste trabalho é que a rugosidade superficial do compósito aumenta de maneira progressiva com o desgaste da ferramenta, viabilizando somente o emprego da ferramenta de diamante em torneamento de acabamento. Em operação de desbaste o metal duro apresentou-se como a melhor solução, pois apesar de sofrer desgaste superior ao diamante é mais barato e dispensa cuidados operacionais especiais.
Palavras-chave: Usinagem - Ferramentas - Materiais Compósitos

Abstract

Experiments were carried out to study the performance of different tool materials. They were tested in turning of carbon and glass fiber reinforced fenolic resin composite. During the experiments, tool wear, surface roughness, and feed force behavior were observed. Experimental results showed that, due to the great influence of tool wear on workpiece surface roughness, only diamond tools are suitable for use in finish turning. In rough turning, the cemented carbide tools showed to be the best solution. Although it showed larger wear than diamond, the cost/benefit ratio is much lower and special precautions are not necessary.
Keywords: Machining - Tool - Composite Material

Introdução

O emprego de materiais compósitos à base de resinas fenólicas reforçadas com fibras tem crescido notavelmente nos últimos anos, especialmente nas indústrias aeronáutica, aeroespacial e automobilística. Como conseqüência do aumento e da diversificação do emprego dos materiais compósitos, cresce cada vez mais a necessidade de usiná-los, para satisfazer as exigências com relação à precisão dimensional e à qualidade superficial dos componentes (Wunsch e Spur, 1988).

Os plásticos reforçados com fibras são moldados e a massa mais importante de sua aplicação até nossos dias é na forma de placas, lâminas e chapas. Nelas incide principalmente operações de corte e furação. Pouco encontra-se em pesquisa e desenvolvimento, relatado ou publicado sobre outras operações como: torneamento, fresamento, retificação etc. (Reinhart, 1987). Este trabalho tem por objetivo contribuir para aplicações alternativas dos plásticos reforçados com fibras, na fabricação de peças e componentes com geometrias diversas, particularmente no caso de torneamento.

Considerando-se estes aspectos, o trabalho apresenta uma experiência de torneamento de um compósito de resina fenólica reforçada com fibras de vidro e carbono, confeccionados nas formas de placas laminadas e tubos bobinados (Fig. 1). No torneamento do compósito de tecido bobinado serão

Manuscript received: June 1993. Associate Technical Editor: Walter L. Weingaertner

avaliados a evolução do desgaste das ferramentas, da força de avanço e da rugosidade da peça, em função do comprimento de corte usinado. Na operação de torneamento do compósito de tecido laminado serão estudados a influência da velocidade de corte no desgaste da ferramenta e da orientação das fibras na rugosidade da peça.

De posse dos resultados obtidos, apresenta-se neste trabalho a escolha da melhor ferramenta para o processo de torneamento do compósito, em operações de desbaste e acabamento.

Procedimentos Experimentais

Material, Ferramenta e Equipamentos. O material compósito ensaiado apresenta as seguintes propriedades: Tecido híbrido de fibra de carbono (70%) e fibra de vidro (30%); resina fenólica (35 a 40% em massa) e densidade de 1,4 a 1,5 g/cm^3.

As ferramentas utilizadas foram: metal duro classe ISO K10, cerâmica pura (Al_2O_3+ZrO_2), cerâmica mista (Al_2O_3+TiC), cerâmica reforçada com whiskers (Al_2O_3+SiC), SIALON (Al_2O_3+Si_3N_4), nitreto de boro cúbico (CBN) e diamante policristalino (PCD). As ferramentas de metal duro, CBN e diamante tinham geometria ISO SNUN 120412 e as cerâmicas tinham geometria ISO SNUN 120712.

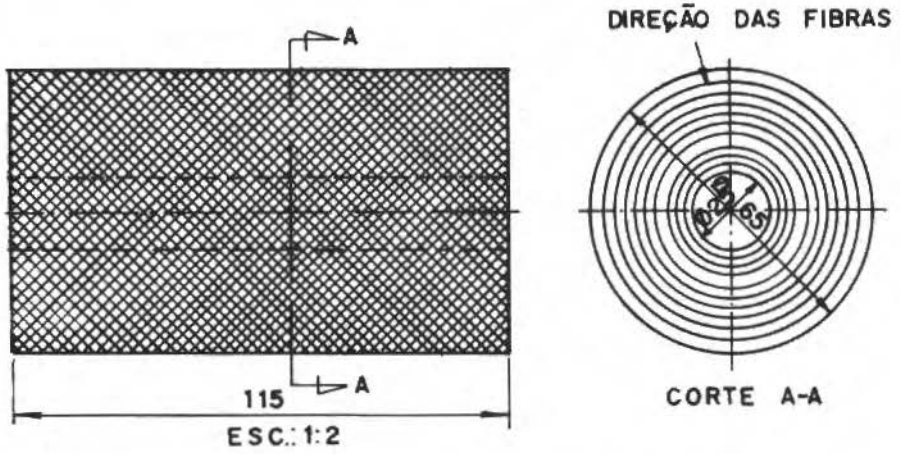

Fig. 1 a) Corpos de prova de material compósito - tecido bobinado

Nomenclatura

a_p = profundidade de corte
α = ângulo de posição das fibras relativa à direção de corte
C_{af} = custo de afiação da ferramenta
C_f = custo da ferramenta
C_{ft} = custo da ferramenta por vida
C_p = custo da ferramenta por peça
C_{pf} = custo do porta-ferramenta
f = avanço de corte
F_f = força de avanço
l_c = comprimento de corte
n_1 = número de afiações da ferramenta
n_2 = número de vidas da ferramenta
n_3 = número de vidas do porta-ferramenta
R_a = rugosidade média
S_h = salário do operador
S_m = salário da máquina
T = vida da ferramenta
t_a = tempo de aproximação e recuo da ferramenta
t_c = tempo de corte
t_{ft} = tempo de troca da ferramenta
t_i = tempos improdutivos
t_p = tempo de preparação da máquina
t_s = tempos secundários
t_t = tempo total de confecção por peça
V_c = velocidade de corte
V_B = desgaste de flanco
Z = número de peças do lote

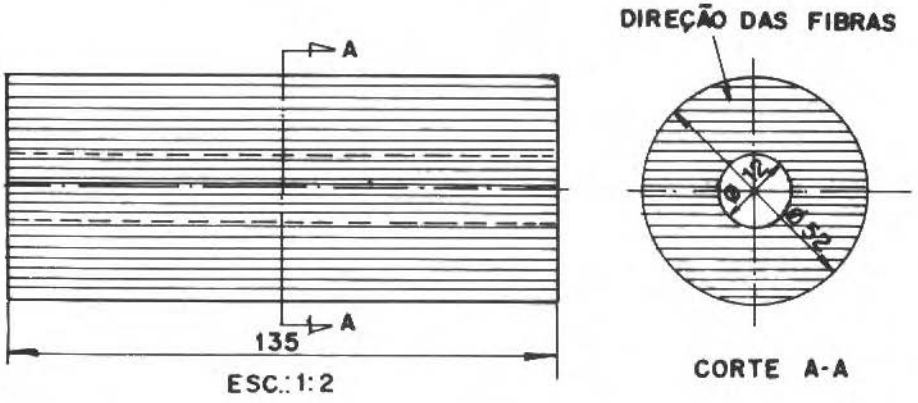

Fig. 1 b) Corpos de prova de material compósito - tecido laminado

Os equipamentos utilizados foram: Torno CNC com potência de 22kW, rugosímetro digital, microscópio com mesa de duas coordenadas, aspirador de pó industrial e equipamentos de proteção individual.

Método Experimental. No torneamento do compósito de tecido bobinado fez-se uma comparação do desempenho de todas ferramentas ensaiadas. Para isto, adotou-se uma condição de corte constante para todas as ferramentas: velocidade de corte V_C=320 m/min, avanço f= 0,1 mm/rot e profundidade de corte a_p=1 mm. Para cada condição de ensaio ferramenta-peça foram medidos o desgaste da ferramenta, a força de avanço e a rugosidade superficial da peça. Este ensaio serviu para classificar as ferramentas baseado no desempenho de cada uma delas.

No torneamento do compósito de tecido laminado, trabalhou-se com ferramentas de metal duro e diamante, as escolhidas do ensaio anterior. Com o metal duro estudou-se a evolução do desgaste da ferramenta com as seguintes velocidades de corte: 25, 100, 200, 320 e 450 m/min. Com a ferramenta de diamante verificou-se a variação da rugosidade superficial da peça em relação ao ângulo de posição das fibras do laminado. As condições de corte utilizadas foram: velocidade de corte V_C=200 m/min, profundidade de corte ap=1 mm e três avanços diferentes, f=0,1, 0,2 e 0,3 mm/rot.

Resultados e Discussões

A Fig. 2 mostra a evolução do desgaste das ferramentas em função do comprimento de corte usinado, no torneamento do compósito de tecido bobinado. As ferramentas de materiais cerâmicos apresentam um fraco desempenho no torneamento do compósito reforçado com fibras de vidro e carbono, exemplificado pela ferramenta de SIALON que sofreu o maior desgaste entre todas as ferramentas ensaiadas. O mecanismo de desgaste provável neste caso foi por abrasão mecânica, pois não foi observado nenhuma quebra ou avaria da ferramenta no ensaio. O melhor desempenho entre as ferramentas mecânicas obteve-se com a alumina reforçada com whiskers de SiC, mas devido ao elevado custo da ferramenta comparado ao metal duro, não justifica seu emprego.

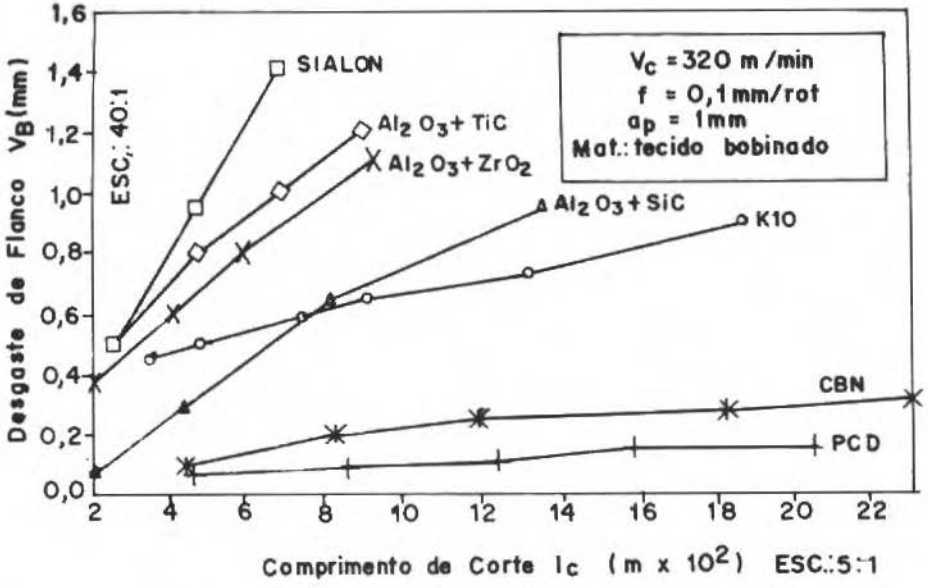

Fig. 2 Desgaste de flanco das ferramentas versus comprimento de corte

A Tabela I mostra os custos por vida, por aresta e as vidas das ferramentas para um critério de desgaste de flanco V_B=0,9 mm.

A ferramenta de CBN apresentou um desempenho superior às ferramentas de cerâmicas e metal duro, mas ficou aquém da ferramenta de diamante. O custo do CBN de US$ 142,00 por aresta, superior ao do diamante (US$ 93,00) inviabiliza a sua aplicação no torneamento do compósito. Portanto, a escolha da ferramenta fica entre o metal duro por apresentar o menor custo por aresta e por vida, a cerâmica pura que apresentou o menor custo por aresta e por vida em relação as cerâmicas, e o diamante que apresentou o melhor comportamento de todas as ferramentas.

Tabela I. Custos por aresta e por vida das ferramentas

Ferramentas	Custo/ar. (CR$)	Custo/ar. (US$)	Vida lc(m) VB=0,9 mm	Custo/Vida (CR$/m)
Cerâmica pura	141,60	3,54	750	0,19
Cerâmica mista	180,00	4,50	580	0,31
Cerâmica ref. SiC	900,00	22,50	1280	0,70
SIALON	450,00	11,25	450	1,00
Metal duro	29,20	0,73	1850	1,57
CBN	5680,00	142,00	lc = 2300 m VB = 0,32 m	2,47
Diamante (PCD)	3720,00	93,00	lc = 2300 m VB = 0,32 m	1,86

Em operação de desbaste deve ser feito um estudo mais detalhado, pois o custo por aresta da ferramenta de diamante é 127 vezes o custo da ferramenta de metal duro. Em função disto deve ser realizada uma análise de custo/benefício de usinagem.

Levantando-se alguns dados sobre o torneamento do compósito de tecido bobinado especificamente, pode-se fazer uma comparação dos custos relativos à usinagem entre as ferramentas de metal duro, cerâmica pura e diamante. O custo relativo à usinagem por peça (C_p) é dado por (Ferraresi, 1977):

$$C_p = t_t \frac{(S_b + S_m)}{60} + \frac{t_c}{T} C_{ft} \qquad (1)$$

sendo:

$$t_t = t_c + t_s + t_a + \frac{t_p}{Z} + \left(\frac{t_c}{T} - \frac{1}{Z}\right) t_{ft} \qquad (2)$$

$$C_{ft} = \frac{C_f}{n_2} + C_{af}\frac{n_1}{n_2} + \frac{C_{pf}}{n_3} \quad \text{p/ inserto reafiável} \qquad (3)$$

$$C_{ft} = \frac{C_f}{n_2} + \frac{C_{pf}}{n_3} \quad \text{p/ inserto descartável} \qquad (4)$$

A Tabela II mostra os valores dos tempos e custos de usinagem para as ferramentas de metal duro, cerâmica pura e diamante, no torneamento de um peça de compósito de tecido bobinado.

Os valores obtidos na Tabela II mostram que a utilização de ferramentas de diamante e de cerâmica pura em operação de torneamento de desbaste de compósito de tecido bobinado apresenta um custo de usinagem por peça superior ao metal duro. Isto abrange as demais cerâmicas pois a relação custo/vida destas ferramentas foram maiores que a obtida para cerâmica pura. Portanto, para uma relação de custo/benefício o metal duro mostrou ser a melhor de todas as ferramentas ensaiadas no torneamento de desbaste do compósito.

Em operação de acabamento, a Fig. 3 mostra o comportamento da rugosidade (R_a) da peça em relação ao comprimento de corte usinado para todas as ferramentas ensaiadas.

A rugosidade aumentou drasticamente nas peças usinadas com ferramentas cerâmicas, devido aos elevados desgastes ocorridos nestas ferramentas. Enquanto que nas peças usinadas com ferramentas de metal duro, CBN e diamante, a rugosidade apresentou menor taxa de crescimento. A ferramenta que assegurou o melhor acabamento superficial foi o diamante.

Tabela II. Tempos e custos/peça de usinagem para as ferramentas

Descrição	MD K10 VB = 0,5 mm	Cer. pura VB = 0,5 mm	Diamante VB = 0,5 mm
Tempo de corte da peça tc (min)	5,78	5,78	5,78
Tempos improdutivos ti (min)	3,7	3,7	3,7
Tempo de troca ferram. t_{ft} (min)	0,5	0,5	0,5
Número de peças do lote Z	10	10	10

Descrição	MD K10 VB = 0,5 mm	Cer. pura VB = 0,5 mm	Diamante VB = 0,5 mm
Tempo total confec. peça t_t (min)	11,43	12,60	9,54
Vida das ferramentas T (min)	1,44	0,91	25,73
Número de afiações n_1			5
Número de vidas da ferramenta n_2	8	8	6
Salário do operador Sh (US$/h)	3,00	3,00	3,00
Salário da máquina Sm (US$/h)	20,00	20,00	20,00
Custo da ferramenta Cf (US$)	5,84	28,32	93,00
Custo ferramenta/vida Cft (US$)	1,06	3,54	30,55
Custo afiação ferramenta Caf (US$)			13,95
Custo porta-ferramenta Cpf (US$)	131,00	131,00	131,00
Custo de usinagem/peça Cp (US$)	9,63	29,40	10,52

Isto acontece devido as delaminações das fibras e os sulcos formados pela presença de resina no material compósito. Sendo que estes sulcos e delaminações aumentam de intensidade com o crescimento de desgaste da ferramenta (Takeshita e Wehara, 1985). Portanto, quanto mais resistente ao desgaste é a ferramenta, melhor seu comportamento em relação ao acabamento da peça.

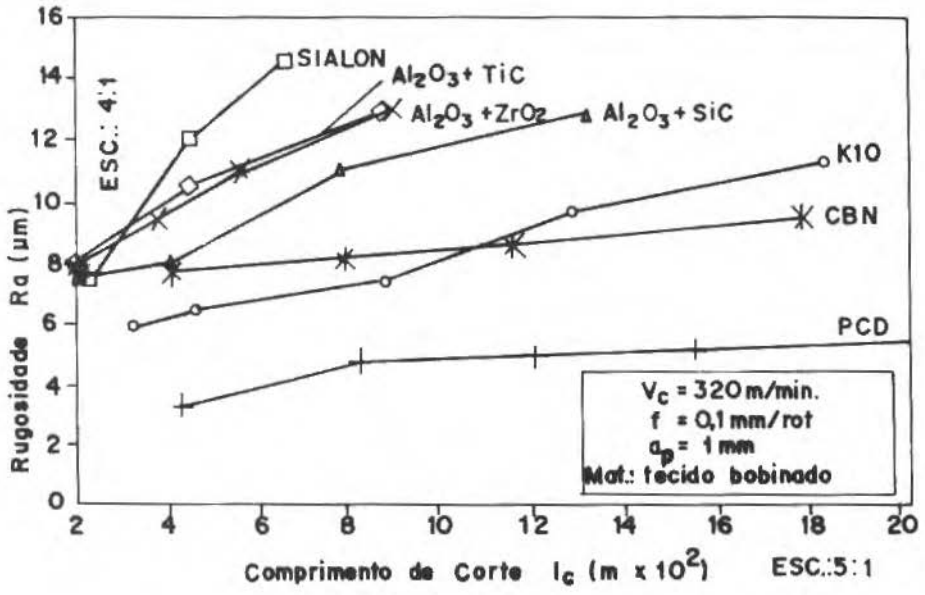

Fig. 3 Rugosidade R_a versus comprimento de corte

Observa-se também que as médias dos valores da rugosidade do compósito apresentaram uma taxa de crescimento aproximadamente constante com o comprimento de corte. Explica-se este fato pelo mecanismo de desgaste da ferramenta desenvolvido na usinagem de compósito reforçado com fibras. O desgaste neste caso é predominantemente abrasivo, ocorrendo uma espécie de polimento somente na superfície de folga da ferramenta (Fig. 4a). Neste caso não são observados os desgastes de cratera e de entalhe, presentes nas ferramentas de metal duro quando da usinagem de aços dúteis (Fig. 4b), onde há grande variação na rugosidade da peça (Ferraresi, 1977).

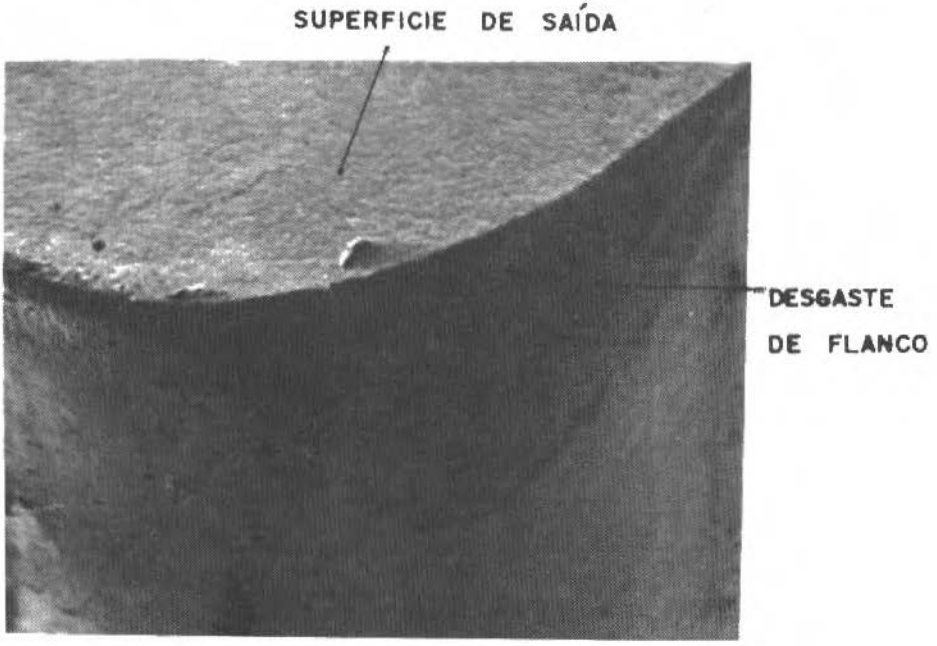

a. Torneamento de material compósito - Metal duro K10

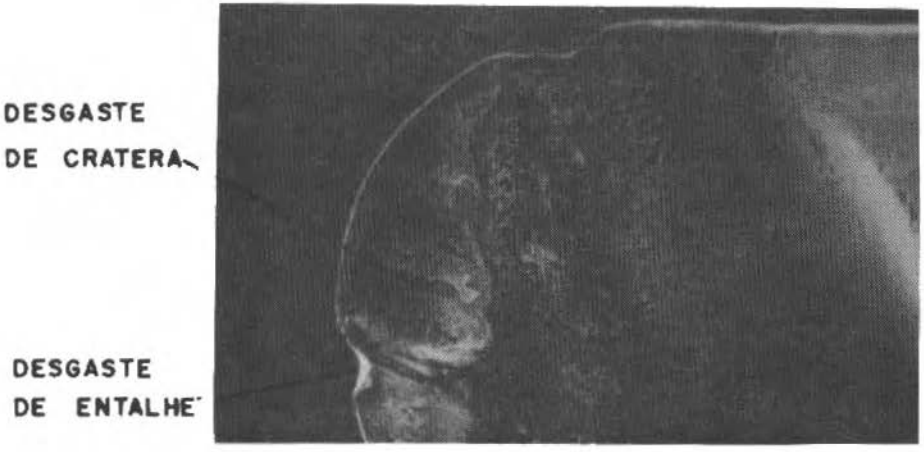

b. Torneamento de aços dúteis (SAE/ABNT 1045) - Metal duro P20

Fig. 4 Mecanismos de desgaste da ferramenta de metal duro

A Fig. 5 mostra a variação da força de avanço com o comprimento de corte. Para alguns materiais de ferramentas como as cerâmicas, o crescimento da força é acentuado. Para o diamante e o CBN, a força de avanço permaneceu quase constante. Justifica-se este fato pela intensidade do desgaste sofrido pelas ferramentas, confirmando os resultados obtidos na Fig. 2.

O valor da força de avanço medida no torneamento do compósito com ferramenta de diamante foi de 5 kgf. Este valor de força de avanço é da mesma ordem de grandeza das obtidas no corte de aços (Ferraresi, 1977). O material compósito apesar de apresentar baixa densidade requer grandes forças de usinagem, provavelmente devido às suas boas propriedades mecânicas.

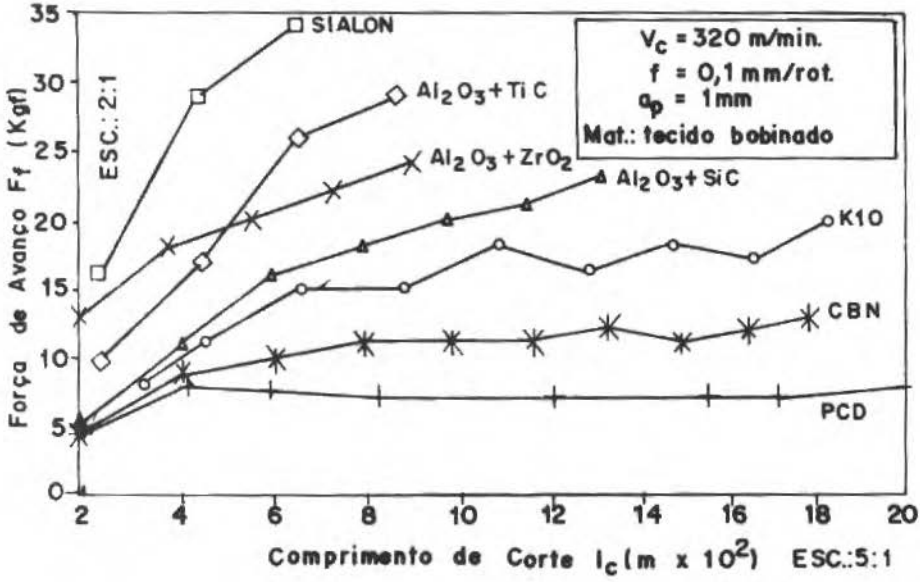

Fig. 5 Força de avanço versus comprimento de corte

No torneamento do compósito de tecido laminado observou-se a influência da velocidade de corte no desgaste da ferramenta de metal duro, como também a variação da rugosidade com a direção das fibras no laminado.

A Fig. 6 mostra a evolução do desgaste da ferramenta de metal duro com a velocidade de corte. Observa-se que até a velocidade de 320 m/min, o desgaste da ferramenta variou pouco. De 320 m/min a 450 m/min houve um rápido crescimento do desgaste, devido ao maior atrito ferramenta-peça e à menor resistência ao desgaste da ferramenta em temperaturas mais elevadas, onde ocorreu inclusive a queima da resina fenólica (Hasegawa, 1984)

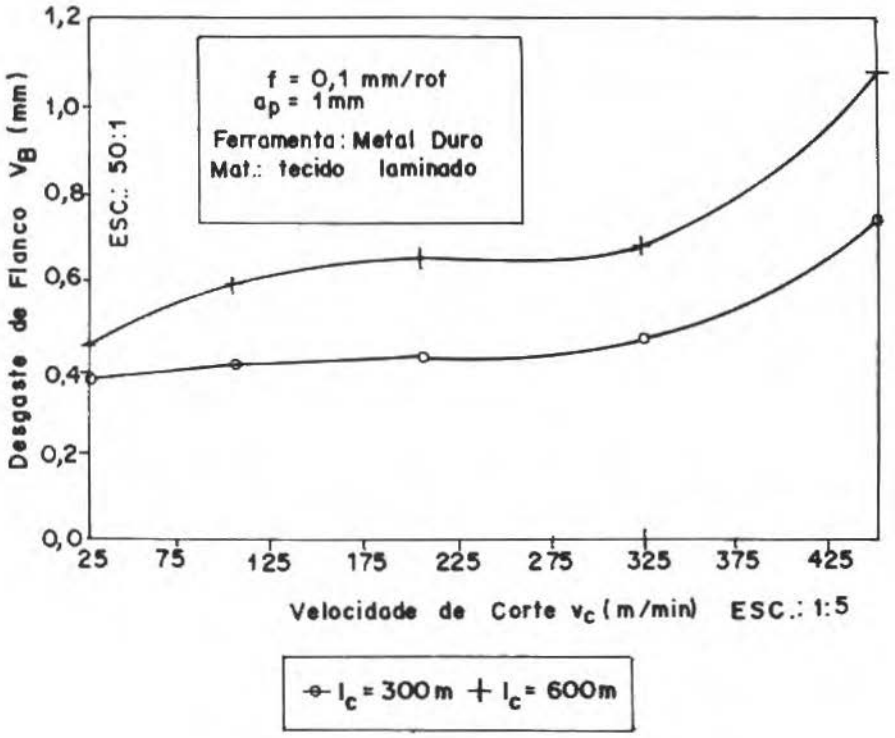

Fig. 6 Desgaste de flanco versus velocidade de corte

A Fig. 7 mostra a variação da rugosidade com o ângulo da direção das fibras (α) em torno de 45 e 225 graus em relação à direção de corte, pois nesta posição a tendência da ferramenta é de delaminar as fibras, deixando a superfície do compósito mais áspera. Na Fig. 7, também pode ser observado uma forte influência do avanço (f) na rugosidade da peça, de maneira similar como na usinagem dos metais (Wunsch e Spur, 1988).

Para finalizar, observou-se a influência da disposição das fibras do material compósito no desgaste da ferramenta. A Fig. 8 apresenta as curvas de desgaste das ferramentas de metal duro em função do comprimento de corte. O comportamento dos desgastes das ferramentas são comparados entre os torneamentos dos compósitos de tecidos bobinado e laminado.

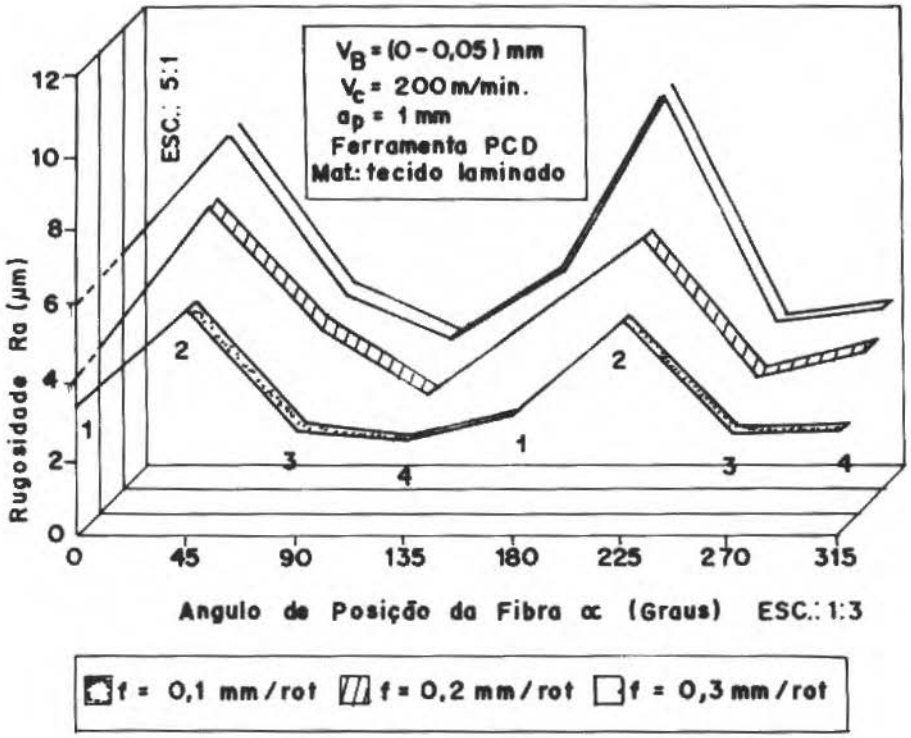

Fig. 7 Rugosidade R_a em função do ângulo de posição das fibras

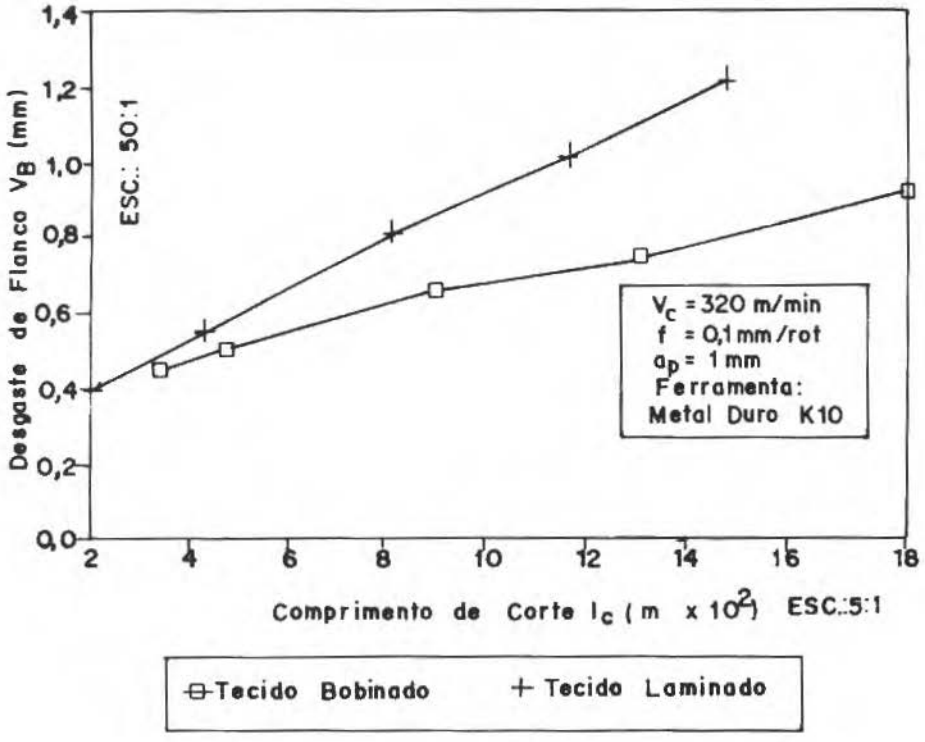

Fig. 8 Desgaste de flanco versus comprimento de corte

A ferramenta de metal duro se desgasta mais rapidamente no corte do compósito de tecido laminado do que no bobinado. A maior abrasividade do tecido laminado deve-se ao fato da variação da orientação das fibras em relação à direção de corte no torneamento, onde se tem a cada instante uma nova posição da fibra em relação à ferramenta.

Conclusões

- Em função dos resultados obtidos pode-se tirar as seguintes conclusões:
- Conforme as considerações efetuadas nas Tabelas I e II, o uso de ferramentas cerâmicas e de CBN no torneamento de compósito não é viável do ponto de vista técnico e econômico;
- A rugosidade da peça aumenta de maneira progressiva com o desgaste de flanco da ferramenta podendo levar à delaminação das fibras;
- Existe uma grande dispersão na medida da rugosidade do compósito, devido aos defeitos originados por delaminação e sulcos na superfície da peça;
- Em operação de acabamento, somente a ferramenta de diamante pode assegurar uma qualidade superficial com rugosidade R_a na faixa de 2,5 a 5,0 μm;
- Apesar do compósito ser um material leve mediram-se forças de corte nos patamares alcançados em corte de aços;
- Devido à presença do desgaste de flanco e à inexistência de desgaste de cratera na ferramenta, a força de avanço aumentou notavelmente com a evolução do desgaste;

- O compósito de tecido laminado é mais abrasivo à ferramenta do que o compósito de tecido bobinado, e
- Em operação de desbaste, a utilização da ferramenta de metal duro apresentou-se como a melhor solução, pois apesar de sofrer desgaste superior ao diamante, resulta numa relação custo/benefício mais vantajosa e dispensa cuidados operacionais especiais.

Agradecimentos

Ao CTA - Centro Técnico Aeroespacial, pelo fornecimento do material compósito. À Dífer Diamantes Industriais, Sandvik, SKF Ferramentas, Brasimet e Winter do Brasil, pelo fornecimento de ferramentas. À FINEP pelo apoio financeiro e ao aluno Frederico Ueda pelo auxílio dado nos ensaios.

Referências

Ferraresi, D. (1977) "Fundamentos da Usinagem dos Metais", Editora Edgard Blucher, São Paulo.

Hasegawa, Y. (1984) "Characteristics of Tool Wear in Cutting GFRP", 5th International Conference on Production Engineering, pp. 185-190, Tokyo.

Koplev, A. e Lystrup, A. (1983) "The Cutting Process, Chips, and Cutting Forces in Machining CFRP", Composites, vol. 14-4, pp. 371-376.

Malhotra, S.K. (1989) "High Speed Steel Tool Wear Studies in Machining of Glass Fiber-Reinforced Plastics", Wear, vol. 132, pp. 327-336.

Reinhart, T.J., (1988) "Engineering Materials Handbook", Composites, Vol. 1, ASM International, Ohio.

Takeshita, H. e Wehara, K. (1985) "Cutting Mechanism of Some Composite Materials", Second International Metal Cutting Conference, Tokyo University, Japan.

Wunsch, U.E. e Spur, G. (1988) "Turning of Fiber-Reinforced Plastics", Manufacturing Review, Vol. 1, pp. 124-129.

RBCM - J. of the Braz. Soc. Mechanical Sciences
Vol. XIV - nº 2 - 1993 pp. 124-135

ISSN 0100-7386
Printed in Brazil

Mechanical Systems Identification through Fourier-Series Time-Domain Technique

Identificação de Sistemas Mecânicos Através das Séries de Fourier - Técnica no Domínio do Tempo

G. P. Melo
Mech. Eng. Department
FEIS/UNESP
15378 Ilha Solteira - SP
Brazil

V. Steffen Jr.
Mech. Eng. Department
Univ. Fed. Uberlândia
38400 Uberlândia - MG
Brazil

Abstract

A time-domain technique based on Fourier series is used in this work for the parameters identification of mechanical systems with multi-degrees of freedom. The method is based on the orthogonality property of the Fourier series which enables the integration of the equations of motion. These equations are then converted to a linear algebraic model that is solved to obtain the unknown parameters. This way the method can be summarized as follows:

1. Expansion of the input and output signals in Fourier series;
2. Integration of the equations of motion using an operational matrix to integrate the series;
3. The parameters are calculated through a least-square estimation method.

Keywords: parameter identification, modal analysis, time-domain technique, Fourier series.

Resumo

Apresenta-se neste trabalho um método para identificação de Sistemas Mecânicos com vários graus de liberdade operando no domínio do tempo. O método baseia-se na expansão das funções de excitação e de resposta do sistema em termos de séries de Fourier e na transformação das equações diferenciais do movimento em equações algébricas por meio de integrações sucessivas e da utilização de uma matriz operacional para integração das funções que formam aquelas séries. Desta forma, o método pode ser sumarizado em três etapas fundamentais:

1. Expansão da excitação e da resposta em séries de Fourier;
2. Integração das equações de movimento e emprego de uma matriz operacional para integração das séries de Fourier;
3. Estimativa dos parâmetros pelo método dos mínimos quadrados.

Palavras-chave: identificação de parâmetros, análise modal, técnica no domínio do tempo, séries de Fourier.

Introduction

In recent years a great number of methods for the identification of dynamical systems using orthogonal functions have been developed. Most of applications are however devoted to control problems. Walsh (Chen and Hsiac, 1975), Block Pulse (Jiang and Schanfelberger, 1985) and Fourier (Chun, 1987) functions and Chebyshev (Paraskevopoulos, 1983), Jacobi (Lin and Shih, 1985), Laguerre (Hwang and Shih, 1987) and Hermite (Paraskevopoulos and Kerkeris, 1983) polynomials are examples of such orthogonal functions used to identify linear-time-invariant lumped parameters systems. In a previous work a method based on the expansion of the input and output time functions in terms of Fourier series was presented by one of the authors of this paper (Steffen, 1991) focusing mechanical vibrations problems.

In the presented paper the method is tested for different mechanical engineering applications: dynamical seal; three d.o.f. system; external force identification. Numerical simulations and experimental tests confirm the applicability of the method. The influence of noise was analysed.

Manuscript received: January 1993. Associate Technical Editor: Agenor de Toledo Fleury

Basic Governing Equations

The method is now briefly presented for linear time-invariant mechanical systems with N degrees of freedom. For those systems a widely used model is

$$[M]\{\ddot{x}(t)\} + [C]\{\dot{x}(t)\} + [K]\{x(t)\} = \{f(t)\} \tag{1}$$

were $[M]$, $[C]$ and $[K]$ are respectively the inertia, damping and stiffness N-order matrices; $\{x(t)\}^T = \{x_1(t)\ x_2(t) \ldots x_n(t)\}$ is the vector of displacements and $\{f(t)\}^T = \{f_1(t)\ f_2(t) \ldots f_n(t)\}$ is the vector of input forces.

This equation can be rewritten in the following state-form equation:

$$\begin{bmatrix}\{\dot{x}(t)\}\\ \{\ddot{x}(t)\}\end{bmatrix}_{2N\times 1} + [A]_{2N\times 2N}\begin{bmatrix}\{x(t)\}\\ \{\dot{x}(t)\}\end{bmatrix}_{2N\times 1} = [B]_{2N\times N}\{f(t)\}_{N\times 1} \tag{2}$$

where

$$[A]_{2N\times 2N} = \begin{bmatrix}[O]_{N\times N} & : & [I]_{N\times N}\\ \ldots & \ldots & \ldots\\ [M]^{-1}[K]_{N\times N} & : & [M]^{-1}[C]_{N\times N}\end{bmatrix} \quad \text{and}$$

$$[B]_{2N\times N} = \begin{bmatrix}[O]_{N\times N}\\ [M]^{-1}\end{bmatrix}$$

Matrix $[A]$ contain all the dynamic characteristics of the system: eigen-values (natural frequencies and modal damping factors) and eigen-vectors can be extracted.

After double integration Eq. (2) becomes

$$\begin{bmatrix}\int_C^t \{x(\tau)\}\,d\tau\\ \{x(t)\}\end{bmatrix} - \begin{bmatrix}\{0\}\\ \{x(0)\}\end{bmatrix} - \begin{bmatrix}\{x(0)\}\\ \{\dot{x}(0)\}\end{bmatrix}t +$$

$$+ [A]\begin{bmatrix}\iint_{00}^{tt}\{x(\tau)\}\,d\tau^2\\ \int_0^t \{x(\tau)\}\,d\tau\end{bmatrix} - [A]\begin{bmatrix}\{0\}\\ \{x(0)\}\end{bmatrix}t = [B]\left\{\iint_{CC}^{tt}\{f(\tau)\}\,d\tau^2\right\} \tag{3}$$

$x_i(t)$ and $f_i(t)$, i=1, N are now expanded in Fourier series:

$$x_i(t) = \{X_i\}\{\varnothing(t)\},\ i = 1,N$$

$$f_i(t) = \{F_i\}\{\varnothing(t)\},\ i = 1,N \tag{4}$$

where

$$\{\Phi(t)\}^T_{r2} = [1, \cos(2\pi t/T), \ldots, \cos(2\pi rt/T), \sin(2\pi t/T), \ldots$$

$$\ldots, \sin 2\pi rt/T\,], (r2 = 2r+1)$$

$$\{X\}^T_{r2} = [x_0, x_1, \ldots, x_r, x^*_1, \ldots, x^*_r] \quad \text{and}$$

$$\{F\}^T_{r2} = [f_0, f_1, \ldots, f_r, f^*_1, \ldots, f^*_r]$$

It is possible to write:

$$\{x(t)\}_{N\times 1} = [X]^T_{N\times r2}\{\Phi(t)\}_{r2\times 1} \quad \text{and}$$

$$\{f(t)\}_{N\times 1} = [F]^T_{N\times r2}\{\Phi(t)\}_{r2\times 1} \tag{5}$$

where

$$[X] = [\{X_1\}\ \{X_2\} \ldots \{X_N\}] \quad \text{and}$$

$$[F] = [\{F_1\}\ \{F_2\} \ldots \{F_N\}]$$

Substituting Eq. (5) into Eq. (4) gives:

$$\begin{bmatrix}[X]^T[P]\\ [X]^T\end{bmatrix}_{2N\times r2} - \begin{bmatrix}\{x(0)\}\{e\}^T[P]\\ \{x(0)\}\{e\}^T + \{\dot{x}(0)\}\{e\}^T[P]\end{bmatrix}_{2N\times r2} +$$

$$+A\begin{bmatrix}[X]^T[P]^2\\ [X]^T[P]\end{bmatrix}_{2N\times r2} - [A]\begin{bmatrix}\{0\}\\ \{x(0)\}\end{bmatrix}_{2N\times r2}\{e\}^T[P] = [B][F]^T[P]^2_{N\times r2} \tag{6}$$

In this equation t was written as $t = \{e\}^T[P]\{\varnothing(t)\}$ and $[P]$ is the operational matrix of integration which is determined from the following integral property of the basis vector $\{\varnothing\}$ of the orthogonal series:

$$\int_0^t \cdots \int_0^t \{\Phi(\tau)\}(d\tau)^n = [P]^n\{\Phi(t)\} \tag{7}$$

n times

and

$$[P]_{r2\times r2} = \left[\begin{array}{c|c|c} T/2 & [0] & -T/\pi\{\bar{e}\}^T_r \\ \hline \{0\} & [0]_{r\times r} & T/2\pi\{\bar{I}\}_{r\times r} \\ \hline T/2\pi\{\bar{e}\}_r & -T/2\pi[\bar{I}]_{r\times r} & [0]_{r\times r} \end{array}\right]$$

where

$$\{\bar{e}\}_r = \begin{bmatrix} 1 \\ 1/2 \\ 1/3 \\ \vdots \\ 1/r \end{bmatrix}, \quad [\bar{I}]_{r\times r} = \begin{bmatrix} 1 & 0 & 0 & \dots & 0 \\ 0 & 1/2 & 0 & \dots & 0 \\ 0 & 0 & 1/3 & \dots & 0 \\ \vdots & \vdots & \vdots & \vdots & \vdots \\ 0 & 0 & 0 & 0 & 1/r \end{bmatrix}$$

For a given set of initial conditions Eq. (6) can be rearranged as

$$[A][D] - [B][G] = [E] \tag{8}$$

where

$$[D] = \begin{bmatrix} [X]^T[P]^2 \\ [X]^T[P] - \{x(0)\}\{e\}^T[P] \end{bmatrix}_{2N\times r2},$$

$$[G] = \left[[F]^T[P]^2\right] \quad \text{and}$$

$$[E] = \begin{bmatrix} (\{x(0)\}\{e\}^T - [X]^T)[P] \\ \{x(0)\}\{e\}^T + \{\dot{x}(0)\}\{e\}^T[P] - [X]^T \end{bmatrix}_{2N\times r2}$$

Then

$$[J]^T[H]^T = [E]^T \tag{9}$$

where

$$[H] = \left[[A] : -[B]\right]_{2N\times 3N} \quad \text{and} \quad [J] = \begin{bmatrix} [D] \\ [G] \end{bmatrix}_{3N\times r2}$$

A least-square technique is used to obtain the unknown parameters (natural frequencies, modal damping factors).

$$[H]^T = ([J][J]^T)^{-1}[J][E]^T \tag{10}$$

The equations above can be easily adapted for the identification of the excitation forces.

Applications

Three applications are now presented to demonstrate the performance of the above methodology.

1. The method was firstly applied to a two degree of freedom system which represents a dynamic seal as shown in Fig. 1.

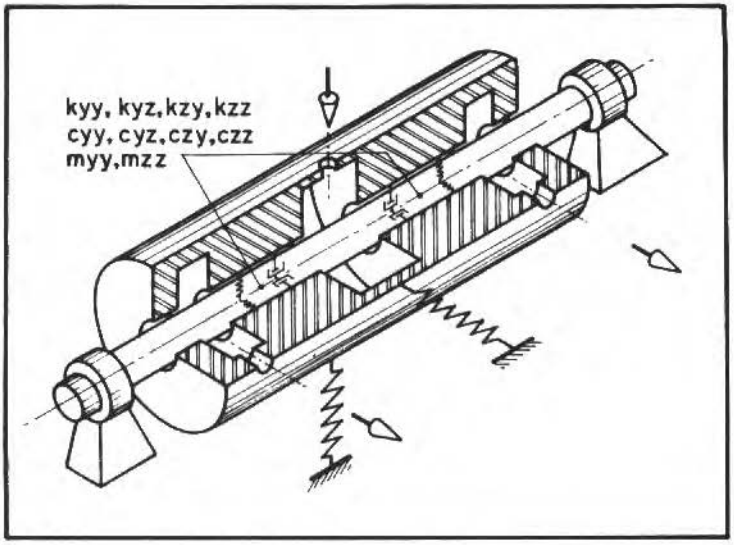

Fig. 1 Dynamic seal

The equation of motion which represents the dynamics of the seal is:

$$[M]\{\ddot{x}(t)\} + [C]\{\dot{x}(t)\} + [K]\{x(t)\} = \{f(t)\} \qquad (11)$$

where

$$[M] = \begin{bmatrix} M_{yy} & 0 \\ 0 & M_{zz} \end{bmatrix}, \quad [C] = \begin{bmatrix} C_{yy} & -C_{yz} \\ C_{zy} & C_{zz} \end{bmatrix}$$

$$[K] = \begin{bmatrix} K_{yy} & -K_{yz} \\ K_{zz} & K_{zz} \end{bmatrix} \quad \text{and}$$

$$\{x(t)\} = \begin{bmatrix} y(t) \\ z(t) \end{bmatrix}, \quad \{f(t)\} = \begin{bmatrix} f_y(t) \\ f_z(t) \end{bmatrix}$$

where M_{yy}=26.200 Kg, M_{zz}=26.200 Kg, C_{yy}=C_{zz}=1124.000 Ns/m, C_{yz}=C_{zy}=720.000 Ns/m, K_{yy}=K_{zz}=468430.000 N/m, K_{yz}=K_{zy}=42811.000 N/m, $f_y(t)$=$f_z(t)$=$y(0)$=$z(0)$=0.000, $\dot{y}$ = 1000, $\dot{z}$ = 0,000 and $0{,}00 \le t \le 0{,}08$s.

The response $\{x(t)\}$ is obtained using a fourth-order Runge-Kutta technique. $\{x(t)\}$ and $\{f(t)\}$ are expanded on Fourier series to permit the identification of the model parameters presented in Table I.

Table I - Theoretical and identified parameters
*** - percentual magnitude differences**

Mode	Parameters	Theoretical Values	Identified Values	Relative Difference
1	ω_n (rd/s)	121.689	120.418	1.04
	ω_d (rd/s)	119.012	118.010	0.84
	ξ	0,209	0,199	-
	Eigen Values	-25.384 ∓ i 119.012	-23.966 ∓ i 118.010	1.04*
	Eigen Vectors $\frac{y2}{y1}$	0.000 + i 1.000	-0.061 + i 1.017	1.88*
2	ω_n (rd/s)	147.536	147.826	0.20
	ω_d (rd/s)	146.493	146.824	0.26
	ξ	0.119	0.116	-
	Eigen Values	-17.516 ∓ i 146.493	-17.184 ∓ i 146.824	0.20*
	Eigen Vectors $\frac{y2}{y1}$	0.000 - i 1.000	-0.039 - i 1.038	3.80*

2. A real three degree-of-freedom system as shown in Fig. 2 was used for identification purposes. The equations to represent the undamped dynamic model of the above system are given by:

$$I_x\ddot{\alpha} + (4KL^2 + 2K_aL^2)\alpha = 0$$

$$I_y\ddot{\beta} + 4KB^2\beta = 0$$

$$M\ddot{z} + (4K + 2K_a)z = 0 \qquad (12)$$

where

I_x, I_y and M are the inertia and mass coefficients;

K and K_a are stiffness coefficients;

L and B are lengths, and

α, β, z are angular and linear displacements

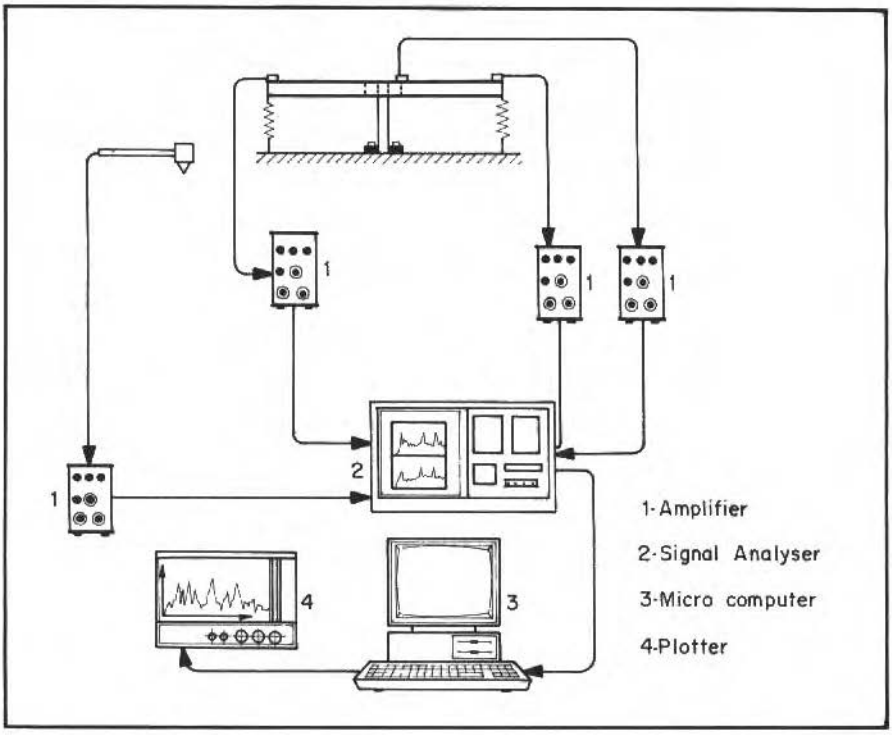

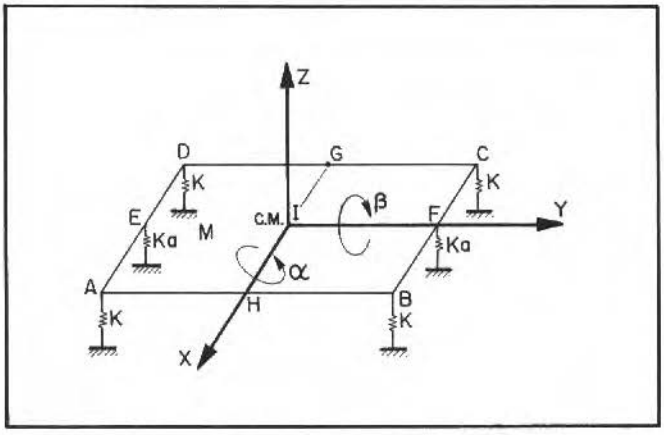

Fig. 2 a) 3 D.O.F. Test rig scheme b) 3 D.O.F. Model

Three accelerometers were used to measure the system response. The signals were manipulated to obtain $\alpha(t)$, $\beta(t)$ and $z(t)$. Three sets of 1024 points-sampling were used. The sampling time was T=0.7 seconds.

These accelerometers were placed at points D, G and F of the structure

Table 2 shows theoretical and identified parameters.

Table 2 - Theoretical and identified parameters
*** - percentual magnitude differences**

Mode	Parameters	Theoretical Values	Identified Values	Relative Difference
1	ω_n (rd/s)	175.889	174.671	0.69
	ω_d (rd/s)	175.899	174.656	0.71
	ξ	0.000	0.001	-
	Eigen Values	0.000 ∓ i 175.899	-0.160 ∓ i 174.620	0.72*
	Eigen Vectors $\frac{y1}{y1}$	1.000 + i 0.000	1.000 - i 0.000	-
	Eigen Vectors $\frac{y2}{y1}$	0.000 + i 0.000	0.037 + i 0.017	-
	Eigen Vectors $\frac{y3}{y1}$	0.000 + i 0.000	-0.032 - i 0.053	-
2	ω_n (rd/s)	219.908	221.058	0.52
	ω_d (rd/s)	219.908	221.059	0.52
	ξ	0.000	0.002	-
	Eigen Values	0.000 ∓ i 219.908	-0.650 ∓ i 221.060	0.52*
	Eigen Vectors $\frac{y1}{y3}$	0.000 + i 0.000	-0.001 + i 0.004	-
	Eigen Vectors $\frac{y2}{y3}$	0.000 + i 0.000	0.009 - i 0.008	-
	Eigen Vectors $\frac{y3}{y3}$	1.000 + i 0.000	1.000 + i 0.000	-
3	ω_n (rd/s)	304.481	290.339	4.64
	w_d (rd/s)	304.481	290.338	4.64
	ξ	0.000	0.003	-
	Eigen Values	0.000 ∓ i 304.481	-0.092 ∓ i 290.340	4.64*
	Eigen Vectors $\frac{y1}{y2}$	0.000 + i 0.000	-0.020 + i 0.006	-
	Eigen Vectors $\frac{y2}{y2}$	1.000 + i 0.000	1.000 - i 0.000	-
	Eigen Vectors $\frac{y3}{y2}$	0.000 + i 0.000	-0.039 - i 0.064	-

3. The last application deals with force identification of a single-degree-of-freedom system where M=10.0 kg, C=40.0 Ns/m and K=1000.0 N/m. For simulation purposes the system response for an excitation force f(t)=50.0 N ($x(0) = \dot{x}(0) = 0,0$) was calculated and is given by:

$$x(t) = e^{-2t}(-0,050\cos(9,798t) - 0,010\sin(9,7898t)) + 0,05 \qquad (13)$$

Using Eq. (13) 1024 points were generated for $0,00 \leq t \leq 1,50$ seconds and the Fourier coefficients were calculated.

The results are presented for different situations:

A - Parameters identification retaining five terms in Fourier expansions (Table 3)

B - Parameters identification retaining ten terms in Fourier expansions (Table 4)

C - Influence introduced in the identified parameters when considering the introduction of 10% of random noise in the answer x(t) - (Table 5)

D - Identification of the excitation force f(t) - Fig. 3

Table 3 - Theoretical and identified parameters (r=5)

	Theoretical Values	Identified Values	Relative Difference (%)
a_i	4.000	4.054	1.34
a_o	100.000	100.256	0.25
b_o	0.100	0.100	0.00
d_o (m)	0.000	0.007	-
d_1 (m/s)	0.000	-0.001	-
M (kg)	10.000	9.980	0.20
C (Ns/m)	40.000	40.455	1.13
K (N/m)	1000.000	1000.555	0.05
ξ	0.200	0.202	1.00
ω_n (rd/s)	10.000	10.013	0.12
ω_d (rd/s)	9.798	9.793	0.05

Table 4 - Theoretical and identified parameters (r=10)

	Theoretical Values	Identified Values	Relative Difference (%)
a_i	4.000	4.044	1.09
a_o	100.000	100.163	0.16
b_o	0.100	0.100	0.00
d_o (m)	0.000	0.004	-
d_1 (m/s)	0.000	-0.001	-
M (kg)	10.000	9.990	0.10
C (Ns/m)	40.000	40.398	0.99
K (N/m)	1000.000	1000.628	0.06
ξ	0.200	0.202	1.00
ω_n (rd/s)	10.000	10.008	0.08
ω_d (rd/s)	9.798	9.801	0.3

Tables 3 and 4 permit to observe that increasing the number of retained terms in Fourier series decrease the relative difference between theoretical and identified parameters.

Table 5 - Theoretical and identified parameters (r=10) - 10% of random noise

	Theoretical Values	Identified Values	Relative Difference (%)
a_i	4.000	4.026	0.64
a_o	100.000	100.583	0.58
b_o	0.100	0.105	5.00
d_o (m)	0.000	0.050	-
d_1 (m/s)	0.000	0.016	-
M (kg)	10.000	9.569	4.30
C (Ns/m)	40.000	38.228	4.44
K (N/m)	1000.000	952.485	4.75
ξ	0.200	0.201	0.50
ω_n (rd/s)	10.000	10.029	0.29
ω_d (rd/s)	9.798	9.824	0.26

Remark: The random noise introduced in the answer signal is obtained as follows:

1) The RMS of the sampled data x(t) is obtained and the value NR=10% RMS is determined

2) N random numbers are produced each one of them is associated to each element of x(t)

3) The product NR by the random numbers is evaluated, with (0.0) average and (1.0) standard deviation.

Fig. 3 shows the results retaining five and ten terms in the Fourier series.

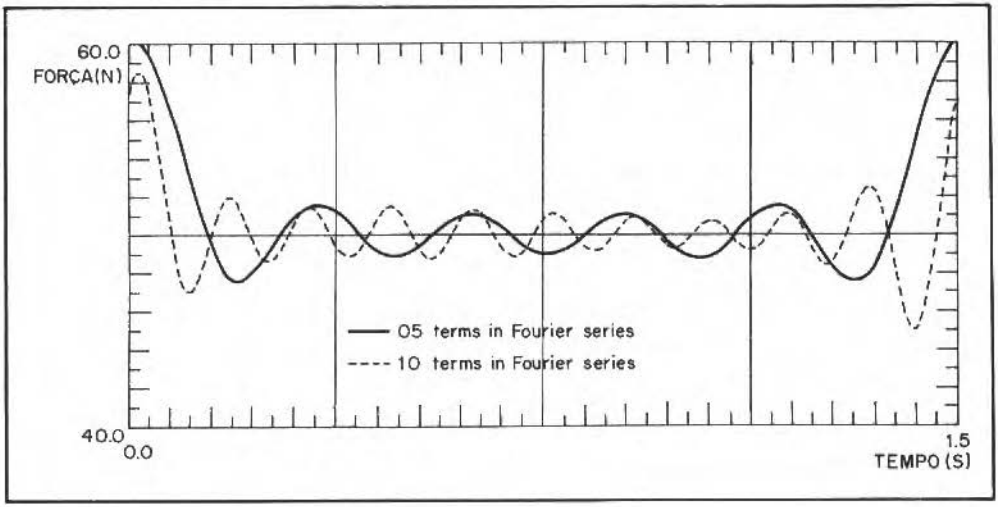

Fig. 3 Excitation force identification

Conclusion

This paper presented a time-domain technique for identification based on the Fourier series expansions of the system excitation and response. The integration of the series is made using an operational matrix. Simulation and experimental results obtained for different mechanical engineering systems show that the method is very simple to be implemented and very little sensitive to noise. It was observed that the quality of the results is improved when increasing the number of harmonics taken in the Fourier expansions.

References

Chen, C. F. and Hsiac, C. H. (1975) "Time Domain Sysnthesis via Walsh Functions", Proc. IEEE, 122: 565-570.

Chun, H. Y. (1987) "System Identification via Fourier Series", International Journal of Systems Science, 18: 1191-1194.

Hwang, C. and Shih, Y. P. (1982) "Parameter Identification via Laguerre Polynomials", International Journal of Systems Science, 13: 209-217.

Jiang, Z. H. and Schanfelberger, W. (1985) "A New Algorithm for Single-Input-Single-Output System Identification via Block Pulse Functions", International Journal of Systems Science, 16: 1559-1571.

Lin, C. C. and SHIH, Y. P. (1985) "System Analysis, Parameter Estimation and Optimal Regulator Design of Linear Systems via Jacobi Series", Int. J. Control, 42: 221-224.

Melo, G. P. (1992) "Identificação de Sistemas Mecânicos através do Método das Séries de Fourier - Um Método no Domínio do Tempo", Tese de Mestrado - Universidade Federal de Uberlândia, 114p.

Paraskevopoulos, P. N. and Kerkeris, G. TH. (1983) "Hermite Series Approach to System Identification, Analysis and Optimal Control", Proc. 6th Int. Symp. on Methods and Appl. of Measurement and Control, Acta Press, Canada, 1: 146-149.

Paraskevopoulos, P. N., Sparis, P. D. and Mouroutsos, S. G. (1985) "The Fourier Series Operational Matrix of Integration", International Journal of Systems Science, 16: 171-176.

Paraskevopoulos, P. N. (1983) "Chebychev Series Approach to System Identification, Analysis and Optimal Control", Journal of the Franklin Institute, 316: 135-157.

Steffen Jr., V. and Rade, D. A. (1991) "An Identification Method of Multi-Degree-of-Freedom Systems Based on Fourier Series", The International Journal of Analytical and Experimental Modal Analysis, pp. 271-278, oct.

RBCM - J. of the Braz. Soc. Mechanical Sciences
Vol. XV - nº 2 - 1993 - pp. 136-149

ISSN 0100-7386
Printed in Brazil

Updating Rotor-Bearing Finite Element Models Using Experimental Frequency Response Functions

José Roberto F. Arruda
Department of Computational Mechanics
State University of Campinas
Campinas 13083-970, Brazil

Marcus A. V. Duarte
Department of Mechanical Engineering
Federal University of Uberlândia
Uberlândia 38400-080, Brazil

Abstract

Most Finite Element model updating techniques require experimental modal parameters, which are obtained from modal tests. In the case of real rotor-bearing systems it is frequently unfeasible to perform complete modal tests due to difficulties such as exciting a rotating shaft and dealing with bearing nonlinearities. In this paper, the possibility of updating the Finite Element model of a rotor-bearing system by estimating the bearing stiffness and damping coefficients from a few measured Frequency Response Functions is investigated. The proposed model updating procedure consists of applying a nonlinear parameter estimation technique to correct a few FE model parameters chosen a priori. The parameter estimation problem is presented in its general form, from which the various methods can be derived, and then particularized to a nonlinear least squares problem where the objective function to be minimized is the sum of the square differences between the logarithm of the theoretical and experimental Frequency Response Function (FRF) magnitudes. The importance of using the logarithm of the magnitudes and its equivalence to the maximization of the correlation between the theoretical and experimental functions is pointed out. A closed form expression for the sensitivity matrix of the logarithm of the FRF magnitudes is derived, and it is shown that the finite differences approximation produces sufficiently accurate results at a much lower computational cost. The issues of identifiability and parameter estimation errors are addressed. A numerical example of a flexible rotor supported by two orthotropic bearings is presented to illustrate the proposed method.

Introduction

Although the tools for theoretical dynamic analysis are increasingly sophisticated and refined models can be treated at a relatively low cost and high speed with modern computers, dynamic testing is still of foremost importance due to the difficulties in predicting the dynamic behavior of certain structure components, e.g., mechanical joints. Rotor systems always include a nonlinear, nonconservative kind of joint which influences dramatically its dynamic behavior, namely the bearings. Fluid/structure interaction is also very difficult to model. In both cases, linearized models may be obtained by the experimental estimation of some linearized parameter values which describe the system behavior for the operating dynamic load levels. This estimation is done by comparing theoretical model predictions with measured data and updating the former so that the predictions fit the experimental data. Different approaches exist to the problem of updating theoretical models of structures (Imregun and Visser, 1991). The most suitable when a small set of physical parameters of a FE model are to be corrected is the so-called inverse sensitivity approach. Inverse sensitivity methods are usually applied in the modal domain (Lallement and Zhang (1988), Natke (1988), and Carneiro and Arruda (1990)), and are usually referred to as indirect methods.

In the case of industrial rotor systems, however, it is extremelly awkward, when feasible, to perform a thorough modal test and extract modal parameters. This is related to experimental difficulties in exciting and measuring the responses on a rotating structure as well as to modal parameter estimation problems due to the variation of the modal parameters with the rotating frequency and to the nonlinear behavior of bearings and seals. Hence, in the case of rotor systems, it is desirable to use model updating techniques that need only a few measured system responses, those

Manuscript received: July 1993. Associate Technical Editor: Agenor de Toledo Fleury

which can be easily measured. Using dynamic responses in the updating procedure is usually referred to as the direct approach (Natke, 1986). When using direct inverse sensitivity rotor Finite Elements (FE) model updating methods, unbalance responses and Frequency Response Functions (FRFs) are examples of experimental dynamic response functions which can be used. In previous papers (Arruda, 1987 and 1989), one of the authors proposed the FE model updating of rotors based on the unbalance response curve fit. The method was shown to work with simulated data, but the problem with its implementation is the experimental difficulty in measuring steady-state unbalance responses near the rotor critical speeds.

When updating a FE model, one has to choose the theoretical parameters to be corrected. They are either known a priori or have to be "localized". The localization problem is usually based on a sensitivity analysis (Blakely and Walton, 1984). In the case of rotor-bearing systems, the rotor is usually well modeled, while the bearing and seal stiffness and damping coefficients are quite poorly predicted theoretically. Hence, the parameters which must be estimated when updating the model are known a priori. In this paper, the possibility of updating FE rotor models by the estimation of bearing stiffness and damping coefficients using measured FRFs is investigated. In practical applications, the FRFs may be obtained by exciting a few accessible shaft locations with an impact hammer. The FRF curve fit is implemented using a nonlinear parameter estimation method which, in its most general form, is a Regressive Maximum a Priori method and, in its simplest form, when there is no information about either the statistics of the estimated parameters or the statistics of the experimental data, is the Ordinary Nonlinear Least Squares method. The importance of using the magnitudes of the FRFs in logarithmic scale is pointed out and it is shown that this improves the smoothness of the objective function, which becomes similar in shape to the complement of the correlation coefficient between theoretical and experimental FRFs as a function of the parameters.

Two methods for calculating the sensitivity matrix- finite differences and analytical formulation- are implemented and compared. The problems of identifiability and error estimates are adressed and the techniques used to reduce the computational efford are discussed. A numerical example consisting of a flexible rotor supported by two orthotropic bearings illustrates the use of the proposed methodology.

Nomenclature

$B(\omega)$ =dynamic stiffness matrix
C = viscous damping matrix
c_{yy}
c_{zz} = bearing linearized damping coefficients
$D(\Omega)$ =generalized damping matrix including gyroscopic effect
F = any dynamic response function, e.g., a FRF
F_t = predicted dynamic response function
F_{t_i} = element of vector F_t
F_x = measured dynamic response function
$\overline{F}_x$ = scaled measured function in maximum correlation method
G = coriolis matrix (gyroscopic effect)
$h^{(k)}$ = step taken in the search direction to minimize $J(p)$
$H(\omega)$ =frequency response matrix
$H_{ij}(\omega)$ =frequency response function (FRF)
H_R = real part of a FRF
H_I = imaginary part of a FRF
i = $\sqrt{-1}$
$\Im$ = imaginary part of the sensitivity
$J(p)$ = objective function of the parameters p
$J(\hat{p})$ = objective function for the estimated parameters $\hat{p}$
K = stiffness matrix
k_{yy}
k_{zz} = bearing linearized stiffness coefficients
M = mass matrix
n_e = number of elements of vector F_x
n_p = number of elements of vector p
p = vector whose elements are the parameters to estimate
$\hat{p}$ = estimate of the parameters p
p_0 = initial theoretical guess values for parameters p
p_k = model parameter, kth element of vector p
$\hat{p}^{(k)}$ = estimate of the parameters at the kth iteration step
$\Re$ = real part of the sensitivity
$S_{(k)}$ = sensitivity matrix at the kth iteration step
S_{ij} = element of the sensitivity matrix
W_F = weighting matrix for the experimental data
W_p = weighting matrix for the model parameters
$var[\hat{p}]$ =variance of the parameter estimates
β = scaling factor used in the maximum correlation method
γ = relative confidence in the theoretical model
δ_j = increment in the parameter values
Δp_j = increment in the parameter values for derivative computation
$\Delta p^{(k)}$ = search direction
ω = frequency in rad/s
Ω = rotating frequency in rad/s
σ^2 = variance

Model Updating Procedure

The estimation of model parameters that update a FE model is done by minimizing the difference between the predicted and the measured responses (outputs) or excitations (inputs). Depending on that the method may be classified as an "output error" or an "input error" method, respectively (Eykhoff, 1974). Frequency Response Functions (FRFs) are obtained by normalizing the system responses with respect to the excitation. As a consequence, estimating parameters from the FRFs characterizes an output error method. Output error methods are not biased by additive Gaussian noise but they are iterative and hence prone to convergence problems (Natke, 1986). Putting the experimentally obtained FRF magnitudes evaluated at different frequencies in a vector called F_x, and accordingly, the values predicted by the theoretical model with a set of parameter values, p, in F_t and given an initial set of guess values for the parameters, p_0, the model parameters are obtained by minimizing the objective function (Beck and Arnold (1977), Blakely and Walton (1984), and Natke (1988)):

$$J_{LS}(p) = [F_x - F_t(p)]^T W_F [F_x - F_t(p)] + \gamma [p - p_0]^T W_P [p - p_0] \qquad (1)$$

In this expression, W_F is the weighting matrix of the experimental data, expressing the relative confidence (statistically the inverse of the covariance matrix) in the experimental FRFs. W_P is a weighting matrix expressing the relative confidence in the theoretical model parameters (of which the statistics is usually unknown). The scalar γ expresses a global relative confidence between the theoretical and the experimental models. If $\gamma = 0$ and W_F is the inverse of the covariance matrix of the experimental data, the solution leads to the Maximum Likelyhood (ML) estimator. If $\gamma = 1$, W_F is the inverse of the covariance matrix of the experimental data and W_P is the inverse of the covariance matrix of the theoretical parameters, the solution is the Maximum a Posteriori (MAP) estimator (Beck and Arnold, 1977). Finally, if $\gamma \to \infty$ the minimization leads to the trivial solution $p = p_0$, and the experimental data is not taken into account.

The weighting matrices may be chosen empirically in practical situations, giving the dynamicist the possibility of introducing any subjective a priori knowledge about the problem. When the statistics of the data and model parameters are used, the approach is sometimes referred to as Bayesian (Natke, 1988). It is interesting to note at this point that the Kalman Filter formulation does not apply to the model updating problem as stated here because the model parameters are not time-varying by hypothesis, i.e., the FE model parameters are supposed to be constant in time. When $F_t(p)$ is a nonlinear function of the parameters p, the MAP estimator $\hat{p}$, which minimizes $J_{LS}(p)$ of Eq. 1, may be shown to be derived from an iterative process where a new set of parameters $\hat{p}^{(k+1)}$ is obtained from the previous values $\hat{p}^{(k)}$ by the equations:

$$\hat{p}^{(k+1)} = \hat{p}^{(k)} + h^{(k)} \Delta p^{(k)} \qquad (2)$$

$$\Delta p^{(k)} = (W_P + S_{(k)}^T W_F S_{(k)})^{-1} \left[W_P (p_0 - \hat{p}^{(k)}) + S_{(k)}^T W_F (F_x - F_t(\hat{p}^{(k)})) \right] \qquad (3)$$

where $\Delta p^{(k)}$ is the search direction and $h^{(k)}$ is the step taken in the search direction, which is determined via a one-dimensional search algorithm. $S_{(k)}$ is the sensitivity matrix at iterative step k, given by the Jacobian of function F_t with respect to the parameters p, i.e.:

$$S_{(k)} = \frac{\partial}{\partial p} F_t(p) \Big|_{p = \hat{p}^{(k)}} \qquad (4)$$

Introducing the one-dimensional search is a modification of the Gauss's algorithm. Different one-dimensional search methods may be used. In this paper the Box-Kanemasu modification as described by Beck and Arnold (1977) was used. Algorithms for the solution of the nonlinear least squares problem are well-known and will not be detailed in this paper. The algorithm may be made recursive when the measurements are made sequentially. In this case the parameter estimation algorithm may be seen as a filter instead of a curve fit. When the experimental data are FRFs, vectors with complex values at different frequencies in a given frequency range are usually obtained simultaneously using Discrete Fourier Series methods. If all the experimental data is available at once there is no need for sequential estimation algorithms. The so-called direct method (Beck and Arnold, 1977) can help saving memory space if the FRFs are measured sequentially but no intermediate estimation of the parameters is needed, i.e., only the final update after all the experimental data has been used is sought. In the numerical example treated in this paper 4 FRFs were used in each case and the direct sequential method was used. The computation of the sensitivity matrix is discussed in another section of this paper.

Objective Function

In the case of rotor FE model updating by the estimation of bearing stiffness and damping coefficients, there is usually a very low confidence in the initial guess values (theoretical predictions) and it is convenient to make $\gamma = 0$ in Eq. 1. It can be shown that the discretization of the FRF curve in the case of lightly-damped structures may lead to several problems of convergence because of the existence of many local minima in the objective function.

In some of the cases simulated with the numerical example described hereafter, there was no convergence of the iterative nonlinear search. It was observed that when convergence problems occurred the first iteration step generally decreased the square error objective function but it decreased the correlation coefficient between the theoretical and experimental FRFs. A maximum correlation iterative search was sought to improve the convergence in those case. A formulation for parameter estimation by the maximization of the correlation coefficient was presented by Arruda (1992), where it is shown that the same convergence improvement can be achieved using the logarithm of the FRF magnitudes with the nonlinear least-squares estimation. The objective function for the maximum correlation technique is given by:

$$J_{MC}(p) = 1 - \frac{\left[F_x^T F_t(p)\right]^2}{\|F_x\|^2 \|F_t(p)\|^2} \tag{5}$$

where $\|F_t(p)\|$ denotes the Euclidean norm of vector $F_t(p)$. Figure 1 shows the plots of scaled cross-sections of J_{LS} and $J_{MC}(p)$ for F in both linear and logarithmic scales. In this case F is the magnitude of one of the rotor system example FRFs and p is one of the bearing stiffness coefficients of which p_0 is the exact value. As it can be observed in Fig. 1 the shape of $J_{LS}(p)$ and $J_{MC}(p)$ is approximately the same in the neighborhood of the solution p_0 when a logarithmic scale F is used. Arruda (1992) showed that the relation between $J_{LS}(p)$ and $J_{MC}(p)$ was:

$$J_{MC} = \frac{J_{LS}}{\|F_x\|^2} \tag{6}$$

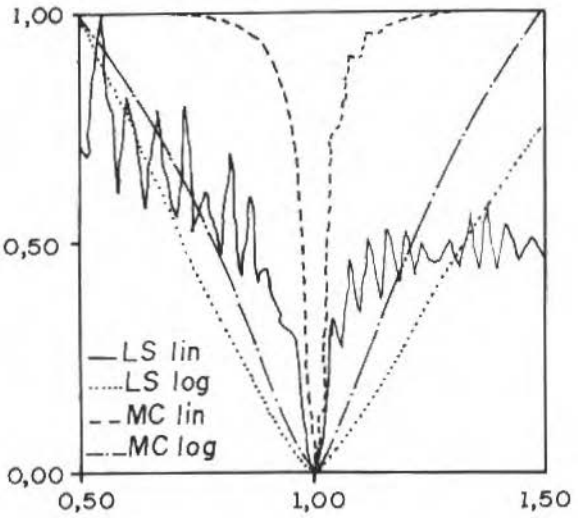

Fig. 1 Cross sections of the different scaled objective functions in the neighborhood of the solution p_0

In the implemented computer code it is possible to choose among the four different objective functions. It was observed that it is usually more efficient to start searching for the maximum correlation with the FRFs in logarithmic scale and, after a high level of correlation is attained, e.g., 0.95, switch to the least squares objective function with the FRFs still in logarithmic scale. The refinement of the solution may be otained taking the FRF in linear scale in the few last iterative steps. Arruda (1992) showed that, in order to minimize $J_{MC}(p)$ it is necessary to introduce another iterative scheme besides the nonlinear least-squares loop. A scaled experimental FRF is introduced:

$$\bar{F}_x = \beta F_x \tag{7}$$

where,

$$\beta = \frac{\|F_t\|^2 + 2(\hat{p}^{(k+1)} - \hat{p}^{(k)})^T S_{(k)}^T F_t + (\hat{p}^{(k+1)} - \hat{p}^{(k)})^T S_{(k)}^T S_{(k)} (\hat{p}^{(k+1)} - \hat{p}^{(k)})}{F_x^T F_t + (\hat{p}^{(k+1)} - \hat{p}^{(k)}) S_{(k)}^T F_x} \tag{8}$$

Initially, $\beta = 1$ and the least-squares search direction is calculated from Eq. 3. The solution $\Delta \hat{p}^{(k)}$ is then put into Eq. 8 to calculate β which is used to scale F_x in Eq. 7. With the scaled curve $\bar{F}_x$, the search direction is recalculated from Eq. 3. This procedure is repeated until convergence of the values of the search direction $\Delta \hat{p}^{(k)}$. In the one-dimensional search (Box-Kanemasu modification) performed with the calculated search direction the objective function is also given by Eq. 5.

Sensitivity Matrix Calculation

Many recent papers treat the problem of calculating the sensitivity matrix S of Eq. 4 (Adelman and Haftka (1986), Sharp and Brooks (1988), Sutter et al (1986), and Vanhoacker (1989)). In this section the basic formulation of the derivative of the FRF with respect to the structural parameters will be reviewed. Because of the iterative character of the updating method it is interesting to take the simple first order finite differences approximation for the derivative, which has the lowest computational cost:

$$S_{ij} = \frac{\partial F_{t_i}}{\partial p_j} \approx \frac{F_{t_i}(p_j + \Delta p_j) - F_{t_i}(p_j)}{\Delta p_j} \tag{9}$$

The choice of Δp_j may be critical. It should be as small as possible but there are limitations due to numerical truncation. The Brown and Dennis rule (Beck and Arnold, 1977) was used here:

$$\Delta p_j = \min\{\| F_t(p_j) \|, \delta_j\} \tag{10}$$

where,

$$\delta_j = \begin{cases} 10^{-9} & \text{if} \quad |p_j| < 10^{-6} \\ 10^{-3}|p_j| & \text{if} \quad |p_j| \geq 10^{-6} \end{cases} \tag{11}$$

The Frequency Response Matrix of a rotor system may be expressed as:

$$H(\omega) = B(\omega)^{-1} \tag{12}$$

with,

$$B(\omega) = K - \omega^2 M + i\omega D(\Omega) \tag{13}$$

$$D(\Omega) = C + \Omega G \tag{14}$$

where K, M and C are the stiffness, mass, and viscous damping matrices respectively, G is the Coriolis matrix, and Ω is the rotation speed. It is possible to calculate the sensitivity of any FRF with respect to a parameter p_k using the known property for the inverse square matrix derivative (Martinez, 1981):

$$\frac{\partial B^{-1}}{\partial p} = -B^{-1}\frac{\partial B}{\partial p}B^{-1} \tag{15}$$

so that,

$$\frac{\partial}{\partial p_k}B(\omega) = \frac{\partial K}{\partial p_k} - \omega^2\frac{\partial M}{\partial p_k} + i\omega\left(\frac{\partial C}{\partial p_k} + \Omega\frac{\partial G}{\partial p_k}\right) \tag{16}$$

For a given FRF $H_{ij}(\omega)$, the sensitivity matrix elements are given by:

$$S_{lk} = \frac{\partial}{\partial p_k} H_{ij}(\omega_l) \quad l = 1, \ldots, n_e; k = 1, \ldots, n_p \tag{17}$$

The derivatives that appear in Eq. 16 must be obtained analytically, which is usually straighforward. In the case where the parameters are the bearing stiffness and damping coefficients, it is sufficient to replace the parameter value by 1 and watch for the elements of the matrices K and C that vary. The derivative of the elements that do not vary is zero and the derivative of the elements that vary is equal to the new value of the element. The closed-form solution of the sensitivities has a higher computational cost because it is necessary to invert matrix $B(\omega)$, or, numerically, solve a linear system of algebraic equations for each frequency ω at which the FRF has been measured (usually hundreds or thousands of frequency lines). The finite differences approximation gives fairly precise results when compared to the exact, closed-form solution. In the numerical example treated in this paper the sensitivities have been calculated by finite differences and the receptance FRFs (displacement/force) were taken in dB scale with 1 m/N reference. It can be shown that, for:

$$H_{ij}(\omega) = H_R + iH_I \tag{18}$$

$$\frac{\partial}{\partial p_k} H_{ij}(\omega) = \Re + i\Im \tag{19}$$

the sensitivity of the absolute value in dB scale is given by:

$$\frac{\partial}{\partial p_k}(20\log|H_{ij}(\omega)|) = 8{,}6859\frac{H_R\Re + H_I\Im}{H_R^2 + H_I^2} \tag{20}$$

In the investigated numerical examples it was not possible to depict in graphical plots of the sensitivity curves (the columns of the sensitivity matrix) any difference between the sensitivities obtained analytically and by finite differences.

Estimation Errors

The variances of the generalized nonlinear least-squares estimates of the parameters, $\hat{p}$, for additive Gaussian noise may be shown to be approximated by (Eykhoff, 1974):

$$\mathrm{var}[\hat{p}] \approx [S^T S]^{-1}\sigma^2 \tag{21}$$

In the above equation σ^2 is the variance of the noise and can be estimated with:

$$\sigma^2 \approx \frac{J(\hat{p})}{n_e - n_p} \tag{22}$$

where n_e is the number of elements of vector F_x and n_p is the number of elements of vector p. For $(n_e - n_p) \to \infty$ the probability distribution of $\hat{p}$ tends to be Gaussian and the normal confidence intervals for the estimated parameters may be determined (Beck and Arnold, 1977).

Uniqueness and Identifiability

A question that is always present in model updating and parameter estimation problems is whether the models are unique. Given a set of modal parameters (natural frequencies, mode shapes and modal dampings), it is only possible to define uniquely the structure stiffness, mass and damping matrices if the model is complete, i.e., if all the modes are known at every degree-of-freedom. This is practically impossible because real structures are continuous and it is too costly to experimentally identify high order modes (Berman, 1988). So, it is meaningless to try to identify the model of the structure, but, hopefully, it is possible to identify a model consistent with the a priori knowledge about the structure and with the measured data. In the case where only a small set of parameters of the theoretical model is estimated from experimental data, this problem may be formulated as an identifiability problem. The question is whether the parameters may be independently estimated from the available data. There exist different identifiability criteria (Beck and Arnold, 1977). For the specific case of nonlinear least-squares estimation, one of them consists of looking for the number of nonnegligible singular values of the sensitivity matrix, which are related to the linear independence of the columns of this matrix. It may be proved that if the columns of the sensitivity matrix for a given group of parameters are linearly dependent, then that group of parameters are linearly dependent, then that group of parameters cannot be estimated uniquely from the available data (Beck and Arnold, 1977), i.e., the rank of the sensitivity matrix is equal to the number of parameters which can be estimated independently.

Computer Code

The proposed method was implemented in a 16 bit personnal computer. A Finite Element code for rotor systems developed by Berthier, Ferraris and Lalanne (1983) was modified to include the model updating procedure. The calculation of FRFs (Ω constant, ω varying) by inversion of the dynamic matrix $B(\omega)$ with the equilibrium equations reduced using the first eigen-modes of the nonrotating system was implemented. Throughout the iterative process and when calculating the sensitivities by finite differences, the modal data base of the nonrotating system is kept constant and only the finite elements which involve the parameters which are being estimated are re-calculated. When convergence is attained the modal data base is updated before the final results are given. The implemented code is highly interactive so that it is possible, at each iteration step, to change the FRF being curve-fitted, the frequency range and the parameters to be estimated. This allows the use of any nonalgorithmic rule due to the knowledge and experience of the dynamiscist about rotordynamic structural problems.

Numerical Example

A numerical example is presented in this section to illustrate the proposed rotor model updating method. Fig. 2 shows the orthotropic flexible rotor system consisting of a single hollow spool supported by two bearings, which was reported in Chen et al. (1987). The FE nodes, referred to as stations, are depicted in the figure. The bearings are considered to be orthotropic with two unknown stiffness coefficients and two unknown damping coefficients in each bearing. The rotating speed is constant at 5000 rpm. The geometry and material properties of the rotor-bearing system are given in Tables 1, 2 and 3.

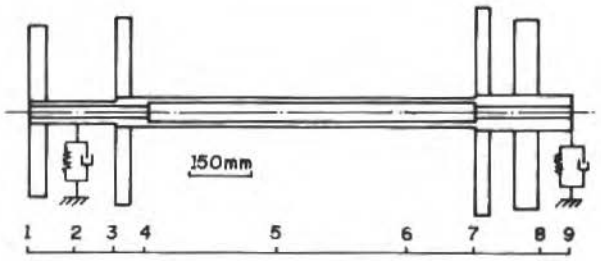

Fig. 2 Scheme of the rotor-bearing system numerical example

Table 1 Rotor-bearing system example - shaft data

Station number	Axial location (mm)	Inner radius (mm)	Outer radius (mm)
1	0000.0	12.70	25.40
2	0088.9	12.70	25.40
3	0203.2	12.70	25.40
4	0274.3	12.70	34.29
5	0591.8	20.32	34.29
6	0896.6	20.32	34.29
7	1049.0	20.32	34.29
8	1193.8	15.24	38.10
9	1270.0	15.24	38.10

Table 2 Rotor-bearign system example - disc data

Station number	Mass (kg)	Diametral inertia ($kg.m^2$)	Polar inertia ($kg.m^2$)
1	11.38	0.0982	0.1953
4	07.88	0.0835	0.1671
7	07.70	0.0880	0.1761
8	21.71	0.2224	0.4448

Table 3 Rotor-bearing system example - bearing data

Bearing	$k_{zz} \times 10^6$ (N/m)	$k_{yy} \times 10^6$ (N/m)	$c_{zz} \times 10^6$ (N/m)	$c_{yy} \times 10^6$ (N/m)
B1	.350	.438	.350	.440
B2	.525	.613	.200	.610

The influence of the excitation and measurement point locations was investigated and results are summarized in Tables 4 and 5. Two response measurement locations were used in each case and at

Table 4 Highest among the bearing parameter estimation errors for different excitation point locations; response measured at stations 2 and 9.

Maximum relative estimation error (%)	Excitation point location								
	1	2	3	4	5	6	7	8	9
station 2 bearing	0.03	1.60	0.45	0.44	0.44	0.44	0.09	0.36	549.1
station 9 bearing	0.92	256.9	285.6	0.66	0.61	0.61	0.02	0.02	1.22

Table 5 Highest among the bearing parameter estimation errors for different response measurement locations (one of the measurement stations is kept fixed while the other is moved; excitation is fixed at station 6).

Maximum relative estimation error (%)	Measurement pont locations at stations 9 and:								
	1	2	3	4	5	6	7	8	9
station 2 bearing	0.23	0.44	0.14	0.26	12.32	33.03	36.5	84.86	-
station 9 bearing	5.00	0.61	0.15	0.09	2.16	3.26	1.91	1.62	-

Maximum relative estimation error (%)	Measurement pont locations at stations 2 and:								
	1	2	3	4	5	6	7	8	9
station 2 bearing	5.90	-	6.89	34.29	0.50	13.50	0.17	3.66	0.44
station 9 bearing	81.11	-	461.3	242.1	1.27	35.15	0.03	27.55	0.61

each location the FRFs on both directions, x and z, were simulated. The 4 FRFs were used sequentially to find the search direction of Eq. 3 at each iteration step. The FRFs were simulated with a frequency resolution of 11.72 cpm in the frequency range 0 - 3000 cpm (0 - 50 Hz). Random Gaussian error of variance equal to 0.5% of the FRFs rms amplitude was added to the FRFs to simulate measurement noise.

In rotordynamic applications, the usual measurement point locations are the bearings, where noncontacting sensors are frequently installed. From the simulated results they have proved to be convenient for the estimation of the bearing parameters. It can be seen from Table 4 that the rotor mid-

span is a good location for the excitation if the two bearings are to be simultaneously identified. If only one bearings is to be identified at a time, the excitation and the measurement point locations may be situated at the bearing itself.

The logarithm of the quotient between the biggest and the smallest singular values of the sensitivity matrix was chosen as an index to quantify the identifiability. Fig. 3 shows the good correlation that

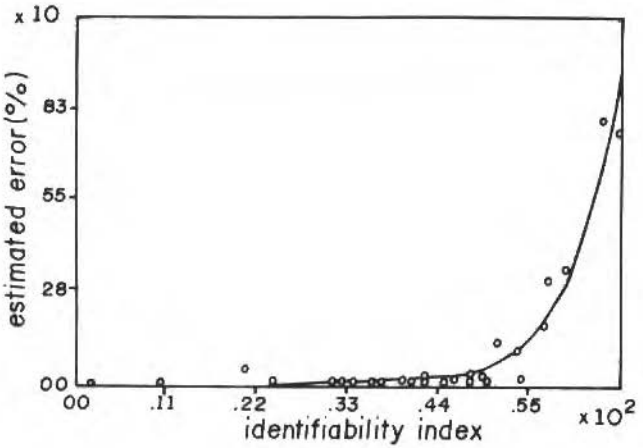

Fig. 3 Correlation between the identifiability index and the maximum estimation error

exists between this index and the estimation errors. Fig. 4 shows the percentage of successful trials

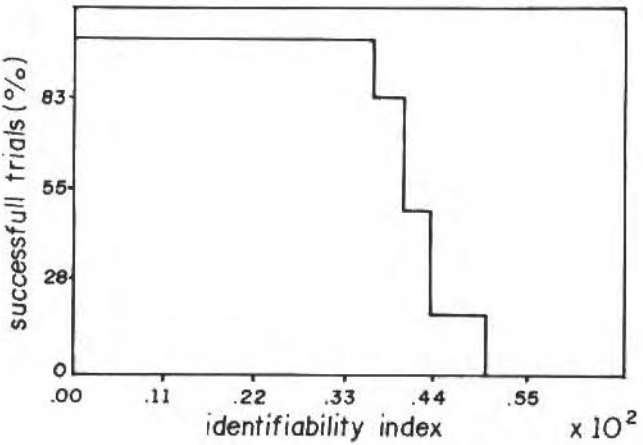

Fig. 4 Percentage of successful trials as a function of the identifiability index

as a function of the identifiability index. In this context, a successful trial means that the parameters were estimated with an error of the same magnitude as the simulated measurement noise.

The additive Gaussian noise level influence is shown in Fig. 5. It can be seen that the sensitivity with respect to the measurement noise is small for noise levels under 4% and acceptable for noise levels up to 10%.

The amount of measured data did not show a strong influence on the precision of the estimates. Table 6 shows some illustrative results relating the number of frequency lines of the FRF used to

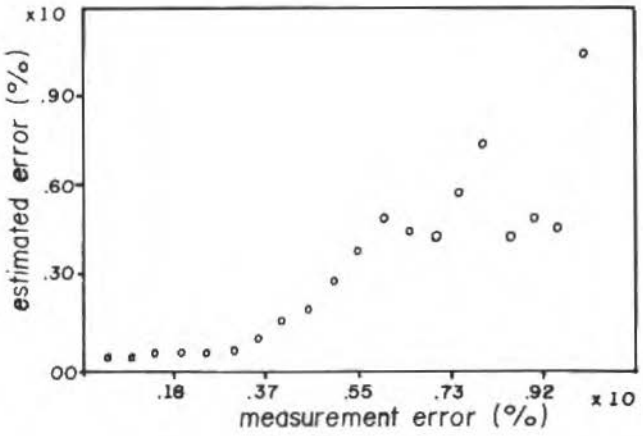

Fig. 5 Influence of the simulated measurement noise on the parameter estimation errors

Table 6 Influence of the number of frequency lines

N. of frequency lines	60	120	256	500	1000	2000
Max. estim. error (%)	1.86	0.70	1.14	0.61	0.94	0.97

update the model and the maximum error found in the estimated bearing parameters. These results were obtained with a 2% additive noise level. For higher noise levels the averaging effect of taking a greater number of frequency lines would have had a more significant effect.

Conclusions

The proposed FE model updating method applies whenever a small number of theoretical parameters selected a priori need to be corrected based on experimental data. Depending on the extent of the knowledge of the statistics of the problem the method can be classified as Ordinary Least Squares, Maximum Likelyhood or Maximum a Posteriori. Its implementation can be recursive or not. The method is versatile and any experimentally obtained dynamic response which can be predicted with the FE model can be used. As the dynamic responses are nonlinear in the structural parameters, a modified Gauss's nonlinear iterative approach is used.

The application of the method to the Finite Element model updating of rotor-bearing systems using measured Frequency Response Functions was presented. The method was used to estimate bearing stiffness and damping coefficients of a rotor-bearing numerical example.

Two methods for the calculation of the sensitivity matrix - closed form and finite differences - were compared and the latter was preferred because it is sufficiently accurate and has a much lower computational cost than the former.

With respect to the influence of the excitation and measurement point locations, it was shown that for two-bearings rotors the bearing locations are adequate for measuring the responses while the shaft mid span is a good location for the excitation. In practical cases a previous numerical simulation can be done to indicate the best among the possible excitation and response point locations.

The identifiability problem was investigated. It was shown that an identifiability index can be used to indicate if a given set of parameters can be estimated from the available measured data. This index is the logarithm of the quotient between the highest and the lowest singular values of the sensitivity matrix. In the numerical example, a good correlation was found between this index and the estimation errors and convergence of the model updating method. The order of magnitude of the parameter estimation errors was shown to be predictable with the proposed method.

References

Adelman, H.M. and Haftka, R.T. (1986) "Sensitivity Analysis of Discrete Structural Systems", AIAA Journal, 24(5): 823-832.

Arruda, J.R.F. (1987) "Rotor Finite Element Model Adjusting" Proc. of the 9th Brazilian Congress of Mechanical Engineering, Florianópolis, Brazil: 741-744.

Arruda, J.R.F. (1989) "Rotor Model Adjusting by Unbalance Response Curve-fitting", Proc. of the 7th Int. Modal Analysis Conference, Las Vegas, USA: 479-484.

Arruda, J.R.F. (1992) "Objective Functions for the Curve-Fit of Frequency Response Functions", AIAA Journal, 30(3): 855-857.

Beck, J.V. and Arnold, K.J. (1977) "Parameters Estimation in Engineering and Science", John Wiley, New York.

Berman, A. (1988) "Nonunique Structural System Identification", Proc. of the 6th Int. Modal Analysis Conference, Orlando, USA: 355-358.

Berthier, P., Ferraris, G. and Lalanne, M. (1983) "Prediction of Critical Speeds, Unbalance and Nonsynchronous Forced Response of Rotors", The Shock and Vibration Bulletin, 53: 103-111.

Blakely, K.D. and Walton, W.B. (1984) "Selection of Measurement and Parameter Uncertainties for FE Model Revision", Proc. of the 2nd Int. Modal Analysis Conference, Orlando, USA: 82-88.

Carneiro, S.H.S. and Arruda, J.R.F. (1990) "Updating Mechanical Joint Properties Based on Experimentally Determined Modal Parameters", Proc. of the 8th Int. Modal Analysis Conference, Kissimmee, USA: 1169-1175.

Chen, W.J. et al. (1987) "Bearing Parameter Identification of Rotor-Bearing Systems Using Nonlinear Programming Techniques", Mechanical and Aerospace Engineering Department Publication, Arizona State University, Tempe, Arizona, USA.

Eykhoff, P. (1974) "System Identification", John Wiley, London.

Imregun, M. and Visser, W.J. (1991) "A Review of Model Updating Techniques", The Shock and Vibration Digest, 23(1): 9-20.

Lallement, G. and Zhang, Q. (1988) "Inverse sensitivity based on the eigensolutions: analysis of some difficulties encountered in the problem of parameter correction of finite element models", Proc. of the 13th Int. Sem. on Modal Analysis, Leuven, Belgium: 19-23.

Martinez, D.R. (1981) "Parameter Estimation in Structural Dynamics Models", Sandia National Laboratories Report SAND80-0135, Albuquerque, USA.

Natke, H.G. (1986) "Improvement of Analytical Models With Input/Output Measurements Contra Experimental Modal Analysis", Proc. of the 4th Int. Modal Analysis Conference, Los Angeles, USA: 409-413.

Natke, H.G. (1988) "Updating Computational Models in the Frequency Domain Based on Measured Data: A Survey", Probabilistic Engineering Mechanics, 3(1): 28-35.

Sharp, R.S. and Brooks, P.C. (1988) "Sensitivities of Frequency Response Functions of Linear Dynamic Systems to Variations in Design Parameter Values", Journal of Sound and Vibration, 126(1): 167-172.

Sutter, T.R. et al. (1988) "Comparison of Several Methods for Calculating Vibration Mode Shape Derivatives", AIAA Journal, 26(12): 1506-1511.

Vanhoacker, P. (1989) "Sensitivity Analysis of Mechanical Structures Based on Experimentally Determined Modal Parameters", Proc. of the 7th Int. Modal Analysis Conference, Las Vegas, USA: 534-541.

RBCM - J. of the Braz. Soc. Mechanical Sciences
Vol. XV - nº 2 - 1993 - pp. 150-164

ISSN 0100-7386
Printed in Brazil

On Geometric Nonlinear FE Solution of Unidimensional Structure Dynamics

C. A. Almeida
J.A. Pires Alves
Department of Mechanical Engineering
Pontifícia Universidade Católica do Rio de Janeiro
Gávea - Rio de Janeiro - Brazil

Abstract

A numerical procedure for geometric nonlinear analysis of framed structures in presented. The finite element model employs 3-D linear to cubically varying space displacements and is capable of transmitting stress only in the direction normal to the cross-section. It is assumed that this normal stress is constant over the cross-sectional area, and that the area itself remains constant, allowing the element for large displacement analysis but under small strain condition. Two algorithms for the automatic incremental solution of the resulting nonlinear equilibrium equations in static analysis are accessed. These include the displacement control technique and the minimization of residual displacements, which allow to calculate the path response of general truss structures, even of those that exhibit unstable configurations. The formulation has been implemented and the results of various examples illustrate the element effectiveness in both static and dynamic analyses.
Keywords: Geometric Nonlinear Analysis, Automatic Incremental Solution, Displacement Control, Minimization of residual displacements.

Resumo

Um procedimento numérico para a análise não linear geométrica de estruturas entreliçadas é apresentado. O modelo de elementos finitos utiliza deslocamentos tri-dimensionais com interpolação espacial de ordem linear a cúbica e é capaz de transmitir tensões apenas na direção normal de seção transversal. Considera-se esta tensão normal constante sobre a área da seção reta que permanece constante, permitindo ao elemento representar grandes deslocamentos mas sob a condição de pequenas deformações. Dois algorítmos para a solução incremental automática das equações de equilíbrio não lineares são apresentados. Estes incluem as técnicas de incremento controlado do deslocamento e de minimização dos deslocamentos residuais que permitem obter a resposta de estruturas de barras em geral, mesmo apresentando configurações instáveis. A formulação foi implementada e os resultados com vários exemplos ilustram a efetividade do elemento em análises estáticas e dinâmicas.
Palavras-chave: Análise Não Linear Geométrica, Solução Automática Incremental, Controle do Deslocamento, Minimização dos Deslocamentos Residuais

Introduction

The important requirements for a reliable nonlinear finite element analysis of structures are, in general, the use of accurate finite element model for geometry and kinematics representation and the use of an efficient procedure for the solution of the incremental equations of motion. For a given solution accuracy, the procedures for assemblage and solution of the equilibrium equations are efficient when de computer costs are low and the numerical solution is obtained in a reliable manner with a minimum amount of analysis effort.

The need of nonlinear analysis of structures in recent years has significantly increased due to the adoption of limit static and optimum design concepts, which have resulted in the use of slender members in framed structures. Since the behavior of these structures near to the limit (pre- and post-buckling) loads is complex, and difficult to predict accurately by observation, much emphasis is currently being placed on the development of more general and automatic solution schemes. Extensive research efforts have been devoted in the past decade, to the development of reliable and efficient numerical algorithms (Batoz and Dhat (1979); Ricks (1979); Ramm (1980); Crisfeld (1981); Yang and MacGuire (1985); Chan (1988)) that differ from the classical Newton-Raphson numeric scheme by the involvement with a large number of degrees-of-freedom. The standard approach relies on the fact that a nonlinear solution can be obtained by successive linearized results in an iterative process at a

Manuscript received: July 1993. Associate Technical Editor: Agenor de Toledo Fleury

constant load. This condition results in failure of convergence in the analysis of structures displaying limit points in the force-displacement relationship (snap through/back behaviors) because the tangent stiffness matrix is ill-conditioned or simply because the load level is beyond the solution path. A comparative study on the advantages and disadvantages in the use of the various solution procedures is reported in Bath and Ciments (1980), Clark and Hancock (1988) and Pires Alves (1992).

The objectives of this paper is to present a methodology that is simple and effective and predicts accurately the significant deformations in general linear and geometric nonlinear analysis of framed structures. The element is a two to four-node isoparametric displacement based finite element with 3-field displacements to represent constant uniaxial stress states normal to the cross-section. Based on the discussions and practical applications reported in Pires Alves (1992), concerning several numerical solution schemes that using surface constraint equations are employed to solve finite element ill-conditioned equilibrium equations, two methods are presented in this work: a) the constant increment displacement and b) the minimum residual displacement. Both methods employ the displacement as a control parameter. However, in the former, the increment of a sole displacement component is used in the marching process to obtain the solution corresponding loading and displacement components that satisfies equilibrium while in the second approach the objective is to minimize (or to eliminate) the displacement vector associated to the unbalance load in the iterative process.

In the next section of this paper we briefly review the formulation of an unidimensional element with emphasis on the geometric nonlinearities incorporated in the finite element equilibrium equations to be solved for. Methods for the numerical solution are presented afterwards. The element has been implemented in the computer and following, we present the analysis results of some problems that demonstrate the validity of the methodology in general nonlinear analysis.

The Truss Element Formulation

The truss element is a structural model that transmits axial forces only. Normal stresses are uniform over the cross-sectional area which remains constant during deformation. As a consequence, although the element can undergo to large displacements, only the small strain condition is allowed in the element model.

Considering a truss with arbitrary orientation in space and described by two to four nodes, as shown in Fig. 1, the global coordinates of the element at times 0 and t are respectively

$$ {}^{0}x_i(r) = \sum_{k=1}^{N} h_k(r)\, {}^{0}x_i^k \quad \text{and} \quad {}^{t}x_i(r) = \sum_{k=1}^{N} h_k(r)\, {}^{t}x_i^k \quad , \quad i = 1,2,3 \tag{1} $$

In Eq. (1) ${}^{0}x_i^k$ and ${}^{t}x_i^k$ are the nodal point global coordinates at times 0 and t respectively, $h_k(r)$ are the Lagrangian interpolation functions defined in Fig. 1, N is the number of element nodes and r is the element local coordinate. Using equation (1) it follows that

$$ {}^{t}u_i(r) = {}^{t}x_i(r) - {}^{0}x_i(r) = \sum_{k=1}^{N} h_k(r)\, {}^{t}u_i^k \tag{2} $$

and

$$ u_i(r) = \sum_{k=1}^{N} h_k(r)\, u_i^k \tag{3} $$

are the total displacement field and the increment displacement field, at time t, respectively, while ${}^{t}u_i^k$ and u_i^k are these quantities at the element nodes. Thus, with the aid of the following definitions

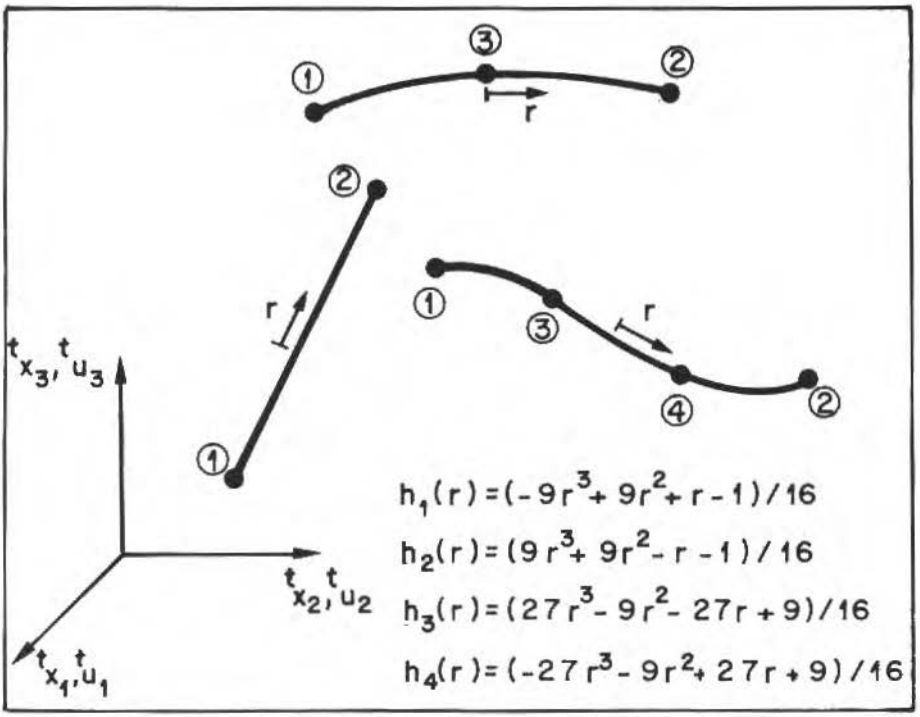

Fig. 1 The isoparametric truss element

$$^0\hat{x}^T = \left[{}^0x_1^1\ {}^0x_2^1\ {}^0x_3^1\ \ldots\ {}^0x_1^N\ {}^0x_2^N\ {}^0x_3^N\right] \tag{4}$$

$$^t\hat{u}^T = \left[{}^tu_1^1\ {}^tu_2^1\ {}^tu_3^1\ \ldots\ {}^tu_1^N\ {}^tu_2^N\ {}^tu_3^N\right] \tag{5}$$

$$\hat{u} = \left[u_1^1\ u_2^1\ u_3^1\ \ldots\ u_1^N\ u_2^N\ u_3^N\right] \tag{6}$$

$$H(r) = [h_1 I\ h_2 I\ \ldots\ h_N I] \tag{7}$$

equations (1) to (3) can be rewritten in the matrix form

$$^0x = H(r)\,{}^0\hat{x};\quad {}^tu = H(r)\,{}^t\hat{u} \quad \text{and} \quad u = H(r)\,\hat{u} \tag{8}$$

Since the only stress component considered is normal to the cross-section area we have, for the corresponding local element longitudinal strain, in the Total Lagrangian formulation (Bathe (1987)),

$$^0\varepsilon 11 = {}^0e 11 + {}^0\eta 11 \tag{9}$$

where the linear component is expressed by

$$ {}_0^{e}11 = \frac{\partial u_1}{\partial {}^0x_1} + \frac{1}{2}\left[\frac{\partial {}^t u_1}{\partial {}^0x_1}\frac{\partial u_1}{\partial {}^0x_1} + \frac{\partial {}^t u_2}{\partial {}^0x_1}\frac{\partial u_2}{\partial {}^0x_1} + \frac{\partial {}^t u_3}{\partial {}^0x_1}\frac{\partial u_3}{\partial {}^0x_1}\right] \tag{10} $$

and the nonlinear term is

$$ {}_0^{\eta}11 = \frac{1}{2}\left[\left(\frac{\partial u_1}{\partial {}^0x_1}\right)^2 + \left(\frac{\partial u_2}{\partial {}^0x_1}\right)^2 + \left(\frac{\partial u_3}{\partial {}^0x_1}\right)^2\right] \tag{11} $$

both defined with respect to the coordinate system attached to the element body at time 0. Plugging in equations (8) into the above results in the strain-displacement transformation matrices; as an example, for a straight two-noded element, with length L and space angles α_1, α_2, α_3, these matrices result in

$$ {}_0^{t}B_L = (1/L)\,[-\cos\alpha_1 \quad -\cos\alpha_2 \quad -\cos\alpha_3 \quad \cos\alpha_1 \quad \cos\alpha_2 \quad \cos\alpha_3] \tag{12} $$

and

$$ {}_0^{t}B_{NL} = (1/2L^2)\begin{bmatrix} 1 & 0 & 0 & -1 & 0 & 0 \\ & 1 & 0 & 0 & -1 & 0 \\ & & 1 & 0 & 0 & -1 \\ & & & 1 & 0 & 0 \\ & & & & 1 & 0 \\ & & & & & 1 \end{bmatrix} \tag{13} $$

In static analysis, considering the linearized equation of motion with incremental decompositions obtained from the principle of virtual displacements, the discretizations in equation (8) yield to the matrix form equilibrium equation

$$ \left[\int_{{}^0V} {}_0^{t}B_L^T \; {}_0^{t}C \; {}_0^{t}B_L \; {}^0dV + \int_{{}^0V} {}_0^{t}B_{NL}^T \; {}_0^{t}S \; {}_0^{t}B_{NL} \; {}^0dV\right]\hat{u} = {}^{t+\Delta t}R - \int_{{}^0V} {}_0^{t}B_L^T \; {}_0^{t}\hat{s} \; {}^0dV \tag{14} $$

where the stress matrix ${}_0^{t}S$ and the vector ${}_0^{t}\hat{s}$ are simply the second Piola-Kirchhoff tensor with a sole non-zero ${}_0^{t}S_{11}$ component, ${}_0^{t}C$ is the linear constitutive matrix and ${}^{t+\Delta t}R$ is the equivalent applied external loading reduced to the nodes degrees-of-freedom at time $t + \Delta t$. These equations are the necessary ingredients for the assemblage of the total equilibrium system of equations. It should be pointed out that the element matrices are obtained in this formulation directly corresponding to the global displacement components. However, and alternative procedure is to use local displacements referred to the coordinate aligned with the element to obtain the element matrices and thus to use a transformation to the global coordinate system.

Numerical Solution Strategies

The essence of an automatic numerical solution is to seek the load-displacement relation such the structure is assumed subjected to a fixed direction varying load. Thus, considering the equilibrium condition in equation (14), at time $t + \Delta t$, the following iterative procedure can be derived from the Newton-Raphson iteration scheme,

$$ {}^{t}K^{(i-1)}\,\hat{u}^{(i)} = {}^{t+\Delta t}R - {}^{t+\Delta t}F^{(i-1)} \tag{15} $$

with

$$ {}^{t+\Delta t}R = ({}^{t+\Delta t}\lambda^{(i)} + \Delta\lambda^{(i)})\,R \tag{16} $$

where the structure displacement increment vector $\hat{u}^{(i)}$, at iteration (i), and the load parameter ${}^{t+\Delta t}\lambda$, at time $t + \Delta t$, are the problem state variables to be solved for. ${}^{t}K^{(i-1)}$ is the coeficient matrix, R is a vector direction of externally applied nodal point loads and ${}^{t+\Delta t}F^{(i-1)}$ is a vector of nodal point forces equivalent (in the virtual work sense) to the internal stresses. When iteraction is performed in the load-displacement space described in equations (15) and (16) the additional equation

$$ f(\Delta\lambda^{(i)}, \hat{u}^{(i)}) = 0 \tag{17} $$

is used to constraint the load step size.

Various constraint equations proposed in the literature for the function f are surveyed by Pires Alves (1992). From those, two numerical schemes were found suitable for general applications in structure analysis, namely, the constant increment displacement component method and the minimum residual displacement method. In the first, a method devised by Powell and Simons (1981), the load vector is modified at each step such the displacement increment is prescribed at a certain degree-of-freedom. During iteration, this displacement increment component is kept constant while the load increment parameter $\Delta\lambda^{(i)}$ is adjusted for equilibrium. From combining equations (15) and (16) the vector displacement increment, at iteration (i), can be decomposed as

$$ \hat{u}^{(i)} = \hat{u}_u^{(i)} + \Delta\lambda^{(i)}\,\hat{u}_r^{(i)} \tag{18} $$

where $\hat{u}_u^{(i)}$ and $\hat{u}_r^{(i)}$ are the unbalance and the residual displacement increments, respectively, obtained from the following systems of equations

$$ {}^{t}K^{(i-1)}\;\hat{u}_u^{(i)} = {}^{t+\Delta t}\lambda^{(i)}\;R - {}^{t+\Delta t}F^{(i-1)} \tag{19} $$

and

$$ {}^{t}K^{(i-1)}\;\hat{u}_r^{(i)} = R \tag{20} $$

For a specified displacement component increment m to remain constant (i.e. $u_{(m)}^{(i)} = 0$), we have

$$u_{(m)} = b^T \hat{u}^{(i)} = 0 \tag{21}$$

in which vector b contains zeroes except for unit at m-th component. Thus, equations (18) and (21) yields the load step constraint equation

$$f(\Delta\lambda^{(i)}) = u^{(i)}_{(m)} + \Delta\lambda^{(i)} u^{(i)}_{r(m)} = 0 \tag{22}$$

which gives

$$\Delta\lambda^{(i)} = -u^{(i)}_{u(m)} / u^{(i)}_{r(m)} \tag{23}$$

Since R is a constant vector, $u_{r(m)}$ is calculated onde during each step cycle - modified Newton-Raphson procedure - and softening or stiffening system behavior is represented by a negative or positive sign of $\Delta\lambda^{(i)}$, respectively. Also, the numerical procedure requires the displacement component ${}^t u^{(i)}_{(m)}$ being monotonically crescent in the solution load interval.

Considering a new step, the load parameter increment for the first iteration is obtained by simply imposing in equation (18) a prescribed value $\bar{u}_{(m)}$ for the m-th component of vector displacement increment with $u^{(i)}_{(m)} = 0$, and resulting in

$$\Delta\lambda^{(1)} = \bar{u}_{(m)} / u^{(1)}_{r(m)} \tag{24}$$

In the second method the constraint equation is obtained by imposing a minimum value for the norm of the increment displacement in each step cycle. In accordance with the iterative procedure objectives, the motivation for this criteria is to eliminate the increment displacement vector by imposing a minimum value of its Euclidian norm. This condition is expressed by the equation

$$\frac{d}{d^{t+\Delta t}\lambda^{(i)}} \left(\hat{u}^{(i)^T} . \hat{u}^{(i)} \right) = 0, \quad \text{for} \quad i > 1 \tag{25}$$

or, considering the increment displacement decomposition in equation (18), in the following vector form

$$\hat{u}_r^{(i)^T} . \left[\hat{u}_u^{(i)} + \Delta\lambda^{(i)} \hat{u}_r^{(i)} \right] = 0, \quad \text{for} \quad i > 1 \tag{26}$$

which gives

$$\Delta\lambda^{(i)} = -\left(\hat{u}_r^{(i)^T} . \hat{u}_u^{(i)} \right) / \left(\hat{u}_r^{(i)^T} . \hat{u}_r^{(i)} \right), \quad \text{for } i>1 \tag{27}$$

Equation (26) states the constraint condition for selection of the load parameter: the displacement increment vector in each iteration is orthogonal to the residual increment displacement vector. The load parameter at the first iteration of each step shall be arbitrarily chosen but should not be too large to ensure convergence in the iteration process. Its size is related to the degree-of-nonlinearity and, in

order to characterize the structure overall behavior, a nondimension quantity is suggested in Bergan et al. (1978) as a current stiffness parameter correction factor of the load increment $\overline{\Delta\lambda}^{(1)}$, used in the first iteration of the first step cycle. Thus,

$$\Delta\lambda^{(1)} = \overline{\Delta\lambda}^{(1)} \left[\frac{R^T . \bar{u}_r^{(1)}}{R^T . \hat{u}_r^{(1)}} \right]^{\gamma} \tag{28}$$

where $\bar{u}_r^{(1)}$ is the residual displacement vector in the first step and γ is an exponent factor assigned by the analyst for control of the load size according to the seriousness of the nonlinearity.

Numerical Analysis

The aforementioned numeric algorithms have been implemented with the truss element formulation. the results of some sample analysis that are reported in this paper illustrate the points made previously and give some insight into how the solution of a specific kind of nonlinear problem should be approached.

Two Rod Arch Structure

The plane structure shown in Fig. 2 is considered for analysis comparison because it is simple and

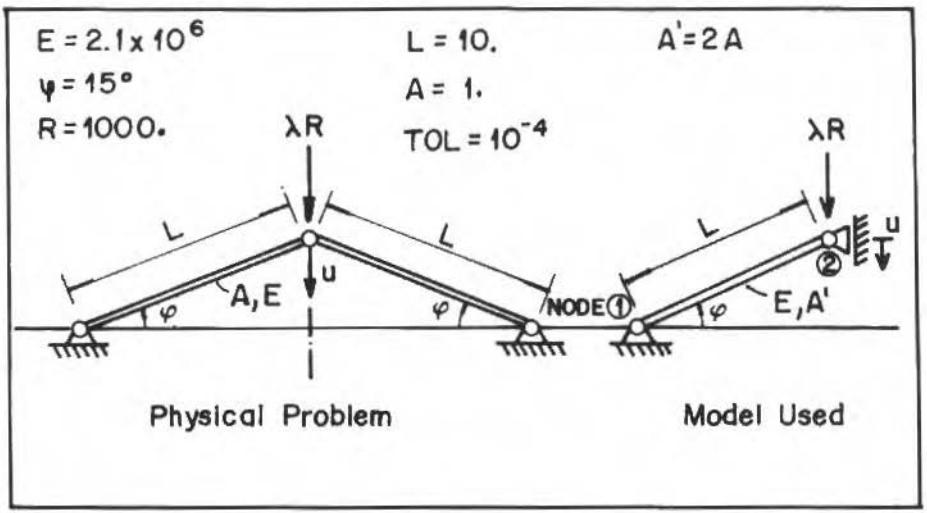

Fig. 2 The two rod arch structure considered (energy tolerance for convergence used = 1×10^{-4}

the analytic solution for static analysis is available in the literature (Bathe, 1987). Because of symmetry one two-node truss element is employed in the numeric representation. The analysis is limited to the material linear behavior and, as shown in Figs. 3, the solutions for the load-displacement relation furnished by the constant increment displacement method and the minimum residual displacement method (with $\gamma = 1$ and $\Delta\lambda^{(1)} = 4.22$) are both in good agreement with analytic results. It should be noted that, for the classical monotonically incremented loading procedure, the displacement path with snap-through from A to B is likely to be followed, instead the stiffness softening path. The same structure was also considered for dynamic analysis with the mass of the bar lumped at the element nodes and the Newmark method with constant average acceleration ($\alpha = 0.5$

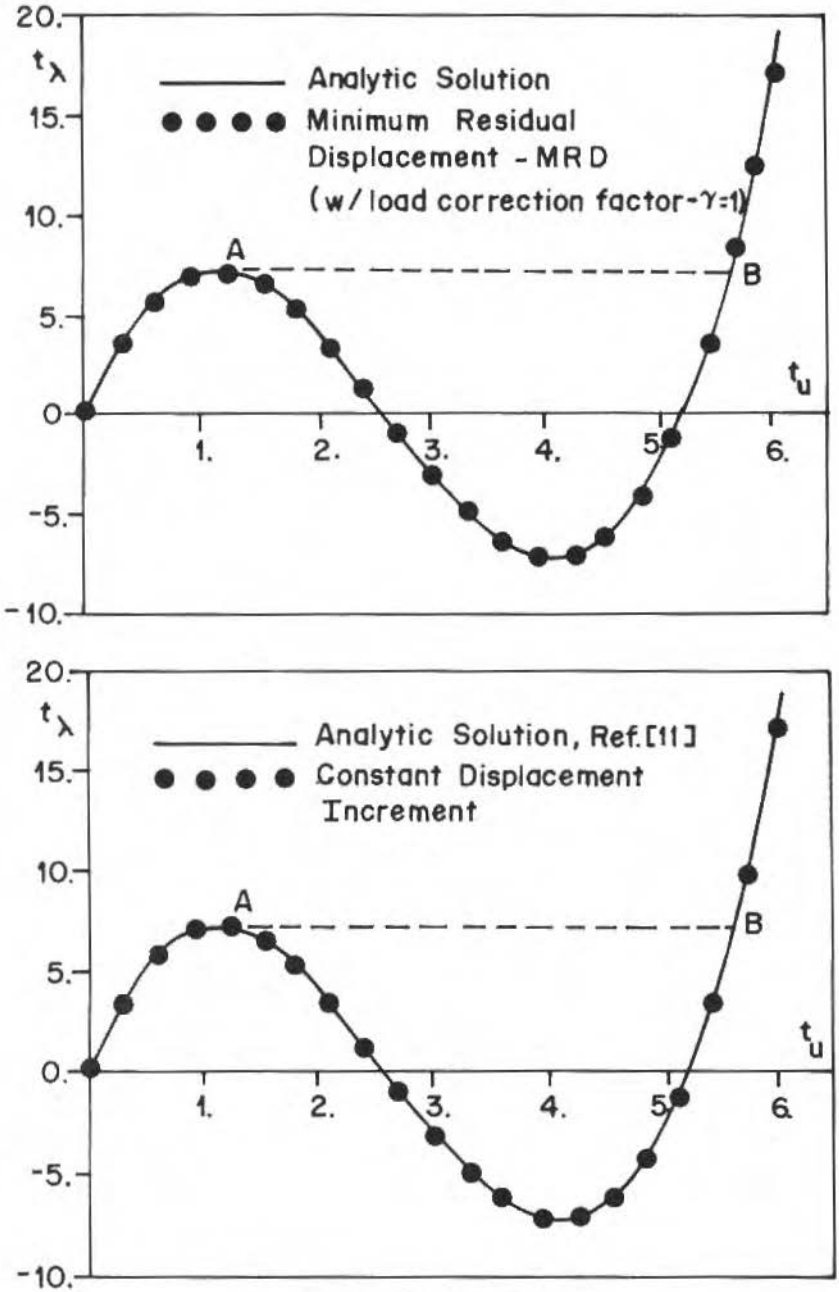

Figs. 3 - Load-displacement comparisons

and $\beta = 0.25$, Bathe (1987) employed to direct integrate the equilibrium equation in the time domain. Solutions for the displacements obtained with different time step integration sizes are shown in Fig. 4 and used for selection of the time integration parameter. The dynamic analysis results with a .01 sec step and three initial conditionsare shown in Fig. 5, in the phase plane. These analysis required three

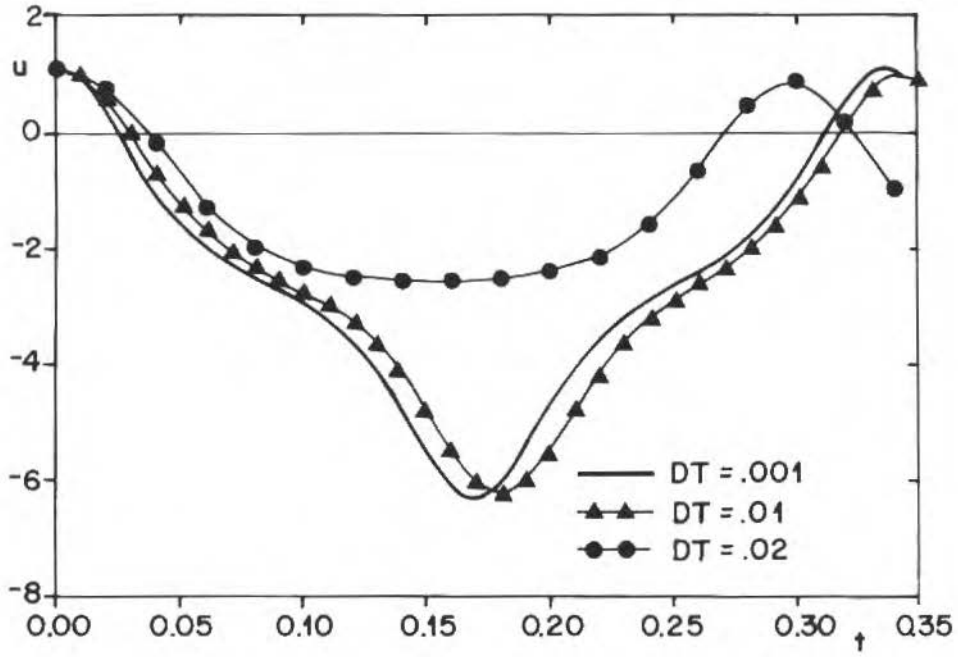

Fig. 4 Time step evaluation in the integration of the equilibrium equation using the Newmark method.

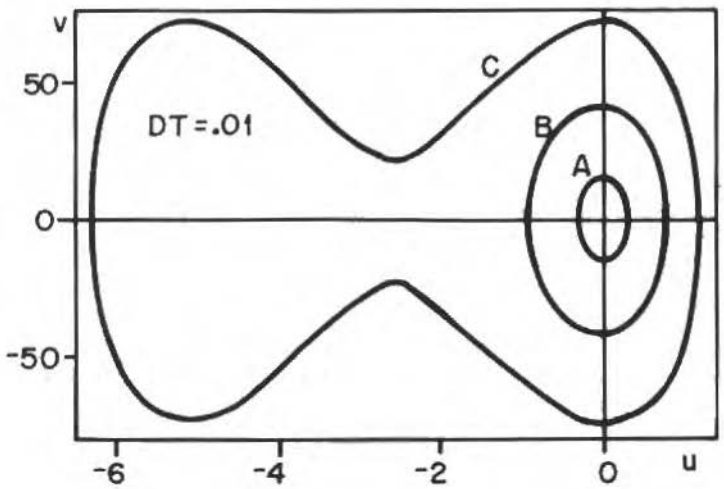

INITIAL CONDITIONS			
CASE	σ_0	u_0	v_0
A	17250	.300	0.
B	43410	.707	0.
C	74818	1.14	0.

Fig. 5 Phase plane solutions for three different initial conditions

iterations, in average, for each step cycle and a total of 35 time steps. Employing the Runge-Kutta

procedure for integration of the equilibrium equation, a step size of .001 sec, smaller than with the Newmark method, was required for convergence and resulting in a solution very close to the obtained with the finite element technique.

Three Rod Inplane Structure

The assemblage of elastic hinged bars in Fig. 6 has been considered for analysis in the literature

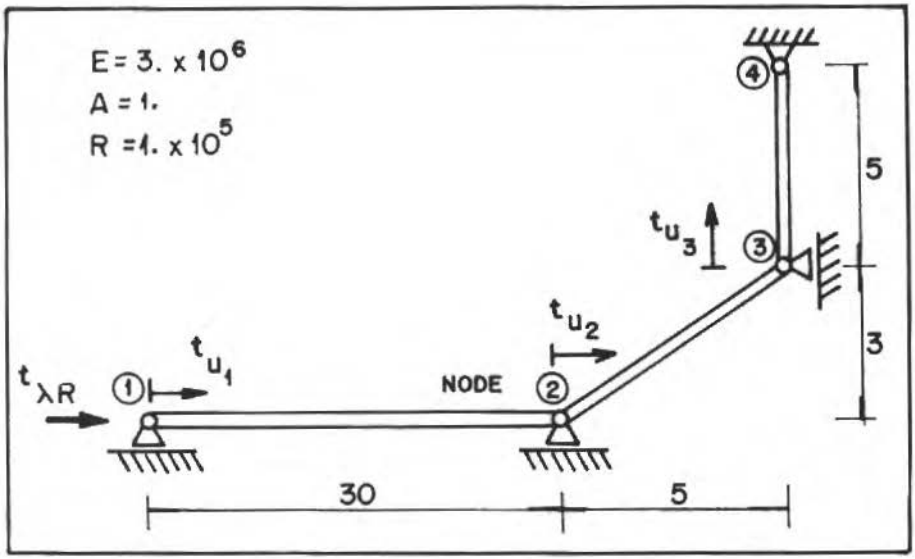

Fig. 6 The three hinged-bar structure considered

using the displacement control method (Powell and Simons, 1981) and the constant work method (Bathe and Dvorkin, 1983). The structure load-displacement responses possess the snap-through and the snap-back behaviors when subjected to a compressive load at node 1. Due to the snap-back behavior of nodes 1 and 3 displacement responses, node 2 displacement should be used as controlling displacement. Numerical solutions employing the displacement control algorithm and the method of minimum residual displacements with a load factor $\Delta\lambda^{(1)} = 1.542$ and $\gamma = 1$ were obtained and the responses automatically traced. As shown in Fig. 7, the agreement of the numerical results with previously obtained solutions is good.

Three-Dimension Rod Structure

The spatial truss in Fig. 8 was loaded vertically and subjected to two sets of boundary conditions at the structure base. First, the condition of all nodes at the base fixed is considered and the problem reduces to the one degree-of-freedom case addressed in the first example. The cross section area of the bars was adjusted to give the same results for the vertical displacement of node 7, as shown in Fig. 3. In the second case, free boundary conditions were considered for all base nodes of the structure except for node 1 kept fixed and for node 6 set free in x_1-direction only, Numerical solutions using the minimum residual displacement and constant increment displacement methods are presented in Figs. 9 for the load-displacement relation at node 7, in the vertical direction and at node 4, in the x_2-direction, respectively.

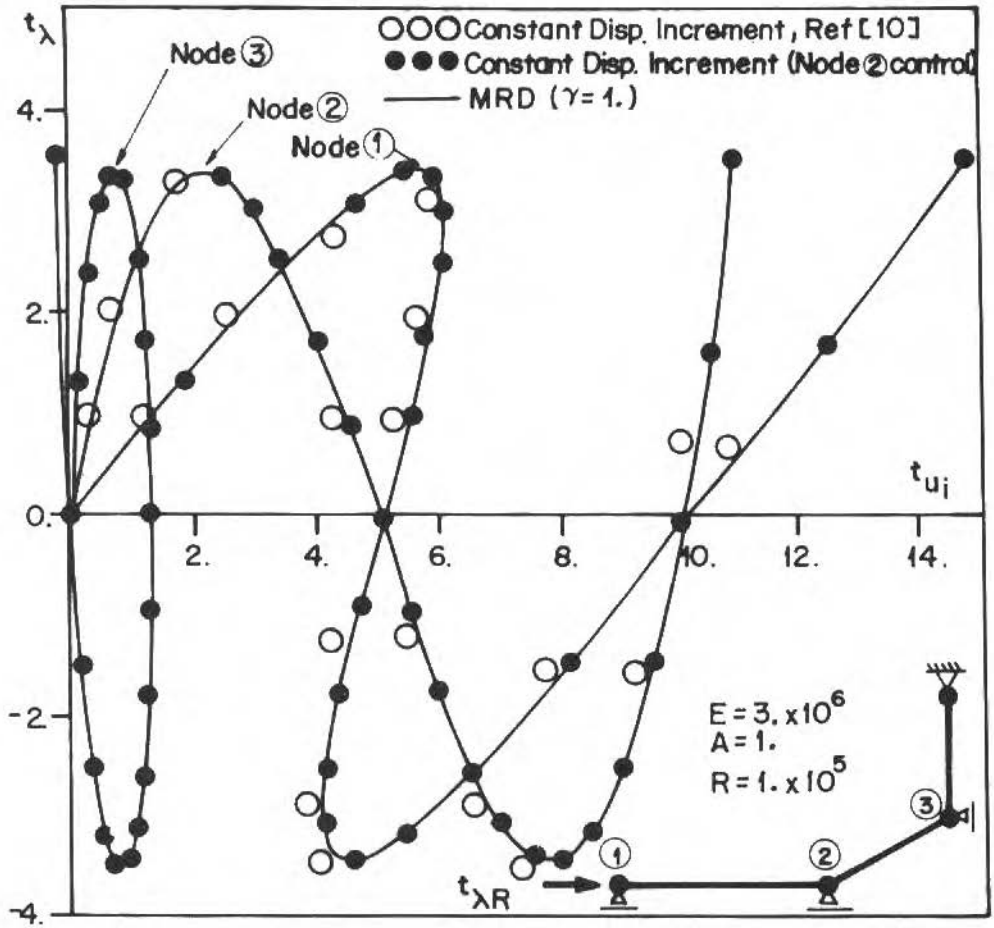

Fig. 7 Force-displacement numerical responses at the nodes of the structure

Free Fall of a Chain

A chain originally fixed between two horizontal points is released at one end. The shape of the hanging chain at rest is obtained numerically by imposing the equilibrium at each joint, considering the weight and the internal forces in each chain segment. First, the chain is held stand by a solenoid, which has the electric current shutted off when a stroboscopic light is activated, releasing the chain fixture at B and allowing it for motion. The numerical simulation of the chain falling, shown in Fig. 10, was obtained using 46 two-node truss elements with lumped mass. The Newmark time integration procedure was employed in a step-by-step solution with a time step of .5E-4 sec., for positions at a time interval of .1464 sec. Due to the solenoid time lag during the chain release, the second numerical position shown at configuration b, corresponds to time .1662 sec., made coincident with the fifth chain exposure in the experimental counterpart of the phenomena presented in Fig.11. The strobe light frequency was adjusted to 27.3 Hz. It is remarkable that the conputed positions follow the experiment even in fine details as the curling of the free end that takes place while the chain flings back across the vertical line. The small differences presented are certainly due to the friction condition not included in the numerical model representation.

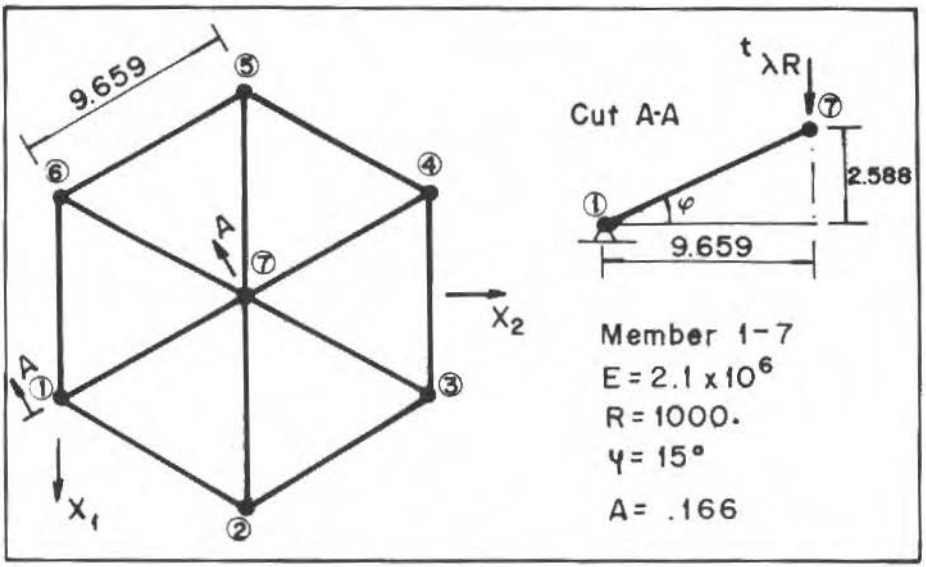

Fig. 8 The 3-D truss structure considered

Conclusions

A finite element formulation has been shown applicable for general truss structure analysis including geometric nonlinearies and dynamics. It enables analysis of structure motions possessing large displacements but under the condition of small strains. Sampling analysis have shown the use of automatic stepping procedure in predicting the load-deflection response of structures presenting snap-through/back behaviors. The examples shown illustrate the applicability of the formulation to a certain extent and the application of the methodology of analysis to more general elasto-plastic behavior is subject of continuing work.

Acknowledgements

The authors wish to acknowledge the financial support provided by the MCT to CTC-PUC/RJ, and by CAPES for the support of J. A. Alves MSc' Studies at the Dept. of Mechanical Engineering.

References

Bathe, K. J. and Cimento, A. P. (1980) "Some Practical Procedures for the Solution of Nonlinear Finite Element Equations", J. Comp. Methods Appl. Mech. Engng., vol. 22, pp. 59-85.

Bathe, K. J. and Dvorkin, E. N. (1983) "On the Automatic Solution of Nonlinear Finite Element Equations", Computers and Structures, vol. 17, n. 5-6, pp. 871-879.

Bathe, K. J. (1987) "Finite Element Procedures in Engineering Analysis", Prentice-Hall.

Batoz, J. L. and Dhatt, G. (1979) "Incremental Displacement Algorithms for Nonlinear Problems", Intl. J. Num. Met. Eng., vol. 14, pp. 1262-1267.

Bergan, P. G., Horrimore, G., Krakeland, B. and Soreide, T. H. (1978) "Solution Techniques for Nonlinear Finite Element Problems", Int. J. for Num. Met. in Eng., vol. 12, pp. 1677-1696.

Chan, S. L. (1988) "Geometric and Material Nonlinear Analysis of Beam/Columns and Frames Using the Minimum Residual Displacement Method", Intl. J. Num. Met. Eng., vol. 26, pp. 2657-2669.

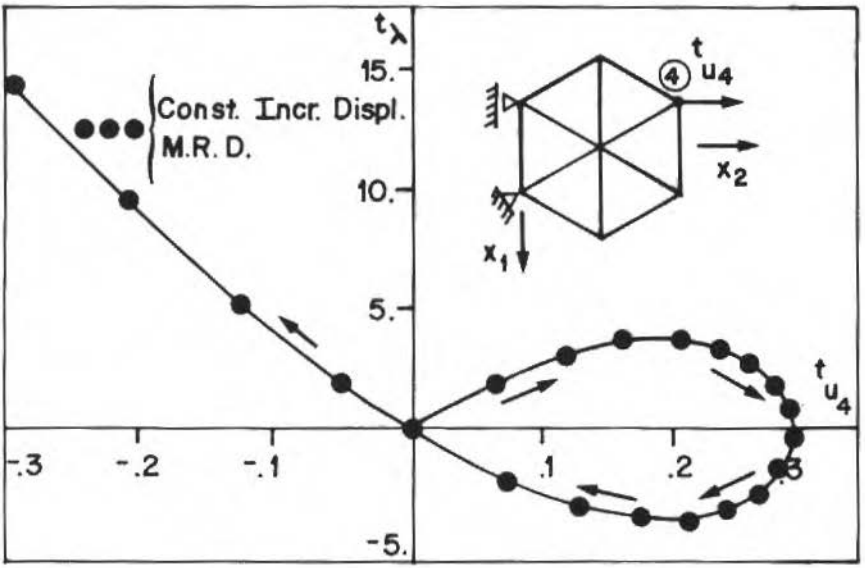

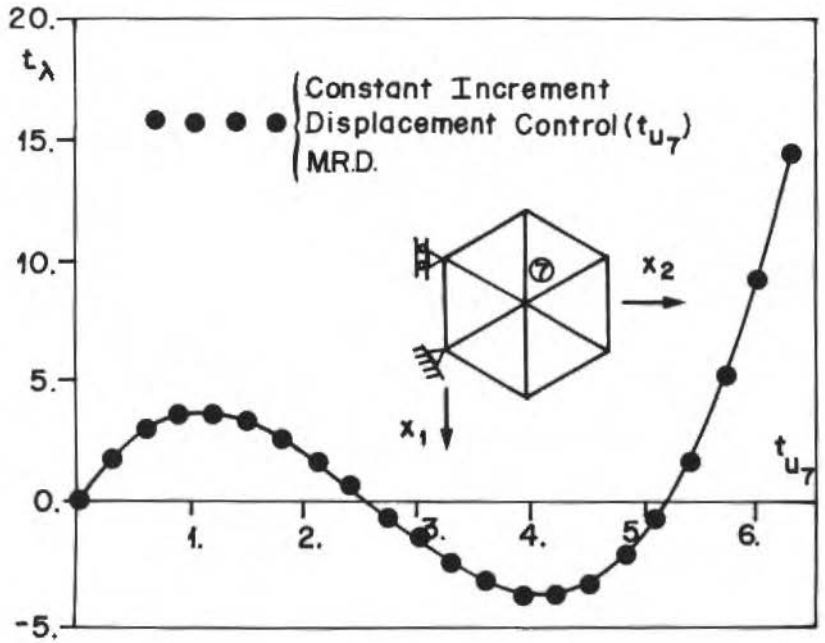

Fig. 9 Load-displacement solutions for the 3-D structure

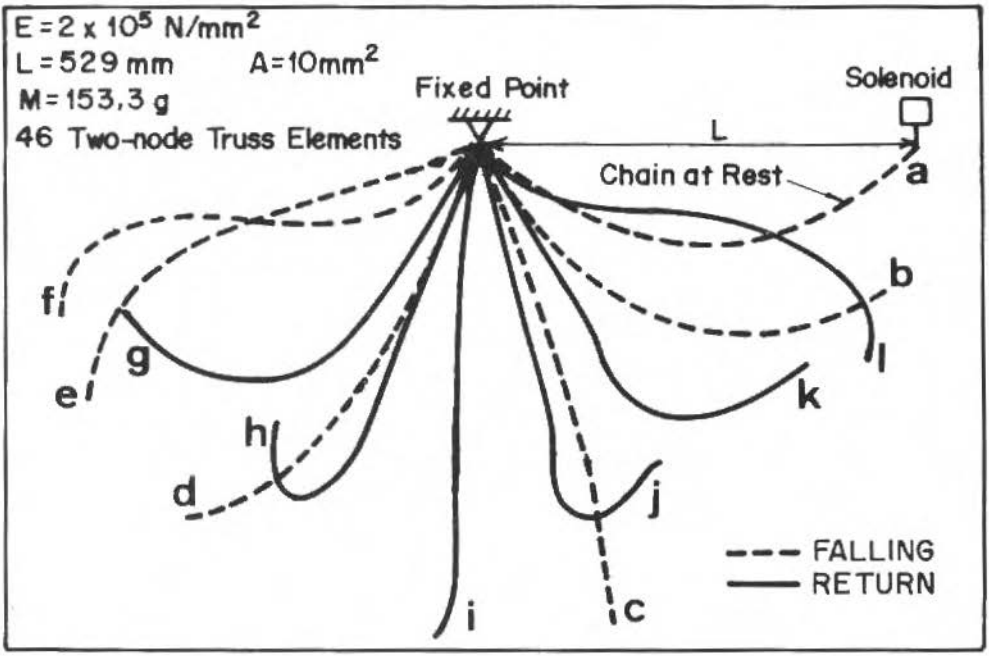

Fig. 10 Chain configuration predicted by the finite element model

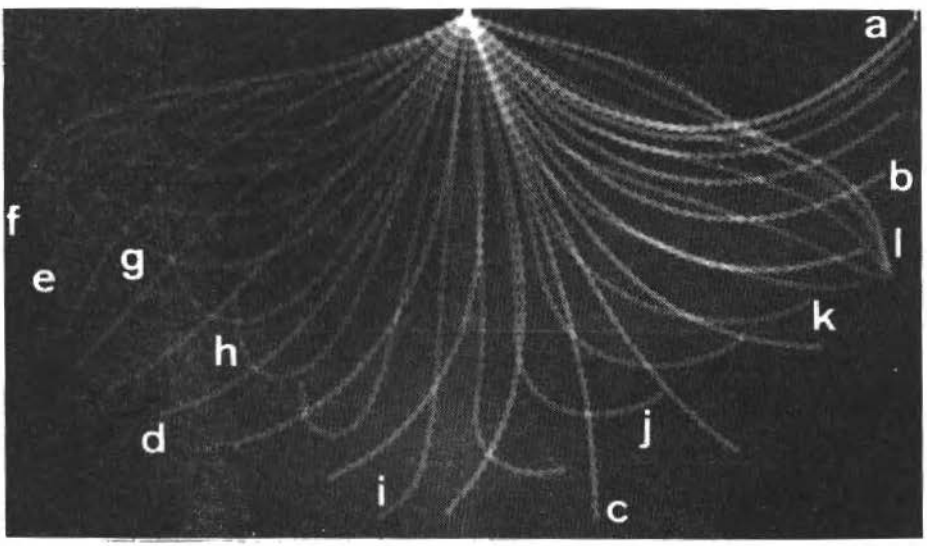

Fig. 11 Configurations of a free falling chain (pendulum like motion)

Clark, M. J. and Hancock, G. J. (1988) "A Study of Incremental-Iterative Strategies for Nonlinear Analysis", Research Report n. R857, The University of Sydney, School of Civil and Mining Eng.

Crisfeld, M. A. (1981) "A Fast Incremental/Iterative Solution Procedure that Handles Snap-Through", Comp. Struct., vol. 13, pp. 55-62.

Pires Alves, J. A. (1992) "Solução Incremental Automática de Treliças com Não-Linearidade Geométrica, Utilizando o Método de Elementos Finitos", Msc. Thesis, DEM-PUC/RJ.

Powell G. and Simons, J. (1981) "Improved Iteration Strategy for Nonlinear Structures", Intl. J. Num. Met. Eng., vol. 17, pp. 1455-1467.

Ramm, E. (1980) "Strategies for Tracing the Nonlinear Response Near Limit Points", Proc. of the Europe-US Workshop on Nonlinear Finite Element Analysis in Structural Mechanics, pp. 63-89.

Riks, E. (1979) "An Incremental Approach to the Solution of Snapping and Buckling Problems", Intl. J. Solids Struct., vol. 15, pp. 529-551.

Yang, Y. B. and Mcguire, W. (1985) "A Work Control Method for Geometrically Nonlinear Analysis", Proc. Int. Conf. on Advances in Num. Met. in Eng, UK, Swansea, pp. 913-921.

RBCM - J. of the Braz. Soc. Mechanical Sciences
Vol. XV - nº 2 - 1993 - pp. 165-171

ISSN 0100-7386
Printed in Brazil

Fundamentos Científicos de la Ingeniería Mecánica

Scientific Foundations of Mechanical Engineering

Juan José Scala Estalella
Departamento de Física Aplicada
Universidad Politecnica Madrid
E.T.S. de Ingenieros Industriales
Jose Gutierrez Abascal, 2-Madrid-España

Abstract

The paper discusses the question of looking for the scientific foundations of technology in preference to the technological foundations of science.
Keywords: Science, Technology, Mechanical Engineering

El análisis de los fundamentos científicos de la ingeniería mecánica es parte de un estudio más general, que nos conduciría a la consideración de cuáles son los fundamentos científicos de la técnica. En cuantas ocasiones he sido invitado a abordar este tema me he planteado la misma pregunta: ¿por qué siempre se buscan los fundamentos científicos de la técnica y sistemáticamente se olvidan los fundamentos tecnológicos de la ciencia?.

Cierto es que en nuestra tradición académica, no compartida por otros países y, en especial, los anglosajones, se suelen presentar los contenidos por la vía lógico-deductiva. Abren camino las matemáticas, seguidas por las físicas y las ciencias del ingeniero, para cerrar el arco con el entramado de las tecnologías, cuyos métodos se ofrecen firmemente apoyados en aquéllas.

Pero forzoso es reconocer que históricamente las cosas no fueron así o, al menos, en bastantes ocasiones siguieron el orden inverso. Muchos capítulos de la matemática nacieron con el afán de formular fenómenos físicos; e incontables avances técnicos tuvieron lugar antes que la física formulara las leyes que los rigen.

Cuando Watt patenta su máquina en 1769 faltan 55 años para que el ingeniero francés Nicolas Léonard Sadi Carnot (1796-1832) presente su estudio sobre la potencia que se puede obtener del calor; faltan 73 años para que Julian Robert Meyer (1824-1878) sugiera la equivalencia y conservación de todas las formas de energía; faltan 74 años para que James Prescott Joule publique sus medidas que dan el equivalente mecánico del calor; faltan 81 años para que Rudolf Julius Emannuel Clausius (1822-1888) y Lord Kelvin (1824-1907) formulen la segunda ley de la termodinámica; faltan 129 años para que Ludwig Boltzmann (1844-1906), después de fundar la física estadística, escribiera desesperado, con una desesperación que le llevó al suicidio: "Soy consciente de ser sólo una persona que lucha débilmente contra la corriente de su tiempo". Así se adelantaba la técnica a la ciencia.

Si esto es cierto para la termodinámica, qué no podemos decir de la mecánica, cuya historia aparece en los albores de la propia historia de la civilización. ¿Qué sabían del esfuerzo cortante los hombres del paleolítico cuando tallaban sus hachas? ¿Quién había introducido el concepto de centro instantáneo de rotación cuando se realizó ese invento inconmensurable de la ingeniería mecánica, que fue la rueda, y que ignoraron importantes civilizaciones, como las del continente americano, tan avanzadas en otras ramas del saber, como la astronomía? ¿Y qué decir de las construcciones de Roma? Y la misma Edad de las Tinieblas, no lo fue tanto en artilugios mecánicos, autómatas, relojes y transmisiones ingeniosas de movimientos en molinos de aire y agua como se desarrollaron en la Edad Media. Nombres tan ilustres en el mundo de la física, desde el siracusano Arquímedes, hasta el hombre típico del Renacimiento, que fue Leonardo da Vinci, bien pueden merecer el título de ingenieros mecánicos. Sería un interesante trabajo de erudicíon estudiar la presencia de la ingeniería mecánica en la historia de la civilización, pero no es esto para lo que me habéis llamado en esta sesión inaugural del congreso.

Lecture at the I Congreso Iberoamericano de Ingenieria Mecanica, Madrid-España - September 1993.
RBCM invited paper

Cuando una rama de la ingeniería tiene un nombre que coincide con el de una parte clásica de la física, como es la mecánica, parece que el tema está bastante centrado. La mecánica es aquélla parte de la física que estudia el movimiento de los cuerpos y las causas que lo producen. La llamada clásicamente mecánica racional, porque maneja entes de razón, es el capítulo de la física que requiere menos hipótesis físicas. Las leyes de Newton y los teoremas de la cantidad de movimiento, el momento cinético y la energía cinética permiten levantar el compacto edificio de la mecánica vectorial o newtoniana, que da cuenta del comportamiento del sólido rígido ante las solicitaciones dinámicas.

Casi como casos particulares, si bien es clásico su tratamiento separado y anterior a la dinámica, están la cinemática, conjunto de relaciones espacio-temporales, verdadera geometría del movimiento, y la estática que estudia las condiciones de equilibrio de los cuerpos.

Sin embargo, forzoso es reconocer que la mecánica teórica no nació al hilo de los pragmáticos problemas de la ingeniería, sino del esfuerzo de unos sabios que trataron de descubrir el orden existente en el Universo, ese orden que San Agustín eleva a uno de los atributos que hace que lo creado por Dios sea bueno. La obsesión por descubrir este orden necesario en el mundo condujo a no pocos errores científicos, como aquéllos en que cayó el propio Kepler.

No obstante, Tycho Brahe ya apuntaba en otro sentido, evitando construir una cosmografía apoyada en especulaciones abstractas y recomendando basarla en la observación para elevarse gradualmente hasta el conocimiento de las causas.

Galileo, como es bien sabido, aplica el método experimental, y Newton introduce un nuevo método en el estudio de la mecánica: el cálculo. A partir del hecho de que los planetas describen elipses alrededor del Sol, situado en uno de los focos, infiere que la fuerza atractiva debe decrecer con el cuadrado de la distancia. Ningún método experimental hubiera permitido llegar a esta conclusión, que Halley y Hooke habían entrevisto por la misma época.

Llegamos así a Joseph Louis Lagrange que en 1788 publica su Mécanique Analytique en la que aplica el cálculo de variaciones a las coordenadas generalizadas para ofrecer una nueva visión de la dinámica: el formalismo lagrangiano, totalmente analítico. Esta modelización de la mecánica culmina cuando Laplace extiende la teoría de la gravitación de Newton al conjunto del sistema solar, lo que constituía un complejo problema. Según las observaciones realizadas desde el tiempo de Tycho Brahe, es decir, durante dos siglos, la órbita de Júpiter se estaba reduciendo continuamente, mientras que la de Saturno se ampliaba. El hecho había sorprendido a Newton quien, al no poder explicar matemáticamente fenómenos tan complejos, supuso una periódica intervención divina para arreglar las cosas y evitar la catástrofe. Laplace desarrolló las soluciones en serie hasta las terceras potencias de las excentricidades y de las inclinaciones, antes despreciadas, concluyendo en la invariancia del movimiento medio planetario. Era el paso más importante en la mecánica celeste desde Newton.

Laplace resumió los resultados obtenidos por medio de cálculos matemáticos y la aplicación de la ley de gravitación de Newton en su gran obra titulada Traité de Mécanique Céleste. En ella demuestra que el Universo, como realización de un magnífico orden, responderá perfectamente a las leyes de la física.

Todo esto era así mirando al cielo, que no es precisamente el trabajo de los ingenieros mecánicos de hoy. Pero aún en esa máquina maravillosa que es el Universo, andaba enredando un fantasma que nunca podemos conjurar. En efecto, Laplace no lo explicó todo, al menos todo lo que hoy sabemos. Por ejemplo, la Tierra no es un cuerpo rígido, los movimientos de los fluidos que afectan al manto y a la corteza, así como las variaciones del nivel global de los mares, debidos a la congelación o fusión del hielo polar alteran el momento de inercia del planeta y modifican a su velocidad de rotación. El sistema no es, además, conservativo, pues los fenómenos de marea frenan los movimientos de los cuerpos celestes y, en el caso de la Tierra, suponen un incremento gradual de casi dos milisegundos por siglo.

Laplace no se planteó estas reservas y afirmó que el sistema está diseñado para una duración eterna, mediante los mismos principios que prevalecían tan admirablemente en la Tierra misma para la conservación de los individuos y para la perpetuidad de las especies.

El fantasma omnipresente dedicado a perturbar el cumplimiento de las leyes en el mundo mecánico es el rozamiento. En efecto, los sistemas son disipativos y la energía mecánica no se conserva. Las leyes de conservación son uno de los pilares de la física. Una de ellas se refiere a la electricidad y es la

conservación de la carga eléctrica, que hasta el momento se presenta inconmovible frente a los modelos cuántico y relativista. Otras dos se inscriben en la física de partículas: la conservación del número de leptones y del número de bariones. Las otras tres se encuadran en la mecánica: la conservación de la cantidad de movimento, del momento cinético y de la energía. Las tres entran en quiebra por la enojosa presencia del rozamiento, pero aún en interacciones instantáneas, en que las fuerzas intervinientes pueden ser representadas por funciones de Dirac, como choques y percusiones, se salvan las dos primeras, pero no la tercera.

En la Mecánica clásica se conservaban dos cantidades: la masa y la energiá. Pero Einstein probó que la segunda no era más que una manisfestación de la primera. Por ello, actualmente se predica sólo la conservación de la energiá, que puede manifestarse de muy diversas formas: cinética, potencial, másica, electromagnética, etc. Puesto que los sistemas mecánicos son disipativos, está siempre presente una transformación de su energiá en calor; el ingeniero mecánico no puede ignorar esta transformación, que genera un calor con frecuencia indeseable y que se ve obligado a difundir al medio ambiente o a sistemas refrigerantes y esto le conduce al mundo de la termodinámica.

Esta degeneración - permítanme utilizar esta palabra - de la energiá mecánica debe ser minimizada. Luego nos ocuparemos de ello. Entretanto, pensemos que el calor es la forma menos noble de la energía. Esperemos no ofender con ello a nuestros colegas de técnicas energéticas, pero ellos lo saben mejor que nadie. La energiá calorífica es, en el fondo, energía mecánica; la temperatura está estrechamente relacionada con la energía cinética media de las moléculas. Entonces, ¿dónde está la diferencia?. Es bien simple. La energía mecánica es ordenada, mientras que la calorífica es desordenada. Siempre es fácil, y casi inevitable, pasar del orden al desorden, pero no recíprocamente. Para extraer del calor energía mecánica hay que encontrar un foco caliente y uno frío. Sólo así se puede recuperar algo, nunca toda. Si éstos no se encontraran se habría llegado al equilibrio térmico, único estado perfectamente estable de un Universo, que sólo podría salir de ahí por una fluctuación afortunada, como puede ser la que dio origen a la vida.

La disimétrica dificultad de ambas transformaciones (energía mecánica en calor o la recíproca) queda bien patente meditando el contexto histórico en que tuvieron lugar. Moviendo entre las manos un palo terminado en punta, con rotación alternativa, sobre una base de madera, o bien haciendo saltar chispas en el golpe entre dos piedras, alguien consiguió generar el fuego. Quién fuera la persona o civilización del invento ha quebrado ignorado en la noche de los tiempos, pero se sabe que ocurrió en el paleolítico medio, cuando el hombre de Neanderthal se movía por la Tierra, varias decenas de miles de años antes de la revolución del Neolítico. Se había pasado de la energía mecánica al fuego. El hecho pasó a la mitología como un regalo de Prometeo a los hombres, después de haber robado el fuego a los dioses, lo que le valió como castigo vivir encadenado a una roca por toda la eternidad.

Pero la transformación del fuego en energía mecánica tuvo que esperar bastante más. Fue durante la Edad Media cuando la tecnología militar conoció un avance ciertamente revolucionario que alteró las reglas del arte de la guerra. Parece que en España lo utilizó por primera vez Alfonso el Sabio en el sitio de Niebla: nos referimos a la pólvora. Las armas de fuego hacen su aparición. No queremos hacer un juego de palabras, sino invitar a la reflexión, considerando que no es el fuego como arma, conocido desde antiguo, primero en la lucha prehistórica del hombre con los animales y, posteriormente, de los hombres entre sí. Los romanos ya arrojaban con sus catapultas objetos ardientes sobre las fortalezas enemigas. Ahora ya no es el fuego el que hiere, sino el que impulsa. La energía del proyectil es, como siempre, mecánica. Pero se ha dado el primer paso de la termodinámica: se ha aprendido a convertir la energía química potencial de la pólvora en energía calorífica, y ésta en energía mecánica. Falta mucho para que el ingeniero militar Sadi Carnot (1796-1832) publique su libro "Reflexiones sobre la potencia motriz del fuego" (1824), que puede, con razón, ser considerado como la piedra fundamental de la ciencia termodinámica.

Pero una cosa es lograr una explosión y otra más difícil es conseguir controlar la generación de energía mecánica con fines útiles, entendiendo por tales los no destructivos. Habían de pasar unos seiscientos años hasta que Nicolaus August Otto (1832-1891) construyera su motor de explosión de cuatro tiempos, del que él mismo decía: "Es brutal, pero funciona". Recordemos que la fusión nuclear conoció también este retraso de su empleo como fuente de energía con respecto a su uso como medio de destrucción.

En mecánica teórica es muy fácil cortar el nudo que supone el carácter disipativo de los sistemas, afirmando, como es cierto, que el problema del rozamiento es de naturaleza termodinámica y refugiándose en el estudio de los sistemas conservativos. Pero al ingeniero mecánico no le es permitido realizar esas piruetas de abstracción intelectual y se verá conducido, de grado o por fuerza, a entendérselas con el mundo de la termodinámica y de la transmisión del calor.

Para disminuir los efectos del rozamiento se introducen capas fluidas entre las superficies de contacto. Aunque se pretendiera separar la ingeniería hidráulica de la ingeniería mecánica, no sería soslayable el uso de las leyes de la mecánica de fluidos en sus aspectos cinemáticos y dinámicos y, como recurso matemático ineludible, la teoría general de campos, que permitirá formular la evolución del fluido.

No siempre se pretende minimizar el rozamiento. En muchas ocasiones se encuentra en él un medio de disipar energía, como en los procesos de frenado, o de transformar la naturaleza del movimiento, como en el caso de la rodadura. Sea como fuere, se hacen presentes simultaneamente fenómenos de interacción molecular, rugosidad y efectos ventosa, cuyo estudio está lejos de ser simple.

La ingeniería mecánica no se limita a mover objetos, sino que debe conformarlos adecuadamente, y la idea de conformar, dar forma, nos está evocando esa parte, hoy tan olvidada de la matemática, que es la geometría. Y no me refiro a la geometría de los hiperespacios curvos de Riemann, tan fructífera para estudiar la relatividad generalizada, o a las geometrías no euclídeas. Quiero llevar nuestra reflexión hacia el peligroso olvido en que se encuentra la geometría métrica, la que se desarolla en el espacio euclídeo tridimensional. Esa geometría, que en el siglo XIX fue mucho más allá de lo que pudiera interesar a un ingeniero, pero que floreció en su máximo esplendor en la Escuela Politécnica de París, con nombres tan ilustres como el de Monge.

Por uno de esos movimientos pendulares de la vida académica, hoy ha caído sobre ella el velo del silencio. Cierto es que en un ambiente universitario en que tanto se premia la investigación, resulta poco atractivo para los matemáticos un campo tan agotado, que dio, entre otros frutos, gruesos volúmenes sobre las propriedades del triángulo. Pero una cosa es su actual esterilidad para la actividad investigadora (afirmación que aún hago con reservas) y otra bien distinta es que no contenga herramientas utilísimas para la ingeniería. Y las ciencias básicas deben servir a esos fines. Por la misma razón podríamos estar tentados los físicos de hacer algo muy parecido con la Mecánica Racional, prácticamente cerrada desde los tiempos de Poincaré. Pero sus leyes siguen siendo válidas y extremamente útiles.

El ingeniero necesita de la geometría. Y no sólo como una ciencia que le ofrece unos entes de razón, sino como unas técnicas de representación que le permitan llevar a cabo su trabajo. ¿Qué es, si no, el dibujo? Hágase sobre un tablero o sobre la pantalla de un computador, siempre quedará el desafío que supone representar métricamente el R3 en el R2.

Definida la forma, es necesario realizarla y no de cualquier manera, sino sobre materiales determinados, con la precisión métrica requerida y dejando las superficies en un estado adecuado. El desarollo en el tiempo comporta procesos espaciales y la geometría, ahora convertida en cinemática, reclama su puesto, tanto para estudiar las fases de mecanizado de una pieza, como para proyectar el movimiento del brazo de un robot. Como un escultor, el ingeniero deberá arrancar la materia a la materia o darle forma pasándola por estado de fluidez, llegando a medidas muy exactas, que cada vez más le acercan a las dimensiones moleculares. Es impensable que en este proceso se ignore la física de la materia y la ciencia de los materiales, como fundamentos científicos para llevar a buen término un trabajo con exigencias crecientes.

Vale la pena pensar cuáles fueron los medios que se utilizaron para arrancar la materia de la materia. Desde tiempos muy remotos se dio por supuesto que para conformar un cuerpo hacía falta otro constituido de material más duro: se cortó la madera o la carne de los animales con hachas de piedra. Pero hubo que dar forma y filo a las propias piedras y no siempre se encontraron cuerpos más duros. Golpeando piedra contra piedra se hacían saltar trozos de una de ellas. La primera idea, consistente en un proceso de corte, evoluciona hacia un proceso de erosión, en el que el agente es la energía.

Esto es lo que ocurre en procesos como el chorro de arena o el corte con chorro de agua y así se evoluciona a las técnica de electro-erosión. Es casi increíble, pero la ingeniería corta y perfora actualmente con partículas como los fotones, ¡que no tienen masa! ¿Quién pudo pensar que la luz sería una herramienta en manos del ingeniero mecánico? Pero esto es así, y la nueva herramienta tiene que ser conducida con las leyes de la óptica. En cuando a su génesis y en la interacción del láser con la materia no se pueden ignorar los fundamentos cuánticos de estos fenómenos. Seamos, pues, muy prudentes al pasar una página de un libro de física afirmando:"Este no es mi campo y, por consiguiente, no me interesa".

Una vez constituidos los elementos mecánicos, éstos están llamados a reunirse en sistemas altamente complejos, interactuando entre sí de todas las formas posibles (rodadura, pivotamiento, deslizamiento, tracción y compresión). Esta capacidad de los conjuntos que integran las máquinas y mecanismos ya entusiasmaron a Leonardo da Vinci (1452-1519), pintor, escultor, pero también científico e ingeniero. El mismo, en una carta a Ludovico Sforza, se considera ingeniero militar e hidráulico. Sus conocimientos geométricos, así como del calor y la óptica, le llevaron a aplicar con todo rigor las leyes de la perspectiva, creando una verdadera "ciencia de la pintura" en la que llegó a confundir la visión con la percepción. Estaba convencido que la fuente del conocimiento consistía en la observación, la experiencia, "saper vedere". Esta preocupación, llevada a la práctica, ha quedado recogida en sus libros de notas, no sólo de arquitectura y pintura, sino también sobre anatomía y, en especial, los que sobre mecánica se encontraron en la Biblioteca Nacional de Madrid.

Leonardo se interesa por todo aquello que, de una forma genérica, podemos designar como cadenas cinemáticas. La transmisión de movimiento por medio de tornillos roscados, engranajes, mecanismos giratorios, elevadores hidráulicos y transmisiones de todo tipo, centra su atención y curiosidad. No solamente se ocupa del sólido rígido, como el movimiento de las flechas en torno a su centro de masa, sino del mucho más complejo movimiento de los fluidos: del agua, a la que llama "vetturale della natura" (portadora de la naturaleza), y del aire, al que observa por la evolución de las nubes y de las masas de humo. Estudia y dibuja con minuciosidad los torbellinos y remolinos que se originan en los vertederos, y desea llevar esos conocimientos a fines prácticos, diseñando compuertas para los canales de la región del Arno y Lombardía, asi como imaginando la manera de remedar las capacidades de aves y peces, en lo que más tarde serán submarinos y aeroplanos.

Mayor misterio encerraba la dinámica. Leonardo era consciente de la acción resistente que ejercen las fuerzas de rozamiento, por lo cual tiene que existir un principio motor. Al buscarlo le falla su capacidad observadora y sitúa a la fuerza en un plano trascendente, llamándola "virtù spirituale", llegando así al concepto escolástico del Primer Motor (Primo Motore). Quizá esto pueda resultar sorprendente, pero Newton seguirá hablando de las fuerzas ocultas de la Naturaleza. ¡Cuál hubiera sido el asombro y entusiasmo de aquellos hombres al contemplar las actuales realizaciones de la ingeniería mecánica!.

La integración de los elementos mecánicos en conjuntos cada vez más complejos plantea nuevos problemas, sobre todo si se tiene en cuenta que los distintos elementos son producidos en lugares distintos por empresas distintas. Es necesario tener una perfecta información sobre las características que tendrá la obra del otro. A las técnicas del control numérico de las máquinas se une el diseño asistido por computador, integrándose con la propia mecanización. Las cosas van hoy más allá, apuntando al CIM, en un esfuerzo para integrar y hacer transparente la información abundantísima que se maneja en el proceso de fabricación.

Nuevas exigencias para el ingeniero mecánico: la informática se introduce en su mundo y el tratamiento automático de la información se hace necesario desde el diseño hasta el montaje. Y con la informática, la automática, que, bueno será recordalo, no fue invento de los electrónicos, sino de los mecánicos. Ahí está, como recuerdo permanente, el símbolo de la especialidad mecánica en el escudo de la ingeniería industrial: el regulador de Watt.

Mucho hemos hablado hasta aquí del movimiento y presiento el malestar de los colegas cuya aspiración es lograr sistemas que permanezcan firmes, inmóviles, resistentes a todas las solicitudes. Decir que la estática es el único fundamento científico de las ciencias de la construcción es simplificar demasiado las cosas. En efecto, las leyes del equilibrio de un cuerpo rígido se reducen a la nulidad de la resultante y del momento del sistema de fuerzas que actúan sobre él.

Pero los elementos resistentes no se consideran como cuerpos rígidos. El ingeniero estudia sus deformaciones hasta el estado plástico y debe analizar su capacidad de resistencia. Su cálculo se introduce en el seno de la materia a través de las ciencias de la elasticidad y la resistencia de materiales. El cálculo tensorial le permitirá estudiar el comportamiento del material en el entorno de un punto y la teoría de la rotura nos enfrenta nuevamente con la constitución de la materia, que estudia la física del estado sólido.

Por otra parte la situación se complica bastante por la naturaleza de las solicitaciones. Estas no son estáticas, sino dinámicas: esfuerzos variables, periódicos o no, choques y percusiones, cargas móviles, etc., hacen que las estructuras puedan presentar fenómenos oscilatorios con los delicados problemas de resonancia.

Una vez más debemos recordar que toda la teoría física de las ondas nació inspirada en el estudio de las oscilaciones mecánicas: cuerda vibrante, tubos sonoros, oscilaciones en placas y membranas, etc. Se llegó así a establecer la ecuación de ondas y fue posteriormente cuando la analogía matemática que ofreciael comportamiento de los campos eléctricos y magnéticos variables, a partir de las ecuaciones de Maxwell, hizo pensar en la naturaleza ondulatoria de la luz y de la radiación electromagnética en general.

Independientemente de este hecho, la ingeniería mecánica hace uso extensivo de las ondas para escrutar el interior de los materiales con que trabaja, tanto su homogeneidad e isotropía, como su continuidad y el estado tensorial a que los someten las solicitaciones externas. Los rayos X, la fotoelasticidad, los ultrasonidos, etc., son actualmente herramientas de uso habitual. La misma metrología ha visto incrementado el nivel tecnológico mediante el empleo de sistemas láser.

Hay un principio general, que conviene tener presente: las leyes físicas son siempre modelizaciones de una realidad más compleja. Los entes que se manejan en la ciencia son idealizaciones (el sólido rígido, el sólido homogéneo e isotrópo, el hilo inextensible y perfectamente flexible, el líquido y el gas ideales, etc). De las variables que intervienen en el fenómeno se retienen unas cuantas que se estiman son significativas.

La ingeniería también modeliza sus situaciones. Al fin y al cabo, un modelo no es más que un sistema ideal que se comporta como el sistema real con un grado de aproximación suficiente, pero que es más sencillo de calcular, más fácil de construir, más rápido en reaccionar o más seguro de utilizar. Cualquiera de estas cuatro situaciones pueden conducir al ingeniero mecánico a modelizar su problema. Pero los modelos son cada vez más complejos, es decir, más próximos a la situación real. Son, sobre todo, los métodos de cálculo los que han propiciado esta complejidad creciente. Los computadores han permitido llevar el cálculo numérico a donde nunca hubiera podido llegar el análisis matemático.

Aun así conviene no prescindir de éste. El análisis puede ofrecer una visión de la realidad física altamente elocuente, cuando un alud de números tienda a ocultar fácilmente la visión global del fenómeno. En ningún caso sería plausible prescindir de las leyes que rigen la naturaleza, para lanzarse a un empirismo ciego o progresar a tientas entre puro cálculo numérico. Análisis, cálculo y experiencia deben ser los sólidos apoyos sobre los que se sostenga el trabajo del ingeniero. Ese trípode dará a sus conclusiones una gran seguridad y estabilidad.

Hago un llamamiento a reflexionar en esta línea a quienes tienen la responsabilidad de definir los planes de estudio por los que han de formarse los nuevos ingenieros. La palabra se repite sin cesar, pero con frecuencia se la traiciona. Los centros de enseñanza deben ofrecer una verdadera formación y no una mera información. La galopante evolución tecnológica exige ser prudente al elegir los sectores en que deba hacerse esa gran inversión intelectual, que es la preparación de los futuros técnicos. Y cuando hablo de sectores, no me refiero a especialidades, sino a esos grandes estratos que son matemáticas, física, ciencias del ingeniero y tecnologías. Como habrán observado he eludido las palabras troncal y troncalidad, porque sencillamente las considero de poco gusto. En efecto, quizá en esta imagen botánica a que nos lleva una nomenclatura legislativa poco afortunada, se descubrirá no tardando que habrá muchas troncales que se anden por las ramas.

Y antes de terminar esta presentación sobre los fundamentos científicos de la ingeniería mecánica, debo confesar que he fracasado en mi intento. Mi primera idea fue ofrecerles una inteligente selección. Creo que esto es lo que se esperaba de mí. Pero al hilo de mis reflexiones, acabaron desfilando todos

los campos de la física y, de su mano, toda la matemática. Al darme cuenta de ello, resonaban en mi memoria de los tiempos de estudiante aquellas palabras que tantas veces nos repetía el gran maestro D. Pedro Puig Adam, catedrático de matemáticas de esta Escuela: "Lo único que no se aplica, es lo que no se conoce".

Nada hay más práctico que una buena teoría. Los profesores de las ciencias básicas somos conscientes de nuestra ignorancia enciclopédica. Por eso nos merece mucho respeto la sabiduría monográfica de los especialistas. Pero éstos deben convencerse que les es conveniente, de vez en cuando, salir de su pozo y recibir la brisa refrescante y confortadora del vasto océano de la ciencia.

RBCM - J. of the Braz. Soc. Mechanical Sciences
Vol. XV - nº 2 - 1993 - pp. 172-198

ISSN 0100-7386
Printed in Brazil

Finite Elements Analysis of Parabolic Problems: Combined Influence of Adaptive Mesh Refinement and Automatic Time Step Control

Paulo Roberto Maciel Lyra
University College of Swansea
Dept. of Civil Engineering
SA28PP - Singleton Park, Swansea - Wales, U.K.

Summary

An adaptive finite element method with mesh refinement, by mesh enrichment, in time and space and an automatic time stepping control is described for a class of parabolic problems. The computational domain is represented by an assembly of 4-noded isoparametric elements. The mesh enrichment is achieved by locally subdividing each element into four new elements in those regions where further resolution is required during the analysis. The Euler backward time marching scheme is used and the time step sizes are gradually adapted. Both the space and the time discretization error estimation adopted involve only the computed approximate solution and those are use to dictate the adaptation. A discussion of the combined influence of time and spatial adaptation in the context of parabolic problems is also presented. Sample model applications are included to demonstrate the efficiency and accuracy, as well as the potentialities for engineering analysis, of the outlined procedure.
Keywords: Finite Element Analysis; Parabolic Problem; Adaptive Mesh Refinement; Automatic Time Step Control.

Introduction

The reliability of an approximate solution computed using the finite element method is directly related to the capacity of the discrete model to represent the physical problem under consideration. Basically two requirements must be fulfilled: the first is to develop techniques which can adequately represent the geometry of the computational domain. This task requires the development of suitable mesh generators and is clearly independent of the problem solution. Since it is unacceptably inefficient to construct a fine discretization everywhere, it is necessary to connect the discretization with the solution. This is the second requirement which can be provided once some techniques that permit an assessment of the error in the solution and a full adaptive process are combined. In this way the discrete model can detect the main features of the problem solution.

Nowadays, there is general agreement that adaptivity will become a standard feature of numerical methods software in the near future. A substantial progress was madé in this area in recent years. However, there are numerous problems that still have to be overcome if adaptivity is to be used with confidence in the solution of practical problems.

The so-called H-version of an adaptive method has received most attention for elliptic problems. In this paper, one possible adaptive procedure based upon the use of such a method is presented to the solution of problems governed by parabolic differential equations.

It is well known that the smoothness of solutions of parabolic problems vary considerably in space and time, exhibiting, for instance, initial transients, where highly oscillatory components of the solution are rapidly decaying. Therefore, efficient computational methods for this class of problems require the use of mesh spacing and time steps which are variable, ideally in both space and time. A discussion of the combined influence of adaptively defining the time step and the mesh spacing is presented in this paper.

An outline of this paper is as follows: In the next section a model parabolic partial differential equation as well as the discretization methods adopted are described. Then, a brief comment on the main characteristics of the equivalent discrete equations and formulations are presented. The following section describes the error analysis used. A brief description of the mesh spacing and the time step control strategies are presented, with the corresponding algorithms. Practical implications associated to

Manuscript received: April 1993. Technical Editor: Leonardo Goldstein Jr.

their implementation are fully discussed. Some numerical results illustrating the performance of the procedures are reported. Finally, the main conclusions are summarized and a brief comment on possible extensions and further optimizations are presented.

The Parabolic Equation

According to the Fourier law for conduction in continuous medium, two-dimensional transient heat conduction problems can be described (Zienkiewicz and Morgan, 1983) by the equation:

$$\left[\frac{\partial}{\partial x}\left(K_x\frac{\partial \phi}{\partial x}\right)+\frac{\partial}{\partial y}\left(K_y\frac{\partial \phi}{\partial y}\right)\right]+\lambda\phi = f(t)+C\frac{\partial \phi}{\partial t} \quad \text{in } \Omega\times I \tag{01}$$

where:

ϕ = temperature;

Ω = space domain $(x, y)\in\Omega\subset\Re^2$;

I = time domain $t\in I(0, T]$;

$f(t)$ = rate of heat generation per unit volume;

K_x, K_y = thermal conductivity ($K_x = K_y = K$ in an isotropic medium);

λ = coefficient of convection or radiation; and

C = heat capacity coefficient ($C = \rho C_p$), where ρ is the density and C_p is the specific heat at constant pressure.

Boundary conditions:

*Dirichlet boundary conditions - the temperature is prescribed $(\bar{\phi})$

$$\phi-\bar{\phi}(t) = 0 \quad \text{on } \Gamma_D\times I \tag{02}$$

*The Cauchy boundary condition

1. Heat flow condition $(\bar{q})$, $(\alpha = 0)$
2. Convection or radiation condition $(\alpha(\phi-\phi_a))$, $(\bar{q}= 0, \alpha\neq 0)$

$$K_x\frac{\partial \phi}{\partial x}n_x+K_y\frac{\partial \phi}{\partial y}n_y+\bar{q}(t)+\alpha(\phi-\phi_a) = 0 \quad \text{on } \Gamma_C\times I \tag{03}$$

in which n_x and n_y are the components of the direction cosines of the unit outward normal to the boundary, α is the convection or radiation coefficient on the boundary, and ϕ_a is the ambient temperature or the temperature of the external radiative source.

To render the initial/boundary-value problem well posed, an initial condition on temperature (ϕ^0) must also be specified at time t^0:

$$\phi = \phi^0 \quad \text{on } \Omega\times t^0 \tag{04}$$

To obtain the equivalent discrete problem the standard finite element procedure was followed (Zienkiewicz and Morgan, 1983). First, a spatial discretization was applied and next, on the resulting system of first order ordinary differential equations, discretization in time by finite difference.

Spatial Discretization

The computational domain which does not vary with time is discretized by linear 4-nodes isoparametric finite elements and an approximation solution is sought in the form

$$\phi \approx \phi_h = \sum_{j}^{nn} N_j(x, y)^* \bar{\phi}_j(t) = \underline{N}_\phi \bar{\underline{\phi}}_h \qquad (05)$$

where nn is the number of nodes in the mesh, N_j are the piecewise linear shape functions associated with node j and $\phi_j(t)$ is the nodal value of the temperature at time t, kept constant.

Applying a Galerkin weight residual procedure, integrating by parts and inserting the approximation ϕ_h in Eq. (01), yields a coupled system of first order ordinary differential equations.

$$\underline{C}\frac{d(\phi_h)}{dt} + \underline{K}\phi_h = \underline{F} \quad \text{with} \quad \phi_h = \phi_h^0 \quad \text{at} \quad t = t^0 \qquad (06)$$

where:

$\underline{K} = \underline{K}^k + \underline{K}^C$ is generically called "stiffness" matrix:

$\underline{K}^k$ is the conductivily matrix;

$\underline{K}^C$ is the convective matrix;

$\underline{C}$ is the consistent capacity matrix;

$\underline{F}$ is the independent term vector which arises due to the imposition of "thermal load" on the domain and/or the boundary conditions.

Time Discretization

Discretization in time by finite differences where

$$\left.\frac{d\phi_h}{dt}\right|^{n+1} \approx \frac{\phi_h^{n+1} - \phi_h^n}{\Delta t^{n+1}} \qquad (07)$$

in which

Δt^{n+1} is a time step at time t^{n+1}

and

$$\phi_h^{n+\theta} \approx (1-\theta)\phi_h^n + \theta\phi_h^{n+1} \qquad (08)$$

where θ is a weight parameter $(0 \le \theta \le 1)$

Inserting Eqs. (07) and (08) into Eq. (06) the problem at time t^{n+1} can be expressed as a system of linear algebric equations, as follows

$$\underline{K}^* \phi_h^{n+1} = \underline{F}^* \qquad (09)$$

$$\phi_h = \phi_h^0 \quad \text{at} \quad t = t^0$$

where:

$$\underline{K}^{*} = \theta \underline{K} + \frac{1}{\Delta t^{n+1}} \underline{C} \tag{10}$$

$$\underline{F}^{*} = [\underline{K}^{*} - \underline{K}] \phi_h^n + \left[\theta \underline{F}^{n+1} + (1-\theta)\underline{F}^{n}\right] \tag{11}$$

in which $\underline{F}^n$, the independent term vector evaluated at time n, and ϕ^0, the initial condition, are known.

Eq. (09) has to be solved at each time step. The parameter θ can vary from 0 (explicit scheme, after lumping the capacity matrix) to 1 (fully implicit scheme).

In this paper, we will concentrate our attention on the Euler/Backward scheme. Eq. (09) becomes in this case:

$$\left[\Delta t^{n+1} \underline{K} + \underline{C}\right] \phi_h^{n+1} = \underline{C} \phi_h^n + \Delta t^{n+1} \underline{F}^{n+1} \tag{12}$$

A discontinuous Galerkin method (Johnson, 1987) can be applied to discretize Eq. (01). It makes use of a finite element formulation to discretize in time, where the approximation functions are polynomials with degree at most g and may be discontinuous in time at the discrete time levels t^{n+1}. Employing constant functions ($g = 0$) on each time interval (I^{n+1}) the following equivalent discrete problem of Eq. (01) is obtained:

$$\left[\Delta t^{n+1} \underline{K} + \underline{C}\right] \phi_h^{n+1} = \underline{C} \phi_h^n + \int_{I^{n+1}} f(t)\, dt \tag{13}$$

This expression can be recognized as a simple variant of the Euler/Backward scheme where the independent term involves the evaluation of an integral of $f(t)$ over I^{n+1} rather than the value of $\underline{F}^{n+1}$ at t^{n+1}. In practice that integral is replaced by an average of $\underline{F}$ over I^{n+1}, if the function $f(t)$ varies smoothly in time.

Discussion About the Time Discrete Formulation

In a mathematical sense, there are basically four requirements to be applied to a numerical scheme in order that it be reliable: Consistency, Stability, Convergence and Accuracy.

The primary requirement of any algorithm is that it must converge, i.e., that the numerical solution approaches the exact solution of the differential equation as the discretization is refined. To establish the convergence one can appeal to the Lax Equivalence Theorem, which may be stated (Hughes, 1987) as: "For a well-posed initial value problem and a consistent discretization, stability is a necessary and sufficient condition for convergence". Therefore it is sufficient to consider only consistency and stability.

We will concentrate on the two-level time stepping scheme represented in Eqs. (08-11). The adoption of that class of methods in heat conduction is extremely popular because of its characteristics of easy programming, little use of memory and sufficiently precise results.

Hughes (1987) has proved that schemes of this class are consistent. Furthermore, the order of accuracy, i.e., the rate at which the discrete formulation goes to the differential equation since Δt tends to zero, is "one" for all $\theta \in [0, 1]$, except for $\theta = 1/2$, in which case it is "two".

Stability establishes a relation between the computed and the exact solution of the discretized equation. It is required that any component of any round-off error should not be amplified without bound.

For linear heat conduction problems, stability criteria can be studied using modal approach (or spectral analysis) and two basic classes can be established for the two-level time stepping methods:

Conditionally stable, in which stability imposes a time step restriction, and

Unconditionally stable, where no time step restriction is necessary.

Whenever $\theta \geq 1/2$ on Eqs. (08-11), unconditionally stable methods arises; otherwise, for $\theta < 1/2$, the time step has to satisfy a limit that, for a one-dimensional problem (Zienkiewicz and Taylor, 1983), since the high frequency is $O(h^{-2})$, can be approximately expressed as:

$$\Delta t_{cr} < \frac{\rho c_p h^2}{2k(1-2\theta)} \tag{14}$$

where h is the element length. In two-dimensional problems, h is a representative element lenght and must be multiplied in Eq. (14) by 1/2 for a regular quadrilateral mesh ($\Delta x = \Delta y = h$) (Press et al., 1988). In practice a safety factor (0.90-1.00) is also adopted to consider any mesh irregularity.

It is important to stress here that even an unconditionally stable scheme can exhibit an undesirable oscillatory behavior if no restriction is imposed to the time step size. This is caused by the existence of very high frequencies in the transient response. The oscillatory limit can be expressed approximately, for one/dimensional problems (Zienkiewicz and Morgan, 1983), as

$$\Delta t_{osc} < \frac{\rho c_p h^2}{4k(1-\theta)} \tag{15}$$

The only scheme oscillation-free in time, within the two-levels class, is the Euler-Backward which satisfies the oscillatory condition whatever value is adopted for the time step. Otherwise, some numerical procedures can be employed to diminish or eliminate these effects either by introducing numerical damping (Tezduyar and Liou,1990) or by weighting the forcing term (Bettencourt, Zienkiewicz and Cantin, 1983), or simple averaging successive time steps solution in some manner (Hughes, 1987). One of these ideas is to employ the Euler-Backward scheme (normally for the first or in severe cases for 2 or 3 time steps) until the effects of the higher thermal frequencies on the transient response have decayed and use other scheme from this point onwards.

Once consistency and stability are verified, convergence is automatic. The accuracy requirement allied with some particular characteristics of the parabolic problems are considered next.

Many heat conduction problems tend eventually to an equilibrium, often over very long time scales. This makes conditionally stable methods look unattractive. Moreover, very refined mesh will normally be necessary to represent accurately the solution behavior and excessively small time steps are required for stability reasons, even if h is only moderately small.

The semi-discrete problem (Eq. 06) is an example of a stiff initial value problem, mainly for the case in which the factor $k/(\rho c_p)$ (diffusivity parameter) becomes small and when highly distorted elements are present. The stiffness is due to the fact that the eigenspectrum of the thermal frequencies is very large. Higher frequencies are dominant in the early stages of a transient response, particularly if drastic changes in initial conditions or thermal load is involved. As the solution tends to the steady state condition it is governed by the lower frequencies. An algorithm which can decrease the amplitude of the higher frequencies will be desirable, and therefore oscillation-free schemes are indicated.

Very little information is available on the stability of general non-linear discretized problems. Within the framework of the Von Neumman method it can be said that the stability of linearized equations, with frozen coefficients, is necessary for the stability of the nonlinear form but it is certainly not sufficient (Hirsch, 1989). The generated high-frequency waves, through a combination of the Fourier modes on finite mesh, will reappear as low-frequency waves and the solution may deteriorate. This non-linear phenomenon is called "aliasing", and can be avoided by providing enough dissipation in the scheme to damp the high frequencies.

For the solution of nonlinear thermal transient problems using the trapezoidal family of methods at time integration, all schemes with $\theta < 1$ become only conditionally stable, as shown by Hughes (1977) and only the Euler-Backward scheme retains its unconditional stability. Furthermore, the Euler-Backward scheme is less sensitive to the gradual deficiency caused when the reduce integration has been used. This, apart from generally reducing the computational cost, is particularly beneficial for coupled problem analysis (Owen and Damjanic, 1981).

From an engineering point of view, besides the mathematical requirements, it is necessary to consider practical questions related to computer efficiency and reliability answers beyond pre-assigned cost.

The choice of the so-called implicit methods requires the solution of a system of equations at each time interval. On the other hand, the Euler-Forward $(\theta = 0)$, when a lumped or diagonal capacity matrix (C) is used, is a fully explicit method, and no system of equations must be solved. The computational advantage of an explicit scheme is accompanied by the severe stability restriction and, as was already stressed, the time step could be prohibitive, even more if we have a refined mesh.

Some technics have been proposed (Hughes, 1987; Smolinski, 1991) in order to improve the efficiency of an explicit scheme. The basic idea is to combine it with a domain decomposition method where the mesh is subdivided in some groups of elements and in each group a maximum allowable time step is used. This is an interesting approach, mainly when combined with an adaptative mesh refinement (Smolinski, 1991). Another idea (Hughes and Liu, 1978; Tezduyar and Liou, 1990) attemps to combine the advantages of both methods. The mesh is again partitioned and the "stiff" part of it is integrated implicitly and the remainder of the mesh explicitly. This is a very efficient scheme when the regions are defined adaptively and coupled problems are being analysed. The main disadvantage of these schemes is the necessity of an appropriate interchange of information across the boundaries of the groups, which requires a specific data structure.

The extra cost involved at each step of an implicit method is more than compensated once larger time steps may be taken. And, normally, they are more efficient methods, particularly if an automatic time step adjustment is available.

In order to satisfy an accuracy requirement very small time steps are necessary during the initial transient. However, outside the transient larger time step may be used. Consequently, one would like to use a method that automatically adapt the size of the time step according to the smoothness of solution. In that way, the number of systems of equations to be solved are reduced and the efficiency improved.

The strong stability and free-oscillation behavior of the Euler-Backward scheme, together with an accuracy control and an adaptive time step size definition presents the best choice to deal with all classes (linear, non-linear, couple, ...) of parabolic problems. Hence, an efficient strategy must be developed to provide cost effective numerical solution and robust tools.

In transient analysis it is generally thought that the accuracy can be improved, indefinitely, as the time steps decrease in magnitude. However, in the finite element approximations very small time steps may cause stability problems, which lead to physically unreasonable results. It is shown by Katz and Werner (1983) that this is due to the violation of the discrete maximum principle. In other words, if a consistent capacity matrix is used, the solution could present an oscillatory behavior if the space discretization and the time step do not satisfy a stability condition which limit the time step size in terms of the element size.

This stability condition can be demonstrated for one dimensional heat conduction problem (Rank and Werner, 1983). Using a parametric study an extension to two-dimension is presented in Murti, Valliappan and Khalili-Naghadeh, 1989, where for an isoparametric element a lower bound for the time step magnitude was proposed to be

$$\Delta t_{min} \geq \frac{\gamma \rho c_p h_{min}^2}{3k\theta} \qquad (16)$$

in which γ is a correction factor introduced in order to take into account other parameters like: the nature of input loading, type of element, aspect ratio, etc. The parametric study carried out by Murti et al., 1989, identifies a realistic value of the correction factor. For an isoparametric linear element in an irregular mesh $\gamma = 2.0$ was recommended.

In a stiff problem normally the accuracy requirements impose a time step size that make it difficult or even impossible to choose a space discretization which satisfies the stability condition (Hughes, 1977). These difficulties can be overcome if a lumped capacity matrix is used. In this case no limit on the minimum size of the time step is imposed, only the accuracy (or physical reasons) will determine the time step size. Therefore, even using an implicit technique a diagonal "mass" matrix is recommended.

A Posteriori Error Analysis

A proper error estimator to deal with a parabolic problem must take into account the two main errors involved in the discretization: the space discretization error and the time discretization error.

Over the past several years substantial progress has been made in the development of a posteriori error estimators: Babuska and Rheinboldt (1978);Gago et al. (1983); Zienkiewicz and Zhu (1987, 1991); and Johnson, Nie and Thomee (1990). These mostly deal with the spatial discretization error in elliptic problems. In this section a brief description of the error estimators adopted in the present paper is presented.

Using the Discontinuous Galerkin method, Johnson, Nie and Thomee (1990) demonstrated a suitable a posteriori error analysis for parabolic problems. Their demonstration was based on the assumptions that: a) The exact solution is bounded; b) The step ratio $\Delta t^{i+1}/\Delta t^{i}$ is also bounded; c) The ratio $\Delta t^{i}/t^{i}$ is sufficiently small; d) The spatial discretization satisfies the regularity condition; e) The initial time steps are selected separately. The derived error estimators for the variant of the Euler-Backward, given in Eq. (13) can be written as

$$\max_{t \in I} \left\| \phi(t) - \phi_h(t) \right\|_{L_2} \le c \left[\left(\max_{m \le N} \Delta t^{n+1} * \left\| \phi t \right\|_{\infty, I_n} \right) * \frac{1}{(\rho c_p)} + \left(\max_{t \in I} h^2 * \left\| \phi t \right\|_{H^2} \right) * \frac{1}{k} \right]$$

$$\text{for } n = 1, \ldots, N \qquad (17)$$

in which $\| \quad \|_{L_2}$ is L_2-norm, $\|v\|_{\infty, I_n} = \sup_{s \in I_n} \|v(s)\|_{L_2}$ and $\| \quad \|_{H^2}$ is the norm corresponding to the Hilbert space $H^2(\Omega)$.

For more details about this expression we recommend Johnson (1987) and Johnson, Nie and Thomee (1990). In Eq. (17) the first term on the right hand side bounds the time discretization error and the second term the space discretization error.

Spatial Discrete Error - Elliptic Problems

Three main types of a posteriori error estimators can be distinguished. First, the residual type of error estimator, presented by Babuska and Rheinboldt (1978) and later by Gago et al. (1983). Second, an interpolation type of estimator (Demkowicz, Devloo and Oden, 1985; and Johnson, 1987). And finally, the post processing type of estimator, which is computed using a recovered higher order finite element solution presented by Zhu and Zienkiewicz (1987).

In the evaluation of the space portion of the discretization error we adopted the third type mentioned, since it is easy to be implemented, with no additional data structure required and fast to compute, because only the first derivatives have to be evaluated. Furthermore, it gives not only global but also element error estimation.

A local solution error is given by

$$\underset{\sim}{e}_{\phi} = \phi - \phi_h \qquad (18)$$

or, in terms of the gradient of the nodal unknowns, by

$$\underset{\sim}{e}_{\sigma} = \sigma - \sigma_h \tag{19}$$

Using the discrete energy norm, the error over an element is defined as

$$\left\| \underset{\sim}{e}_{\phi} \right\|_E^j = \left[\int_{\Omega_j} (\underset{\sim}{e}_{\phi}^T \underset{\sim}{B}^T \underset{\sim}{D} \underset{\sim}{B} \underset{\sim}{e}_{\phi}) \, d\Omega + \int_{\Omega_j} (\underset{\sim}{e}_{\phi}^T \lambda \underset{\sim}{e}_{\phi}) \, d\Omega \right]^{1/2} =$$

$$= \left[\int_{\Omega_j} (\underset{\sim}{e}_{\sigma}^T \underset{\sim}{D}^{-1} \underset{\sim}{e}_{\sigma}) \, d\Omega + \int_{\Omega_j} (\underset{\sim}{e}_{\phi}^T \lambda \underset{\sim}{e}_{\phi}) \, d\Omega \right]^{1/2} \tag{20}$$

where B is an operator that relates the gradient of the variable with itself. The global error is

$$\left\| \underset{\sim}{e}_{\phi} \right\|_E = \left[\sum_{j=1}^{Nelm} \left(\left\| \underset{\sim}{e}_{\phi}^j \right\|_E^2 \right) \right]^{1/2} \tag{21}$$

In order to have a normalized error it is useful to define the parameter η such that:

$$\eta = \frac{\left\| \underset{\sim}{e}_{\phi} \right\|_E}{\left[\left\| \underset{\sim}{e}_{\phi} \right\|_E^2 + \left\| \phi_h \right\|_E^2 \right]^{1/2}} * 100 \, (\%) \tag{22}$$

which provides a measure of the global error of a given finite element mesh, and where

$$\left\| \phi_h \right\|_E = \left[\sum_{j=1}^{Nelm} \int_{\Omega_j} (\sigma_h^T \underset{\sim}{D}^{-1} \sigma_h) \, d\Omega + \int_{\Omega_j} (\phi_h^T \lambda \phi_h) \, d\Omega \right]^{1/2} \tag{23}$$

Other norms may be used, like the L_2 norm in which case the constitutive matrix ($\underset{\sim}{D}$) must be replaced by the identity matrix in the above equations.

In the standard F.E.M. formulation the gradient in a typical element is evaluated by direct substitution of the local variables field in an appropriate constitutive equation:

$$\sigma_h = \underset{\sim}{D} \underset{\sim}{B} \phi_h \tag{24}$$

where $\phi_h = \underset{\sim}{N} \bar{\phi}_h$

Since, only the continuity of the unknown, and not of its derivatives, is imposed in the analysis, the unknown gradients are discontinuous and unrealistic. Indeed that element gradients are mapped completely out of the subspace of the interpolation functions, i.e., they are not in the finite-dimensional subspace of the space containing the actual unknown function ϕ.

Brauchli and Oden (1971) and, independently, Hinton and Campbell (1974) have shown a consistent procedure for calculating stress (gradients) in the F.E.M., which is based on the idea of conjugate approximations. With only a small increase on computation a gradient field consistent with the approximations can be obtained. Moreover, if the unknown approximations are continuous, the consistent gradient will also be continuous and will be more accurate, in a mean square sense.

The procedure presented in Brauchli and Oden (1971), and in Hinton and Campbell (1974) was later extended by Zienkiewicz and Zhu (1990 and 1991) as a local recovery technique which is in fact a particular projection technique to recover the derivatives (gradients) of the F.E. solution. A systematic procedure for computing consistent, continuous gradient distributions in F.E. approximation can be summarized as follows:

Compute the fundamental matrix

$$\underline{M} = \sum_{j=1}^{Nelm} \underline{M}^j = \sum_{j=1} \left[\int_{\Omega_j} \underline{N}_{\sigma}^T \underline{N}_{\sigma} \, d\Omega \right] \tag{25}$$

Compute the discontinuous gradient field using Eq. (24) for each element and evaluate

$$\underline{P} = \sum_{j=1}^{Nelm} \int_{\Omega_j} (\underline{N}_{\sigma}^T \bar{\sigma}_h) \, d\Omega = \left\{ \sum_{j=1}^{Nelm} \left[\int_{\Omega_j} (\underline{N}_{\sigma}^T \underline{D} \underline{B}) \, d\Omega \right] \right\} \bar{\phi}_h \tag{26}$$

The consistent gradient distribution over the entire domain is obtained after solving the following linear system of equations

$$\underline{M} \vec{\sigma} = \underline{P} \tag{27}$$

Noting the best quality of the gradient obtained using the projection technique, Zienkiewicz and Zhu (1987) proposed an error estimator where the exact gradient σ (not available) of the solution is replaced by the consistent gradient σ^* in Eqs. (19-22). The second term in Eqs. (20) and (23) is omitted since it is of higher order.

Reliability of this error estimator has been established mathematically. Also it has been successfully used in adaptive analysis for many types of elements in different physical problems.

Remarks:

a. Eq. (27) can be approximately solved by using a lumped matrix $\underline{M}_L$ such that:

$$\vec{\sigma} = \underline{M}_L^{-1} \underline{P} \tag{28}$$

A successively better solution can be obtained by iteration using

$$\vec{\sigma}^{(n)} = \vec{\sigma}^{(n-1)} + \underline{M}_L^{-1} \left(\underline{P} - \underline{M} \vec{\sigma}^{(n-1)} \right) \tag{29}$$

In practice the iteration must be carried out only a fixed number of times (normally 3 or 4), if it is judged important.

b. The best and most obvious projection (Brauchli and Oden, 1971) is obtained using

$$\underline{N}_{\sigma} = \underline{N}_{\phi} \tag{30}$$

Other projections, even using a simple nodal averaging of the F.E. gradients, give good results (Brauchli and Oden, 1971; and Hinton and Campbell, 1974).

c. It is interesting to stress that the procedure above presented can be used repeatedly in order to determine an approximation to a higher order derivative, as can be seen in Zienkiewicz and Taylor (1989).

d. The continuous gradient field obtained using the projection technique does not satisfy the overall equilibrium conditions. If it is judged important, the residual that results can be minimized by the application of Loubignac's iteration scheme (Cantin, Loubignac and Touzot, 1978). Also, if the procedure described above is to be used in a piecewise homogeneous problem it must be carried out over each material separately, since the gradient jumps are an integrated part of the problem involving multiple material.

e. Based on the well known existence of some exceptional points of the domain, known in advance for certain elements, where the FE solution is superconvergent, Zienkiewicz and Zhu (1990 and 1991) recently proposed a more accurate way to improve the gradient of the solution. They have demonstrated that for even shaped functions the new procedure could represent a big improvement if compared with the projections described before. Nonetheless, for linear elements, the only advantage of the new scheme is the fact that no global system must be solved.

Time Discrete Error - Parabolic Problems

To evaluate the time fraction of the discretization error we adopted the procedure proposed by Johnson (1987), which is very suitable and easy to use as an indicator. It is also efficient in the sense that almost optimal, and not extremely small, time steps are generated when this estimator is used to adapt the time step.

The second part of Eq. (17) can be written as

$$\left\| \underline{e}^{n} \right\|_{L_2}^{time} \leq c \Delta t^{n+1} \left\| \dot{\phi}_h \right\|_{\infty, I_n} = c \left\| \phi_h^{n+1} - \phi_h^{n} \right\|_{L_2} \tag{31}$$

where c is a constant, solution independent in linear problems, and $\left\| \dot{\phi}_h \right\|$ was replaced by the discrete equivalent in central difference. This expression represents an estimate of the time discrete error and must be limited by a pre-assigned tolerance δ during the time integration.

In order to have an efficient algorithm the error estimator must be kept close to the tolerance. In that way we must seek the time step size by solving the following nonlinear problem.

$$\text{Find } \Delta t^{n+1} \text{ such that } \quad c \left\| \phi_h^{n+1} - \phi_h^{n} \right\|_{L_2} = \delta \quad \text{with} \quad \phi_h^{n+1} = f(\Delta t^{n+1}) \tag{32}$$

which can be linearized taking the estimate of $\left\| \dot{\phi}_h \right\|$ by the numerical tangent at the end of the time interval I_n, and the next time step may be estimated as

$$\Delta t^{n+1} = \frac{\delta}{c \left\| \phi_h^{n} - \phi_h^{n-1} \right\|_{L_2}} * \Delta t^{n} = \frac{\delta}{\left\| \underline{e}^{n} \right\|_{L_2}} \quad \text{with} \quad n \geq 1 \tag{33}$$

The error estimator is normalized using the present solution:

$$\mu = \frac{\left\| \underline{e}^{n} \right\|_{L_2}}{\left(\left\| \underline{e}^{n} \right\|_{L_2}^{2} + \left\| \phi_h^{n} \right\|_{L_2}^{2} \right)^{1/2}} \tag{34}$$

Mathematical validity of this simple error estimator can be found in Hughes and Liu (1978). Also some numerical results for one-dimensional problems are presented there.

The error analysis, in which the total error in a specific norm is estimated and the relative contributions of the individual elements is indicated, is by itself important to help in the interpretation of the results. Also, it can be combined with a full adaptive process of refinement to govern the adaptation.

Transient Adaptive Procedure

An adaptive algorithm may be considered to be a computational procedure for constructing a discrete model for a given problem such that, ideally, the error of the corresponding approximate solution is within a given tolerance, in a given norm and such that the number of degrees of freedom to be analysed is minimal.

The main aim of this paper is to present a procedure to deal with parabolic problems where both space and time are adapted automatically, based in an error estimation which involves only the computed solution.

The previous adaptive procedures developed to solve parabolic problems have based their schemes in the interpretation of the parabolic problem as a succession of elliptic problems, and defined the adaptive strategies based only on the spatial error. Since a loss of accuracy at an intermediate step can not be recovered in a future solution it is necessary to choose a very small time step to guarantee that this component of the discrete error is not important when compared to the spatial discrete error. In such a way there is no advantage of the progressively smooth nature of most of the parabolic problems is used.

There exist many other methods in the literature to obtain an automatic time step control for parabolic problems. The adaptation is normally based in certain computation on a local error truncation. The main disadvantage of this procedure is the cost involved, since they require in principle the results of a higher order method.

As stressed above the parabolic problem (Eq 01) can be interpreted as a sucessive solution of elliptic problems. In that way, the time and space discretization can be decoupled and the error analysis and consequent adaptation proceed independently. The proposed strategy which coordinates the adaptation can be summarized as follows:

A. Spatial Control

1. Generate the model;
2. Determine the time step and advance the solution over (see details in the algorithm below);
3. Update the independent vector (F^*);
4. Estimate the spatial discretization error (Eqs. 20, 21, 22);
5. Refine the mesh according to the refinement strategy;
6. If at least one element was refined in the step 5:

Then:

. Reset time over $-\Delta t^{n+1}$;

. Store the solution at $t^{n+1}-\Delta t^{n+1}$ as initial data;

. Go to the step 1;

Otherwise:

. If the time of the analysis has elapsed or the solution reachs the steady-state:

. Stop.

Else,

. Carry on with the time integration;

. Go to step 2;

Remarks:

A.1 - To start the time integration a time step equal to "10E-03 times the stability time step limit for the explicit method" is adopted. This is done to reduce the discrete error [See Eq. (17)] only to the spatial component. In this way, for the first step this algorithm falls back into the steady state algorithm, where the mesh is refined until the error estimated is below the pre-assigned tolerance. And then it works, initially, as a pre-processor in the transient analysis. Moreover, the use of this idea produces an initial solution which will be used to evaluate the error in time after the first time step.

A.2 - In parabolic problems, where the solution changes smoothly in time, the "optimal" grid used at the previous time step should be a very good approximation to the desired grid at the advanced time step. It is sometimes important in terms of computational efficiency to define a number m of steps, after which the spatial error is checked. The number of steps, that the analysis can advance in time before changing the mesh, depends on the problem under consideration, and it is important to keep in mind that if some changing feature of the solution is lost at an intermediate step, then this loss may not be recovered in future solutions.

A.3 - The solution of the resultant system of algebric equations is performed by the Preconditioned Conjugate Gradient algorithm implemented in an element- by-element procedure. The coarser grid solution is also used as an improved initial guess in a similar way as the strategy so-called "nested iteration" (Briggs, 1987).

A.4 - An initial structured mesh is used, and after local refinements non-conforming nodes are introduced and an additional data structure must be used. A tree data structure to define the connectivity is used. To ensure that the method is conforming, restrictions are imposed at element level (Demkowicz, Devloo and Oden, 1985; and Lyra et al., 1988).

A.5 - There are several refinement strategies based on the "Principle of Equidistribution of error". Convergence ratio, reliability and cost depend on the chosen strategy (Lyra et al., 1989). A common problem of adaptive refinement procedures, is that they tend to concentrate an excessive amount of elements about the singularities. The reason is that, as the strategy tends to equidistribute the error, it will sacrifice accuracy in the regions where the solution is smooth to diminish the error at the point/line of singularity. A strategy to provide acceptable results for problems with strong singularities was applied. The basic idea consists of eliminating the error associated with the singularity in order to capture other features in the solution (this strategy is even more important when hyperbolic or advection-dominant parabolic problems are considered). A brief description of the adopted strategy is given below:

. Evaluate the allowable error per element in the whole domain (Ω) :

$$e_{pe} = \text{toll} * \left(\frac{\left\| \underset{\sim}{e}_{\phi} \right\|_E^2 + \left\| \phi_h \right\|_E^2}{\text{Nelm}} \right)^{1/2} \tag{35}$$

. Split the computational domain in two parts:

$$\Omega^* = \{ \bigcup \Omega_e / \text{level}_e = \text{Maxlevel and } \left\| \underset{\sim}{e}_{\phi} \right\|^e \geq e_{pe} \}$$

$$\Omega^{**} = \{ \bigcup \Omega_e / \text{level}_e < \text{Maxlevel or } \left\| \underset{\sim}{e}_{\phi} \right\|_E^e < e_{pe} \} \tag{36}$$

where $\Omega = \Omega^* \bigcup \Omega^{**}$ and $\Omega^* \bigcap \Omega^{**} = \Phi$

. Evaluate the allowable error per element, purging the error that corresponds to the sub domain Ω^* :

$$e_{pe}^{**} = \text{toll} * \left(\frac{\left\| \underset{\sim}{e}_{\phi} \right\|_E^2 + \left\| \phi_h \right\|_E^2}{\text{Nelm}^{**}} \right)^{1/2} \tag{37}$$

Define the elements to be refined using e_{pe}^{**}:

If $level_e < Maxlevel$ and $\left\| e_{\phi} \right\|_E^e \geq e_{pe}^{**}$ then refine element "e".

Another important measure mentioned during the analysis of the numerical results is the normalized error correspondent to the sub domain Ω^{**}:

$$\eta^{**} = \frac{\left(\left\| e_{\phi} \right\|_E^2 \right)_{\Omega^{**}}}{\left(\left\| e_{\phi} \right\|_E^2 + \left\| \phi_h \right\|_E^2 \right)_{\Omega}^{1/2}} * 100(\%) \qquad (38)$$

A.6 - Normally in heat conduction problems there are special features, such as heat sources, heat flux, corners, obstacles, which are assumed at some specified positions. The refinement capabilities are necessary to deal with singularities originated at these special points. Nevertheless, an unrefined capability can represent or not an advantage since a more complex data structure is needed and it is necessary to computation to eliminate elements, nodes and reorganize the data structure. An unrefined capability must be used at hyperbolic or advection-dominated parabolic partial differential problems where the solution migrates over the grid. Another scheme extremely effective is the use of an adaptive unstructured remeshing technique, as presented by Peraire et al. (1987).

B. Time Control

1. Compute ϕ^n;

2. Estimate the time discretization error (Eqs. 31, 34);

3. If the normalized error is smaller than δ:

Then:

. Evaluate Δt^{n+1} using Eq. (33);

. Advance time over Δt^{n+1};

Else:

. Reset time over Δt^n;

. Take: $\Delta t^{n+1} = \frac{\Delta t^n}{2}$

Remarks:

B.1 - The smallest time step obtained at the beginning of the algorithm is kept in memory to be used, as an initial guess, in the case of the existence of more than one transient on the problem solution.

B.2 - Owing to the discrete nature of the finite element, the idealization has to be in such a way that the highest frequency in the finite spectrum to be predicted accurately can be represented. As argued in Hirsch (1987), the shortest reasonable wavelength (λ_{min}) represented on a mesh with size h is $\lambda_{min} = 2h$ (The spacing (h) used to compute the time step is taken as $h = (area)^{1/2}$ of the smallest element). Based on this physical argument and on the time that this fastest decaying component is reduced to 1/10 of its initial value, Sampaio showed, for a one dimensional heat conduction problem, that a time-scale approximately half of the stability limit given by Eq. (14) can be defined for the problem.

This time scale is adopted as the first real time step to start the time integration. This is a very rigorous criteria and using it one can expect no (or only very little) reduction in the time steps at the beginning of the integration in time. The procedure carries on with the time step being adapted (normally increasing) during the interval of the analysis.

If the error tolerance is extremely severe (or if the space discretization is not in agreement with the time discretization dictated by the error) an excessive reduction in the step when the problem presents a sharp initial condition is expected. In real applications, it is not necessary to continue this reduction since it is caused by a singularity in the continuous model that no real problem displays (there is no instantaneous load or change in the boundary conditions), Therefore, in similarity with the space

discretization, a lower limit in the time discretization is imposed. A factor of 1/5 of the stability limit is adopted. In that way only in a extremely small interval the error criteria can not be satisfied, if so, but outside this interval it is guaranteed that the solution is below the pre-assigned tolerance. If a consistent "mass" matrix has been used, the lower bound given by Eq. (16) must be imposed.

B.3 - A limit in the relation between $\Delta t^{n+1}/\Delta t^{n}$ was imposed (normally from "1.5 to 2.0"). This is necessary because of the assumptions on the demonstration of the error (Eq. 17), and thus has a practical interpretation related to the approximate nature of the error estimation. In the examples tested here this restriction was activated only in the initial transient, when the initial step was very conservative and when the problem was close to the steady-state solution, where the step started to grow very steep once the global error decreased fast.

B.4 - There are several ways to construct a lumped "mass" matrix. The "Special Lumping Technique" developed by Hinton, Rock and Zienkiewicz (1976) is adopted. The reason for this choice is that for an arbitrary element it always produces a positive diagonal matrix. For an isoparametric linear element it is equivalent to the row-sum technique or to the nodal quadrature rule.

B.5 - No study was done in order to investigate the constants involved in the error estimator given by Johnson (1987). This could be important if a more sharp error estimation is desired for a special problem.

Using the described procedure, the main objective of bounding the discrete error by a given tolerance, can be achieved, as will be shown in the sample model problems of the next section.

Application

From an efficiency point of view, it will always be beneficial to begin an adaptive approach with a suitable mesh, provided by a pre-analysis based on the analyst experience. However, in order to stress the adaptivity ideas, very coarse initial discretizations are adopted in the following examples. The tolerance adopted in the error analysis is not very tight and the L_2-norm is used in the examples analyzed.

The first application focus on the time step adaptive procedure. The geometry, material property and initial discrete model are described at Fig. 1.

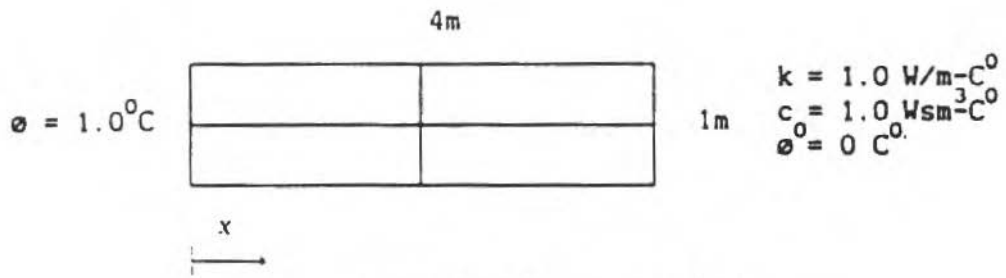

Fig. 1 Initial Discrete Model and Problem 1 Description

The tolerance adopted in both space (η) and time (μ) discrete error was 10%. The maximum level of refinement adopted was 6 and a bound of 3/2 was used in the relation $\Delta t^{n+1}/\Delta t^{n}$.

The final mesh obtained is shown in Fig. 2.

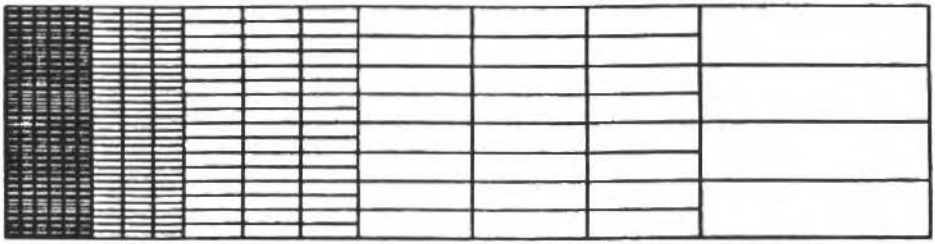

Fig. 2 Final Mesh

If the code has the capability of derefinement, the final mesh expected is the initial one, for this specific problem. But the presented mesh allows the transient solution, as shown in Fig. 3. The results

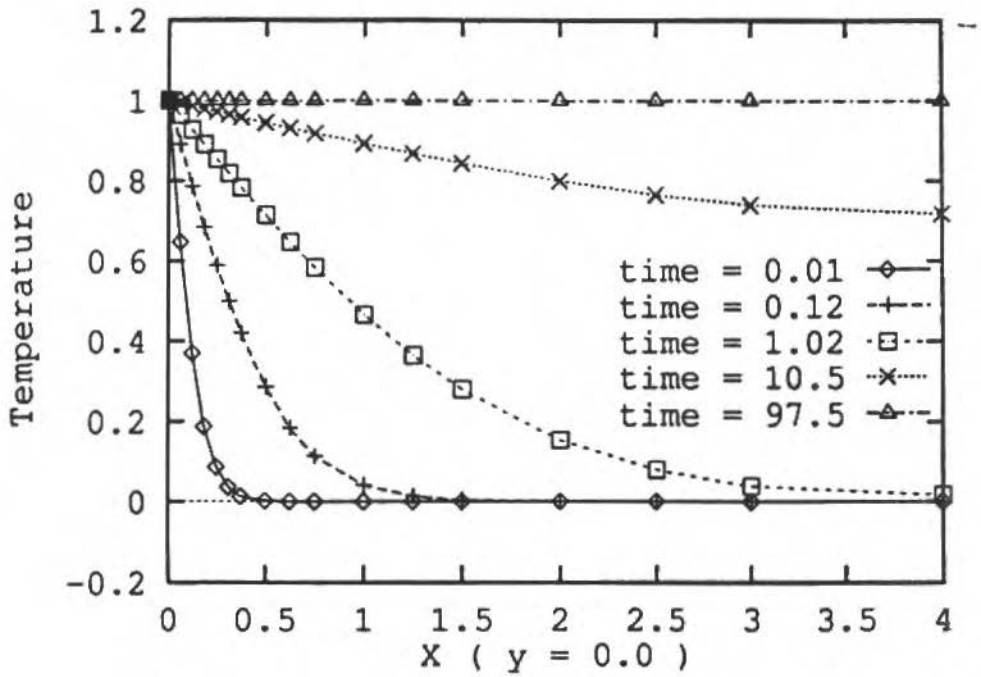

Fig. 3 Temperature Distribution at Sample Times

are in agreement with the analytical solution presented in Damjanic and Owen (1982) and free of any space oscillation.

The time step adaptation can be seen in Fig. 4 and the time discrete error, both the L_2 and

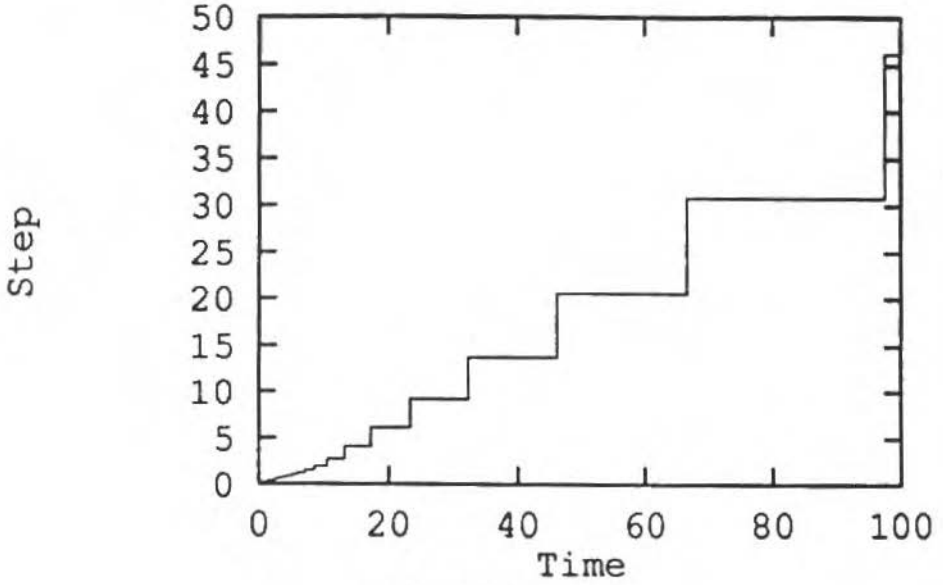

Fig. 4 - Time Step Evolution

maximum norm, in Fig. 5. The temperature against time for some sample points are presented in Fig.6.

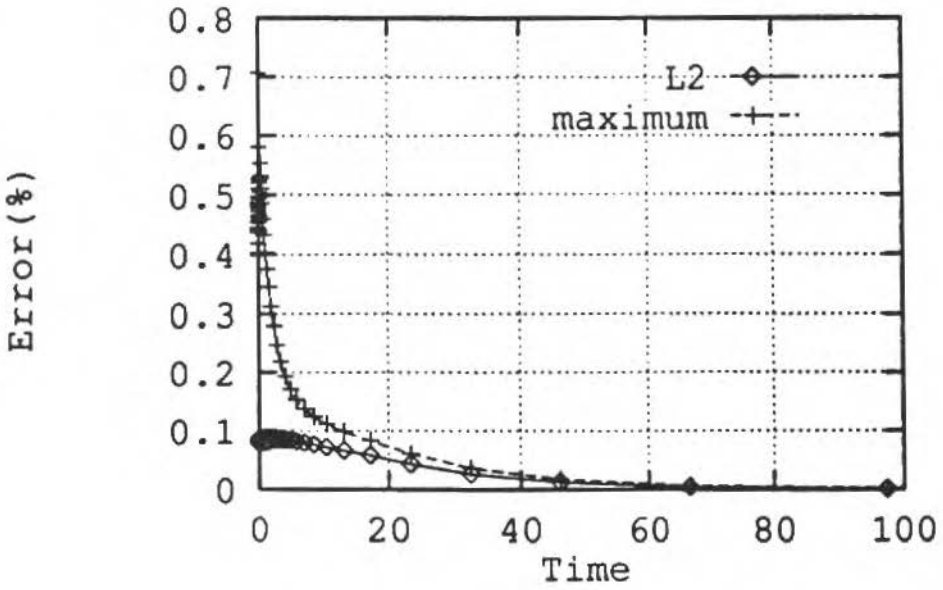

Fig. 5 - Time Discrete Error Evolution

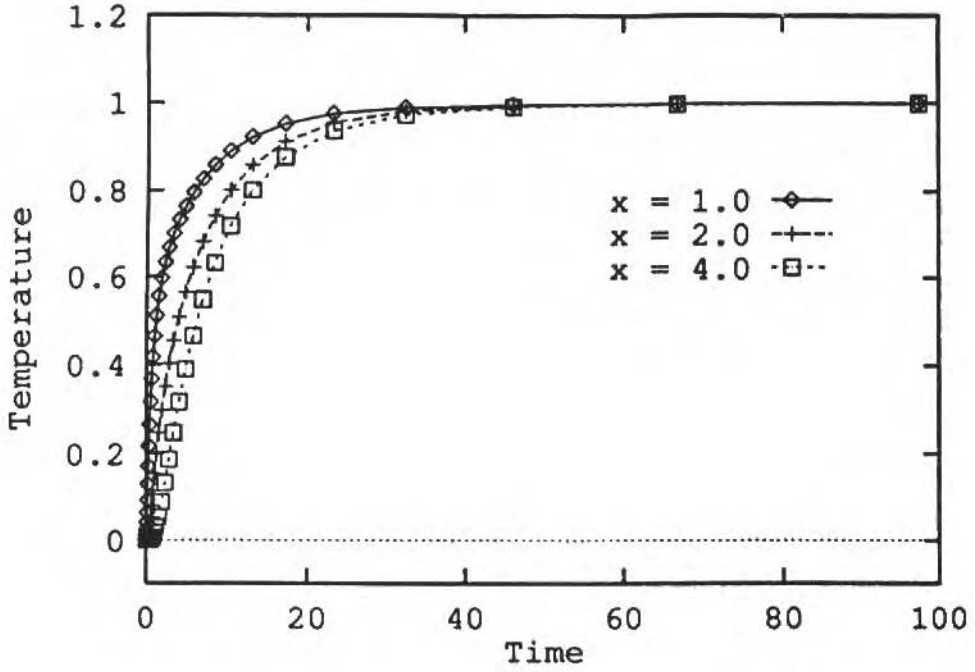

Fig 6 - Temperature vs. Time

Once more no oscillation and an agreement with the analytical solution were obtained.

In order to emphasise the importance and the efficiency of the time step adaptation procedure used, the same problem with the mesh presented in Fig. 2 was computed using a fixed time step equal to the smallest one (Δ t= 2.44E-04) obtained when using adaptivity. A detail of the time error at the beginning of the transient is presented in Fig. 7. It can be seen that the time error is kept below and close to the tolerance adopted (10%), which is in some sense optimal. The spatial errors present similar values, the global estimators (η) are basically the same (5.9%). However, the purged estimators (η^{**}) present some difference, $\eta^{**} = 3.22$ with adaptation and $\eta^{**} = 0.64$ with fixed step. This is an interesting result that demonstrates an interdependence of the two parts of the discretized error. To cover the time of the analysis presented here only 18 steps were necessary against 130 when no adaptation is used. A detail of the solution along the domain at the end of this interval shows no lost of quality in the solution when the adaptation is used (Fig. 8).

It is very important to use a limiter in the relation between the step size in each interval to preserve the quality of the solution. It was observed that a compromise between the cost and quality of the solution is influenced by this parameter. If the maximum norm $\| \ \|_\infty$ was used one could expect more freedom in that choice, but it could be conservative. The use of a technique for eliminating the domain where the solution has converged (presented by Devloo (1987) in a different context) seems to be doubly promising. Firstly, it reduces the number of equations to be computed; and secondly, only the region where the transient solution still exists will contribute to the error evaluation, which results in

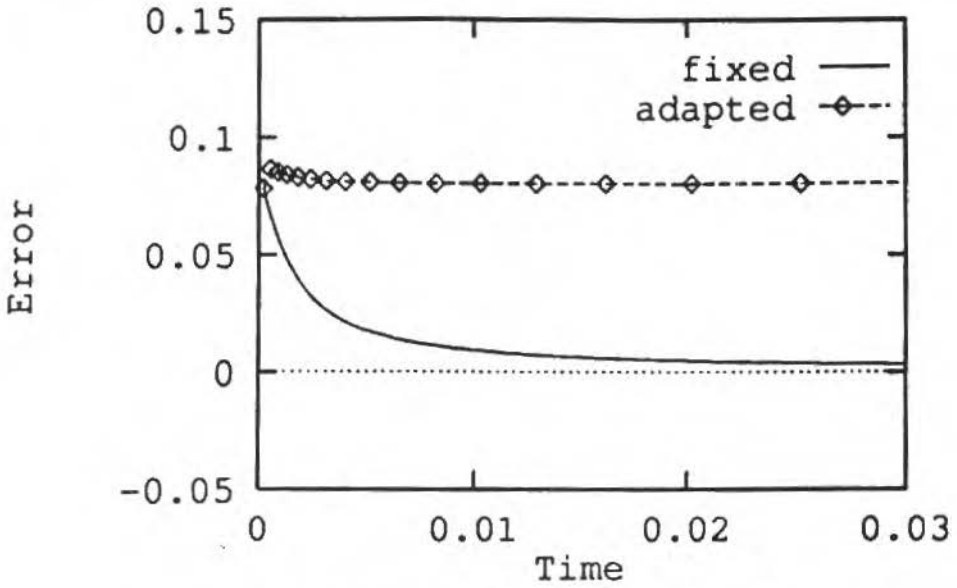

Fig. 7 Time Discrete Error History Using Fixed and Adaptive Time Step

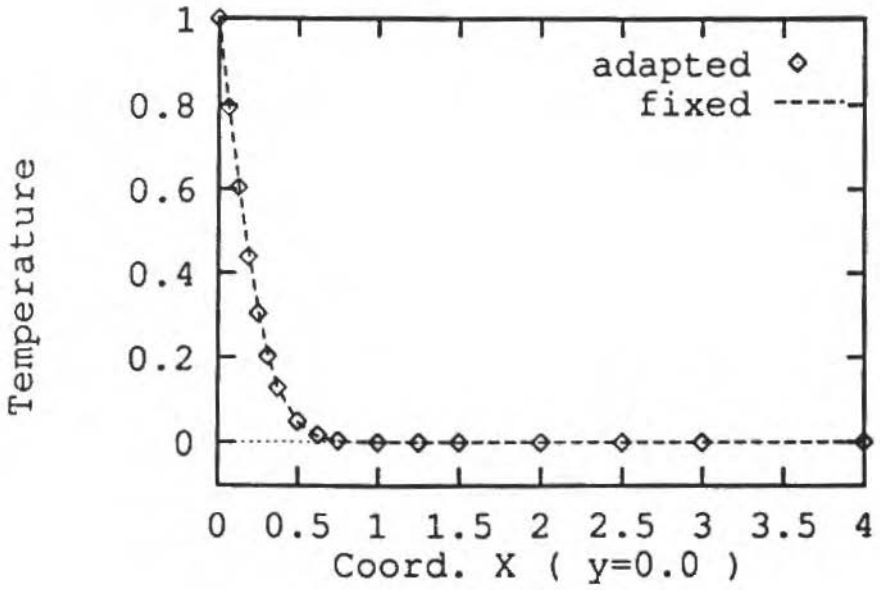

Fig 8 Detail of the Temperature Distribution at Time 3.1E-02

reduction in the increase of the time step. Consequently, good results are expected for the whole domain when the solution is close to the steady-state, even if a bigger value of the limit in time step relation is used.

The second application consists of an "infinite" domain with a punctual heat source. The finite discrete model adopted in the analysis and the physical characteristics are presented in Fig. 9. The

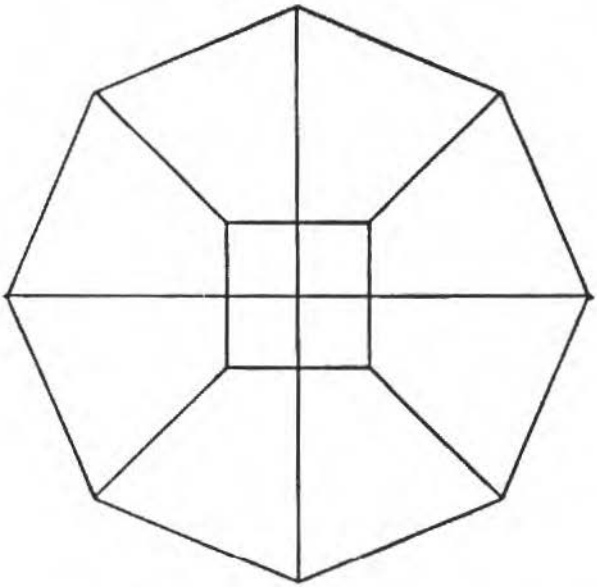

Fig. 9 Initial Discrete Model and Problem 2 Description

domain was truncated at a distance r = 250.0m , the adopted tolerance in both space (η) and time (μ) discrete error was 20%. The maximum level of refinement was again 6 and the limit in the time step relation 2.

Punctual heat source:

$$\text{limit}\frac{\partial\phi}{2\pi rK}\ (t>0)$$

Boundary conditions:

$$\phi = \phi_0 \quad r \to \infty\ (t>0)$$

Initial conditions:

$$\phi = \phi_0 \quad \forall r \geq 0 \text{ at } t = 0$$

where: $\phi_0 = 0.0\,^{\circ}C$
$k = 1.0\ W/m^{\circ}C$
$C = 1.0E\text{-}8\ Wsm^{3}{}^{\circ}C$

$Q = 1.6$ W/m

The final meshes obtained using the transient and also the steady-state strategies are presented in Fig. 10, and are similar. The global error estimators (η) in the steady-state for both strategies are

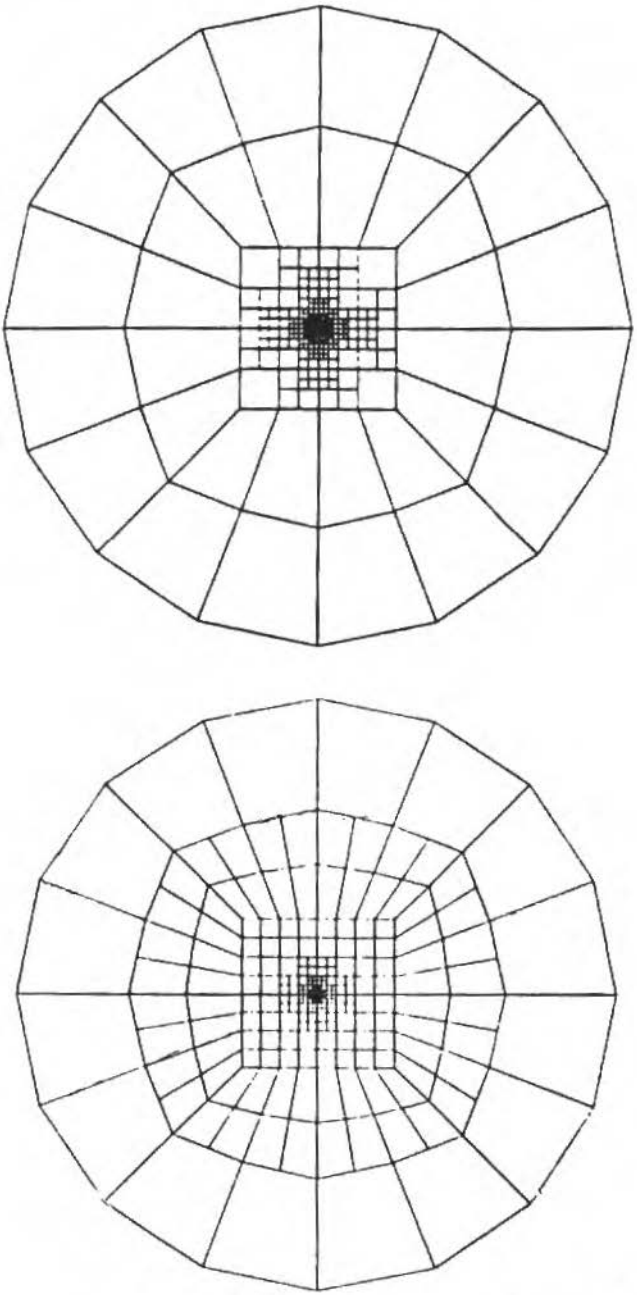

Fig. 10 Final Meshs: a) Transient Analysis; b) Steady-State Analysis

37.33% and 37.59%, and the purged error estimators (η^{**}) are 6.99% and 4.76%, respectively. The criteria adopted to deal with higher order singularities (Remark A.5) was activated in both cases.

An outline of the solution distribution for some sample times is depicted in Fig. 11. The solution at

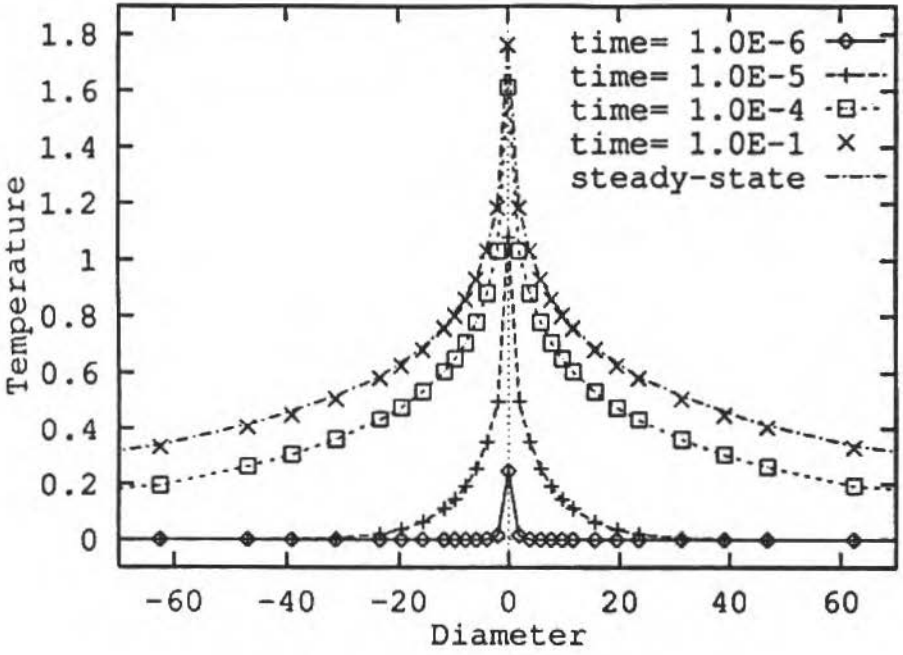

Fig. 11 Temperature Distribution at Sample Times.

time 1.0E-04 and also at the steady-state are presented in Fig. 12, together with the "analytical" solution (in fact, an approximate solution using the second class Bessel functions).

The results are not very good since a crude tolerance in the error analysis was adopted and also because the "analytical" solution could not be exact enough. The space and time discrete error evolution are presented in Fig. 13 and 14.

The incompatible limit in the maximum number of refinement (maxlevel = 6) with the tolerance adopted and also the use of the criteria to deal with higher order singularities can be observed in Fig. 14. More refinement in space must be allowed in order to reduce the global error to the pre-assigned standard (20%); however, outside the neighborhood of the singularity the error was kept well below the tolerance. The error in time also depicts the behavior of the problem, in which a heat source was suddenly activated at the beginning. If no constraint was adopted the time step obtained by the adaptive strategy was 2.33E-12. Once the stability time step limit in that problem is equal to 9.54E-09 the use of the lower limit described in remark B.2 is justified.

The time step evolution presents a similar behavior as the one presented in Fig. 4. The solution for some sample points are presented in Fig. 15.

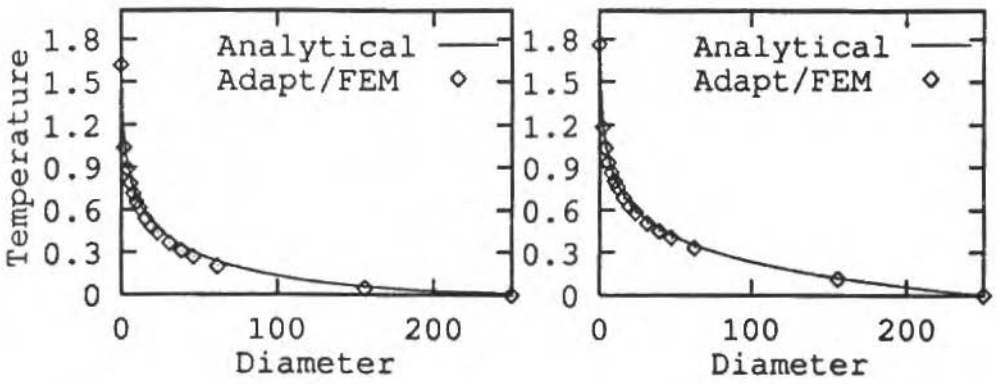

Fig. 12 - Temperature Distribution: a) At time 1.0E-04: b) At Steady-State

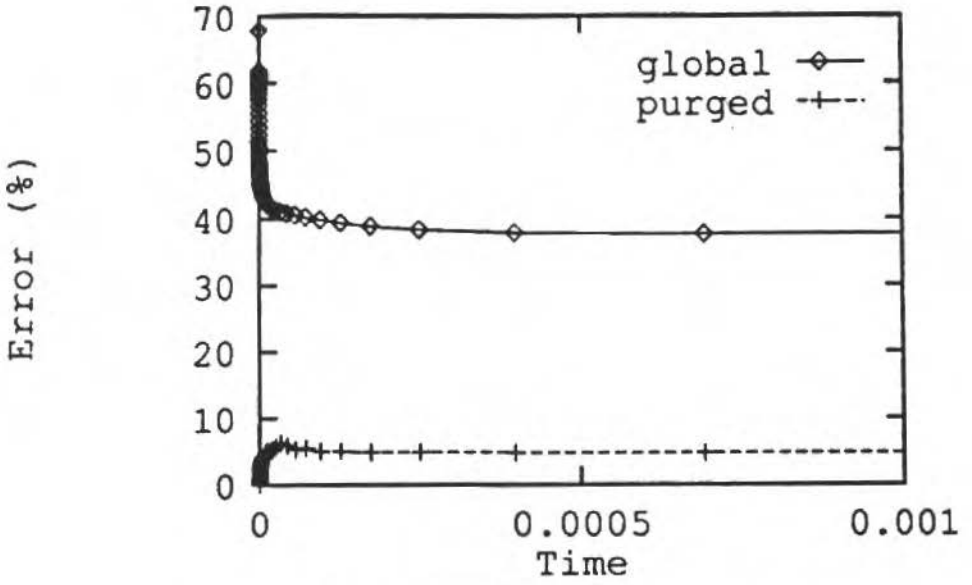

Fig. 13 - Space Discrete Error History

Using the mesh described in Fig. 10a, with a fixed time step equal to the stability limit, the same problem was run. The detail of the beginning of the discrete time error evolution is presented in Fig. 16. It can be noted how conservative and inefficient the use of fixed time step can be, since the error becomes much smaller than the tolerance adopted.

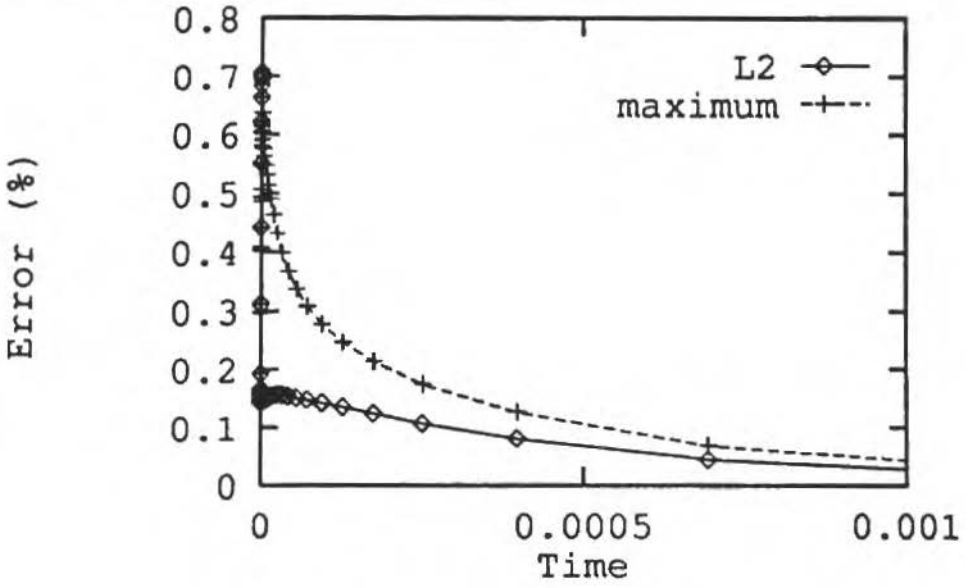

Fig. 14 Time Discrete Error History

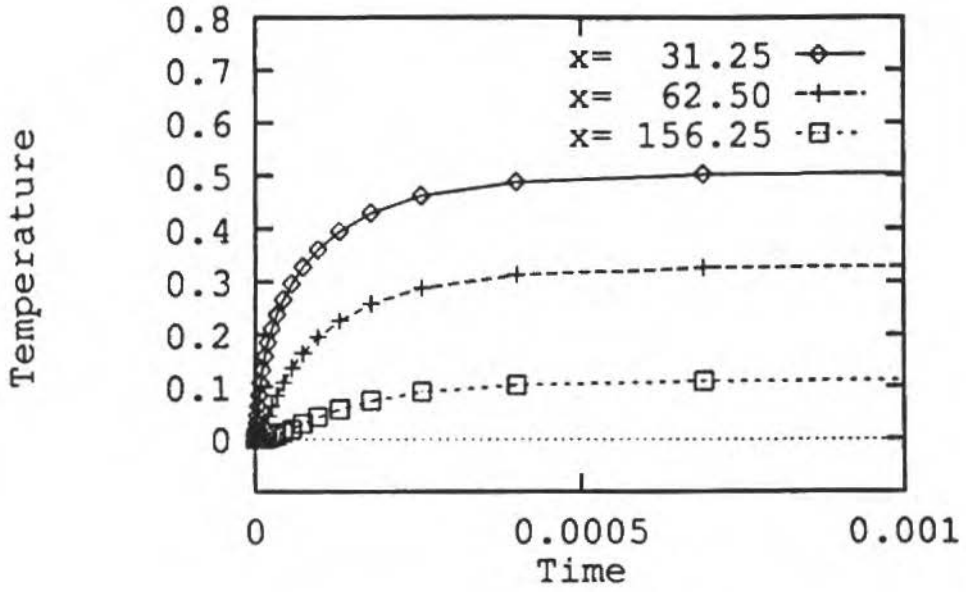

Fig. 15 Temperature Distribution at Sample Points

A reasonable agreement was achieved for the solution using fixed or adapted steps; these results are presented in Figs. 17 and 18. It must be noted that to reach the time level 0.1, which already characterizes the steady-state, only 83 steps were necessary with adaptive time stepping, against approximately 1E+07 steps that would be necessary if the step was kept fixed until the same time level.

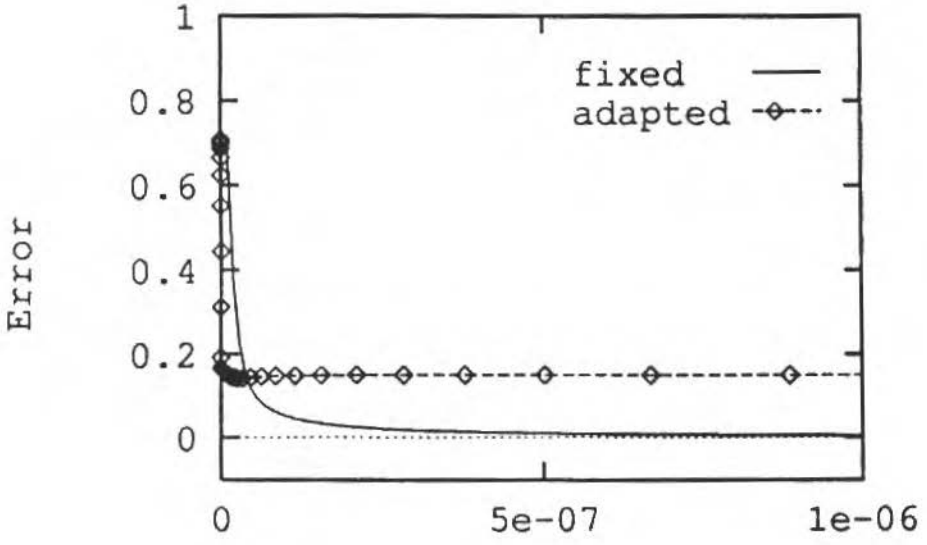

Fig. 16 Time Discrete Error History Using Fixed and Adaptive Time Step

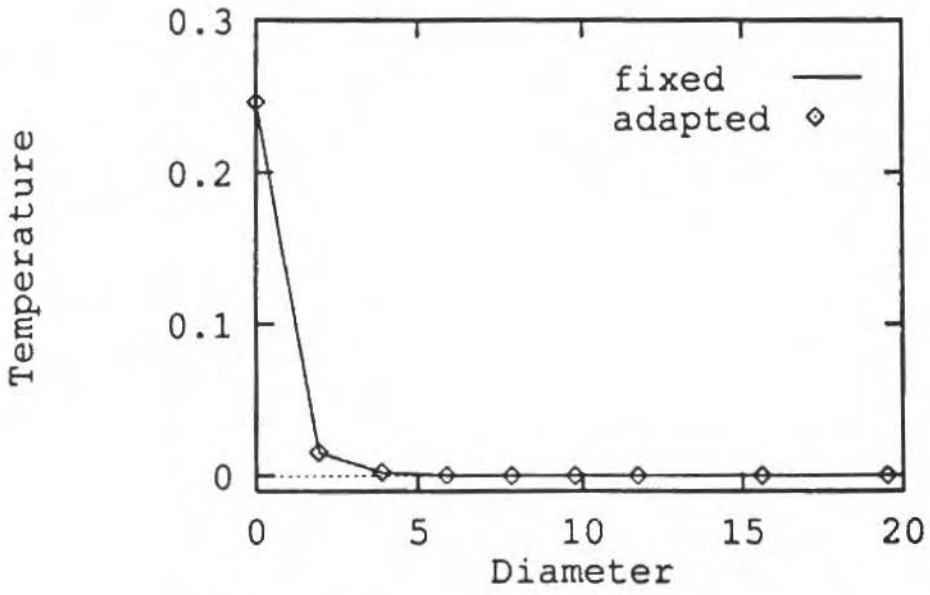

Fig. 17 Detail of the Temperature Distribution at Time 0.36E-05

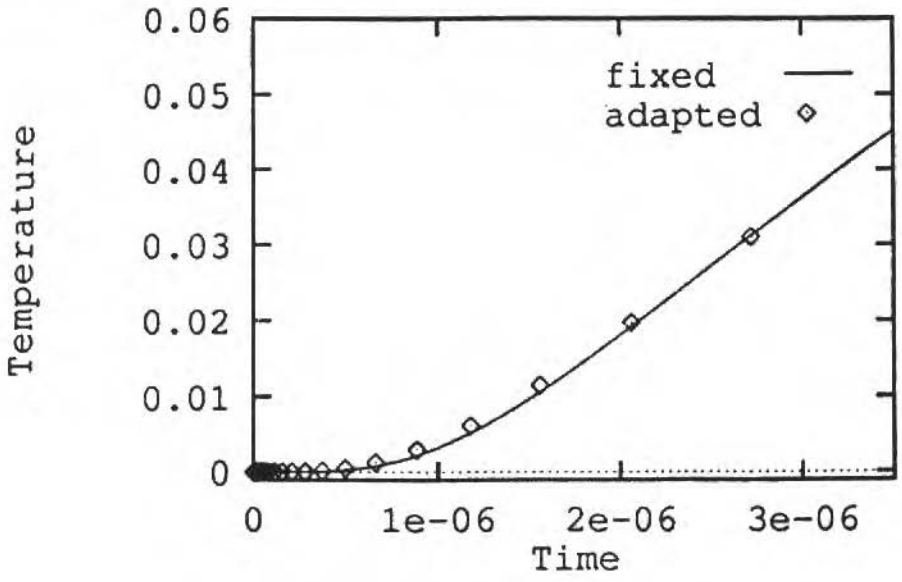

Fig. 18 Temperature at x = 31.25

Conclusions

Adaptive procedures save time in data preparation or mesh input data and provide more efficient and reliable results, mainly with poor predictability or in which the analyst has no previous experience.

Although the analysis presented for the simple model problems described are not conclusive, they give some insight in the characteristics of the proposed transient mesh refinement procedure. It is important to emphasize that the techniques adopted are robust in the sense that they are stable and free from any kind of oscillation.

In order to have a full adaptive scheme for parabolic problem it is necessary to adapt the step also in space. Johnson, Nie and Thomee (1990) have already proposed some ideas in this area. Another approach consists in subdividing the mesh and having an implicit-explicit algorithm where in the implicit part the time step is adapted similarly to the way shown here.

To ensure major flexibility and to allow more complex problems, as for example, when the heat source is moving, Dechaumphai and Morgan (1990) the derefinement capabilty is essential, and the unstructured remeshing technique presents itself as the best choice to be combined with the ideas here described.

Acknowledgment

The author would like to acknowledge the financial support of CNPq (Brazilian Research Council) and to thank his colleague Dr. Marcio M. de Farias for the English revision.

References

Babuska, I., and Rheinboldt, W.C., (1978), "A Posteriori Error Estimates for the Finite Element Method", Int. J. Numer. Methods Eng., Vol. 12, pp. 1597-1615.

Bettencourt, J.M., Zienkiewicz, O.C., and Cantin, G., (1983), "Consistent use of Finite Elements in Time and the Performance of Various Recurrence Schemes for Heat Difusion Equation", Int. J. Numer. Methods Eng., Vol. 17, pp. 931-938.

Brauchli, H.J., and Oden, J.T.,(1971), "On the Calculation of Consistent Stress Distribution in Finite Element Applications", Int. J. Numer. Methods Eng., Vol. 3, pp. 317-325.

Briggs, L.W., (1987), "A Multigrid Tutorial", Society for Industrial and Applied Mathematics, Philadelphia, Pennsylvania.

Cantin, G., Loubignac, G., and Touzot, G., (1978), "An Iterative Algorithm to Build Continuous Stress and Displacement Solutions", Int. J. Numer. Methods Eng., Vol. 12, pp. 1493-1506.

Damjanic, F., and Owen, D.R.J., (1982), "Practical Considerations for Thermal Transient Finite Element Analysis Using Isoparametric Elements", Nuclear Engineering Design, Vol. 69, pp. 109-126.

Dechaumphai, P., and Morgan, K., (1990), "Transient Thermal-Structural Analysis Using Adaptive Unstructured Remeshing and Mesh Movement", First Thermal Structures Conference, University of Virginia, Virginia, November 13-15.

Demkowicz, L., Devloo, P.B.R., and Oden, J.T., (1985), "On an H-Type Mesh Refinement Strategy Based on a Minimization of Interpolation Error", Comp. Methods Appl. Mech. Eng., Vol. 03, pp. 67-89.

De Sampaio, P.A.B., (19__), "A Petrov-Galerkin Formulation for the Incompressible Navier-Stokes Equations using Equal Order Interpolation for Velocity and Pressure", Int. J. Num. Meth. Eng., Vol. 31, pp. 1135-1149.

Devloo, P.B.R., (1987), "An H-P Adaptive Finite Element Method for Steady Compressible Flow", PhD Thesis, The University of Texas at Austin.

Gago, J.P.R., Kelly, D.W., Zienkiewicz, O.C., and Babuska, I., (1983), "A Posteriori Error Analysis and Adaptive Processes in the Finite Element Method, Part II", Int. J. Numer. Methods Eng., Vol. 19, pp. 1621-1656.

Hinton, E., and Campbell, J., (1974), "Local and Global Smoothing of Discontinuous Finite Element Functions Using a Least Square Method", Int. J. Numer. Methods Eng., Vol. 8, pp. 461-480.

Hinton, E., Rock, T., and Zienkiewicz, O.C., (1976), "A Note on Mass Lumping and Related Processes in The Finite Element Method", Earthquake Engineering and Structural Dynamics, Vol. 4, pp. 245-249.

Hirsch, C., (1989), "Numerical Computation of Internal and External Flows, vol. 1: Fundamentals of Numerical Discretization", John Wiley & Sons.

Hughes, T.J.R., (1977), "Unconditionally Stable Algorithms for Nonlinear Heat Conduction", Comp. Meth. in Appl. Mech. and Engng., Vol. 10, pp. 135-139.

Hughes, T.J.R., (1987), "The Finite Element Method: Linear Static and Dynamic F. E. Analysis", Prentice-hall.

Hughes, T.J.R., and Liu, W.K., (1978), "Implicit-Explicit Finite Element in Transient Analysis: Implementation and Numerical Examples", J. Appl. Mech., Vol. 2, pp. 375-378.

Johnson, C., (1987), "Numerical Solution of Partial Differential Equations by the Finite Element Method", Cambridge University Press.

Johnson, C., Nie, Y.Y., and Thomee, V., (1990), "An a Posteriori Error Estimate and Automatic Time Step Control for a Backward Discretization of a Parabolic Problem", SIAM, Journal of Numerical Analysis, Vol. 27 - nº 2, pp. 277-291.

Lyra , P.R.M., Coutinho, A.L.G.A., Alves, J.L.D., and Landau, L., (1988), "An h-Version Auto-Adaptive Refinement Strategy for the Finite Element Method", IX Congresso Ibero-Latino-Americano sobre Métodos Computacionales para Ingenierià, Cordoba, Argentina.

Lyra , P.R.M., Alves, J.L.D, Coutinho, A.L.G.A., Landau, L., and Devloo, P.R.B., (1989), "Comparison of Local Mesh Refinement Strategies for the H-Version of FEM", X Congresso Ibero-Latino-Americano sobre Métodos Computacionais em Engenharia, Vol.2, pp. A/595-A/610, Porto, Portugal.

Murti, V., Valliappan, S., and Khalili-Naghadeh, N., (1989), "Time Step Constraints in finite Element Analysis of Poisson Type Equation", Comput. Meths. Appl. Mech. Engng., Vol. 31, nº 2, pp. 269-273.

Owen, D.R.J., and Damjanic, F., (1981), "The Stability of Numerical Time Integration Techniques for Transient Thermal Problems with Special Reference to Reduced Integration Effects", Num. Meth. in Thermal Problems Conf. Proc., Vol. 2, pp. 487-505, Pineridge Press, Swansea.

Peraire, J., Vahdati, M., Morgan, K., and Zienkiewicz, O.C., (1987), "Adaptive Remeshing for Compressible Flow Computations", Journal of Computational Physics, Vol. 72, pp. 449-466.

Press, W.H., Flannery, B.P., Teukolsky, S.A., and Vetterling, W.T., (1988), "Numerical Recipes: The Art of Scientific Computing", Cambridge U. Press.

Rank, E., Katz, C., and Werner, H., (1983), "On the Importance of the Discrete Maximum Principle in Transient Analysis Using Finite Element Method", Int. J. Numer. Meth. Engng., Vol. 19, pp. 1771-1782.

Smolinski, P., (1991), "A variable Multi-Step Method for Transient Heat Conduction", Computer Methods in Applied Mechanics and Engineering, Vol. 86, pp. 61-71.

Tezduyar, T.E., and Liou, J., (1990), "Adaptive Implicit-Explicit Finite Element Algorithms for Fluid Mechanics Problems", Computer Methods in Applied Mechanics and Engineering, Vol. 78, pp. 165-179.

Zhu, J.Z., and Zienkiewicz, O.C., (1990), "Superconvergence Recovery Technique and A Posteriori Error Estimators", Int. J. Numer. Meth. Engng., Vol. 30, pp. 1321-1339.

Zienkiewicz, O.C., and Morgan, K., (1983), "Finite Elements and Approximation", John Wiley & Sons.

Zienkiewicz, O.C., and Zhu, J.Z., (1987), "A Simple Error Estimator and Adaptive Procedure for Practical Engineering Analysis", International Journal for Numerical Methods in Engineering, Vol. 24, pp. 337-357.

Zienkiewicz, O.C., and Taylor, R.L., (1989), "The Finite Element Method", 4th Ed., Vol. 1, McGraw-Hill, London.

Zienkiewicz, O.C., and Zhu, J.Z., (1991), "Superconvergent Recovery Techniques and a Posteriori Error Estimation in the F.E.M.", part 1: "A General Superconvergent Recovery Technique", Report of INME, University College of Swansea, CR/671/91, also submitted to Int. J. for Numerical Meth. in Engineering.

RBCM - J. of the Braz. Soc. Mechanical Sciences
Vol. XV - nº 2 - 1993 - pp. 199-207

ISSN 0100-7386
Printed in Brazil

Comportamento Mecânico em Compressão Uniaxial de um Compósito Epoxi-Alumina.

Uniaxial Compression Mechanical Behavior of an Alumina-Epoxy Composite

Fabio Horta Motta Marques da Costa
José Roberto Moraes d'Almeida
Dep. Ciência dos Materiais e Metalurgia
Pontifícia Universidade Católica do Rio de Janeiro
22453-900 - Rio de Janeiro - RJ

Resumo

Neste trabalho é feita a análise do comportamento mecânico em compressão uniaxial de um compósito epoxi-alumina e da matriz epoxi sem reforço. A incorporação das partículas de alumina, mesmo em frações volumétricas pequenas, acarreta uma mudança significativa no modo de falha do material. A falha explosiva, característica do comportamento da matriz epoxi em compressão, é alterada para uma falha estável no compósito. O aumento da energia absorvida no processo de fratura do compósito, em relação à matriz epoxi sem reforço, foi atribuído a parcela de energia de propagação. Os mecanismos de aumento da energia de propagação foram identificados como sendo ancoragem e/ou desvio de trinca nas interfaces partícula-matriz.
Palavras-Chave: Compósito, Reforço por Partículas, Ancoragem de Trinca, Energia na Fratura.

Abstract

The mechanical behaviour in uniaxial compression of an alumina-epoxy composite and its neat matrix epoxy resin was analysed. The incorporation of the alumina particles produced a marked change in the failure mode of the composite. The common neat resin burst failure was changed to a stable composite failure, even with the low volume fraction of alumina particles used in this work. The composite has a higher energy at fracture than the epoxy resin matrix and this difference was attributed to the propagation energy term. Crack anchoring and deflexion at the resin-alumina interfaces were identified as the main energy absorbing mechanisms.
Keywords: Composite, Particle Reinforcement, Crack Anchoring, Fracture Energy.

Introdução

Polímeros termofixos são, na atualidade, largamente usados como adesivos e como matrizes em compósitos. Entretanto, estes materiais são frágeis, apresentando valores extremamente baixos tanto para o fator de intensidade de tensões (K_{1c}), como para a taxa de liberação de energia (G_{1c}). Tipicamente, para as resinas epoxi, os valores de K_{1c} e G_{1c} variam entre 0,6-0,8 $MPam^{1/2}$ e 0,1-0,2 kJm^{-2}, respectivamente (Bandyopadhyay, 1990).

Com o objetivo de aumentar a tenacidade pode-se incorporar diferentes cargas aos polímeros termofixos, tais como fibras, elastômeros e partículas rígidas (Low e May, 1988; Bandyopadhyay, Pearce e Mestan, 1985; Kinloch, Maxwell e Young, 1985) ou mesmo polímeros termoplásticos (Bucknall e Gilbert, 1989).

O mecanismo de aumento de tenacidade atuante é função do tipo de interação entre a frente de trinca e as cargas. Para compósitos de matriz polimérica os mecanismos propostos são: i) ancoragem e/ou deflexão da trinca (Low e Mai, 1988; Lange e Radford, 1971), ii) manutenção da união entre as faces da trinca por partículas elastoméricas estiradas ou por fibras (Bandyopadhyay, Pearce e Mestan, 1985) e iii) desenvolvimento de deformação plástica localizada na ponta da trinca (Kinloch, Maxwell e Young, 1985). A incorporação de partículas rígidas acarreta, ainda, um aumento da rigidez do compósito fabricado.

Este trabalho tem por objetivo analisar o efeito da incorporação de partículas rígidas sobre o comportamento mecânico, em compressão uniaxial, de um compósito polimérico com matriz epoxi e partículas de alumina. Os micromecanismos de fratura atuantes no compósito são analisados e comparados aqueles da matriz sem reforço.

Manuscript received: July 1993. Associate Technical Editor: Agenor de Toledo Fleury

Material e Procedimento Experimental

Usou-se como matriz um sistema epoxi de cura a frio, formado pela resina epoxi bifuncional diglicídil éter do bisfenol A (DGEBA, DER 331), tendo como agente de cura uma poliamina alifática (trietileno tetraamina, TETA, DEH 24). Partículas rígidas de alumina (A16SG, ALCOA) com grau de pureza de 99,9% e tamanho médio de 0,26 μm foram usadas como carga. A razão resina/ agente de cura/ carga empregada na preparação dos compósitos foi de 100/13/30 partes, em peso.

Os compósitos foram fabricados pela incorporação da alumina à resina já pré-formulada com o agente de cura. Este procedimento diminui o tempo disponível para a homogeneização da mistura antes do início da gelatinização, porém impede que se forme um gradiente na distribuição das partículas ao longo da espessura da amostra. Antes da incorporação, a alumina foi seca e peneirada para diminuir a tendencia a formação de aglomerados. A mistura homogeneizada foi vazada em molde aberto de alumínio com área de 100×220 mm^2 e 15 mm de espessura. Placas de resina sem reforço foram obtidas de modo similar.

A densidade do compósito fabricado foi medida segundo a norma ASTM D792-86. As frações volumétricas de carga (V_p) e de vazios (V_v) foram obtidas a partir das equações da micromecânica de compósitos (Schoutens, 1984), a saber:

$$V_p = \frac{1}{\rho_p - \rho_m}\left[\rho_c - \rho_m (1 - V_v)\right] \qquad (1)$$

$$V_v = 1 - \rho_c \left(\frac{M_p}{\rho_p} + \frac{M_m}{\rho_m}\right) \qquad (2)$$

onde ρ é a densidade e M a fração em massa. Os índices p, m e c designam a carga de alumina, a matriz e o compósito, respectivamente. Para os cálculos de V_p e V_v foram tomados valores padrões tabelados para as densidades da matriz epoxi e de alumina ($\rho_m = 1160$ kg/m^3 e $\rho_p = 2970$ kg/m^3).

O cálculo das frações volumétricas a partir das equações 1 e 2 foi adotado porque, conforme discutido abaixo, o emprego de microscopia quantitativa não forneceu bons resultados, devido as características da microestrutura do compósito.

Os ensaios de compressão foram realizados em máquina de ensaios de acionamento mecânico, a velocidade nominal constante de $V = 1{,}7 \times 10^{-5}$ m/s. De acordo com a norma ASTM D695M foram usados corpos de prova prismáticos (ou cilíndricos) com 20 mm de comprimento e 10×10 mm de seção (ou 10 mm de diâmetro). Os valores reportados são a média de pelo menos 05 ensaios.

Os corpos de prova fraturados foram analisados por microscopia ótica (MO). As superfícies de fratura foram analisadas por microscopia eletrônica de varredura (MEV) no modo secundário e com voltagem de aceleração do feixe de elétrons entre 15-20 kV. Para evitar acúmulo de carga, as fraturas foram recobertas com uma camada condutora de ouro-paládio.

Nomenclatura

G_{Ic} = taxa de liberação de energia
K_{Ic} = fator de intensidade de tensões
M_m = fração em massa da resina matriz
M_p = fração em massa de partículas
P = carga aplicada
V_p = fração volumétrica de partículas
V_v = fração volumétrica de vazios
U = densidade de energia total
U_{cm} = densidade de energia até a carga máxima
U_p = densidade de energia de propagação
ρ_c = densidade do compósito
ρ_m = densidade da matriz
ρ_p = densidade das partículas
ε = deformação
σ = tensão
σ_r = tensão de ruptura
σ_y = tensão de escoamento
Δl = deslocamento

Resultados Experimentais

A Fig. 1 mostra uma microestrutura típica do compósito fabricado. Dois aspectos podem ser

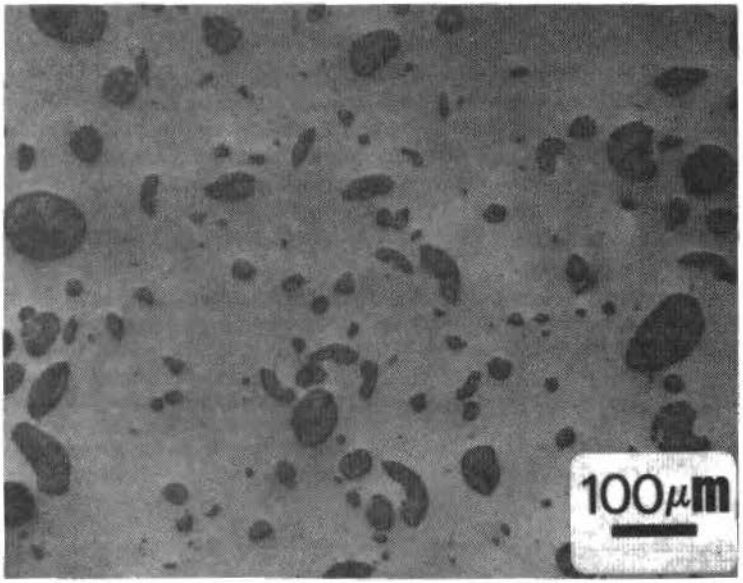

Fig. 1 Microestrutura do compósito epoxi-alumina. As partículas de alumina formam aglomerados com diâmetro variável.

destacados nesta micrografia: i) observa-se um baixo teor de vazios e ii) as partículas de alumina formam aglomerados com tamanhos variáveis. A presença destes aglomerados dificultou a medição da fração volumétrica pelos métodos usuais de microscopia quantitativa (da Silva, Jr et al., 1991) devido a dificuldade de se definir, dentro dos aglomerados, a matriz das partículas de alumina. Na Tab. 1 estão listados os valores das frações volumétricas calculadas pelas equações 1 e 2 e o valor medido para a densidade do compósito.

Tabela 1 Frações volumétricas de partículas e vazios e densidade do compósito

ρ (kg/m^3)	1.400
V_p (%)	8
V_v (%)	~0

Na Fig. 2 está mostrado o aspecto geral das curvas carga, P, vs deslocamento, Δl, obtidas para a resina sem carga e o compósito. Os resultados dos ensaios estão listados na Tab. 2. Como esperado, a incorporação de partículas rígidas acarretou um aumento no módulo de elasticidade e na tensão de escoamento do compósito. Entretanto, a principal diferença entre o compósito e a resina matriz é a mudança no comportamento à fratura. As amostras de resina sem carga fraturam explosivamente, enquanto nos compósitos a fratura ocorre de um modo controlado, sem estilhaçamento dos corpos de prova (Fig. 3).

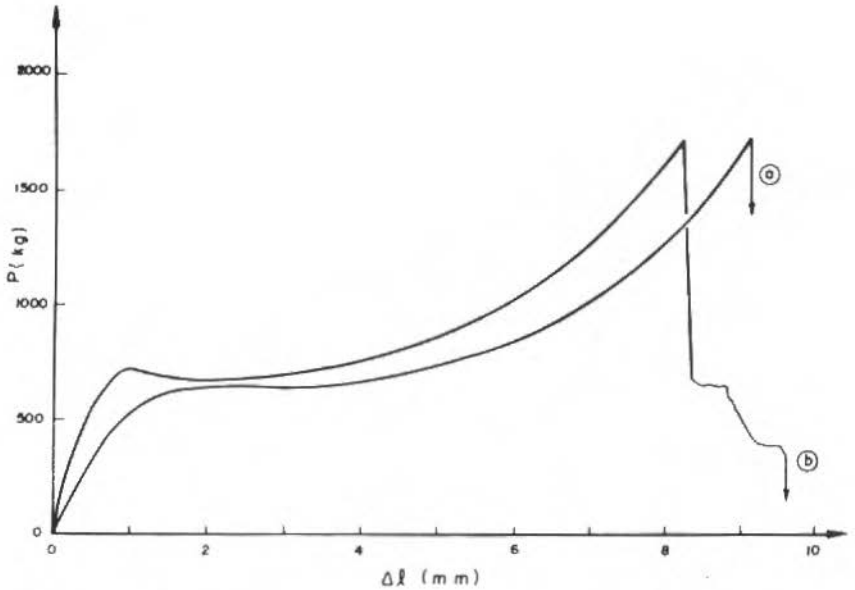

Fig. 2 Forma genérica das curvas experimentais carga (P) vs deslocamento (Δl) obtidas nos ensaios de compressão. a) resina epoxi e b) compósito

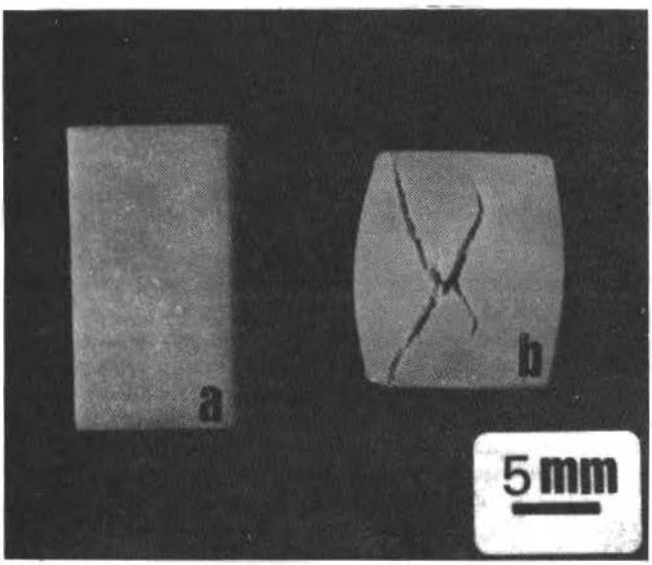

Fig. 3 Aspecto geral dos corpos de prova do compósito antes (a) e depois (b) do ensaio.

Tabela 2 Propriedades mecânicas. Módulo de elasticidade (E), tensão de ruptura (σr) e tensão de escoamento (σy)

	Matriz	Compósito
E(GPa)	2.04∓0.1	2.91∓0.09
σr (MPa)	257∓21	254∓7
σy (MPa)	92∓5	100∓1

Análise dos Resultados

A observação macroscópica do modo de falha das amostras indica que existe uma grande mudança no comportamento à fratura entre o compósito e a resina pura. Na superfície de fratura da matriz epoxi sem reforço existem apenas estrias semelhantes as descritas por Atsuta e Turner (1982) e que são formadas pela junção, através de mecanismos de deformação plástica localizada, de trincas que se propagam em planos próximos (Fig. 4).

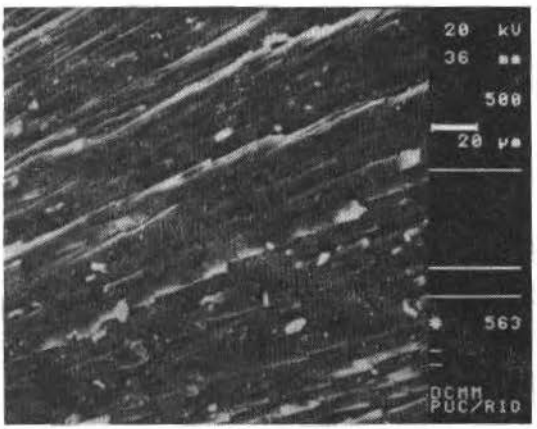

Fig. 4 Superfície de fratura da matriz epoxi. As marcas topográficas são estrias formadas pela junção de trincas que se propagam em planos diferentes.

A ocorrência de plasticidade localizada é o principal mecanismo de deformação em polímeros termofixos (Smith, Kaiser e Roulin-Moloney, 1988). Assim sendo, o comportamento à compressão uniaxial da resina epoxi DGEBA/TETA é governado pela capacidade deste material sustentar um processo de deformação plástica. Uma vez exaurido este processo a ruptura ocorre de forma abrupta, com a propagação instável de trinca, que leva a um estilhaçamento dos corpos de prova. O estilhaçamento, que é provocado pela ramificação das trincas, indica que estas já haviam atingido sua máxima velocidade de propagação e que a energia extra disponível foi liberada pela criação de novas superfícies (Ravi-Chandar e Knauss, 1984; Cantwell, Roulin-Moloney e Kaiser, 1988). Em alguns casos foi possível identificar na superfície de fratura regiões de transição mostrando estrias e, também, uma área com superfície lisa (Fig. 5). A morfologia lisa é característica de fratura instável em regiões sob compressão (d'Almeida e Graça, 1990).

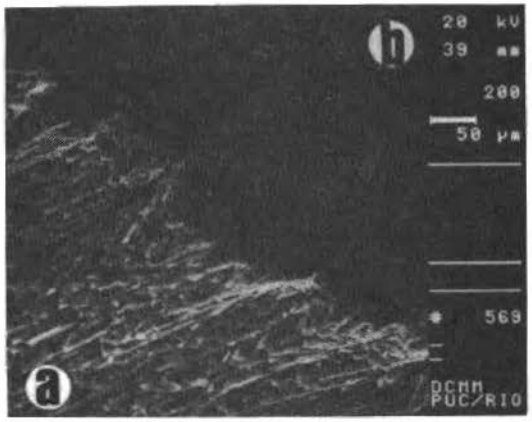

Fig. 5 Região de transição na fratura da matriz epoxi. a) estrias e b) região lisa caracteristica de fratura instável.

Por outro lado, na superfície de fratura do compósito foram observadas diferentes marcas topográficas superficiais (Fig. 6). Além das marcas de deformação plástica na matriz epoxi, observam-

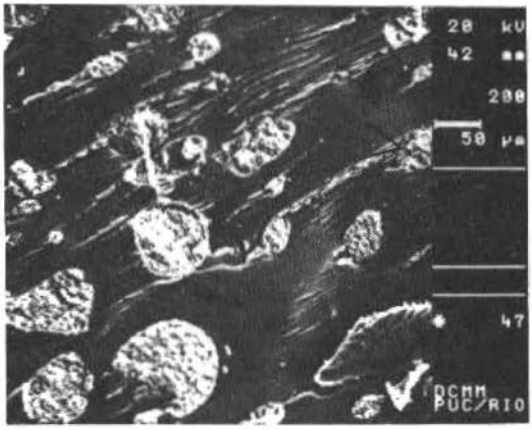

Fig. 6 Superfície de fratura do compósito mostrando marcas características de ancoragem de trinca (⟶) interfaces rompidas (—▷) e deformação plástica localizada na matriz epoxi (➡).

se marcas características de ancoragem de trinca e decoesão na interface partícula-matriz. Estes dois últimos aspectos topográficos indicam que o processo de fratura dos compósitos alumina-epoxi, aqui estudado, pode ser subdividido em duas etapas distintas, a saber:

i) nos primeiros estágios do carregamento, com a matriz rigidamente ligada às partículas, a resina epoxi, que tem propriedades elásticas menores que as das partículas, tem a sua deformação restringida pelas partículas. Esta restrição à deformação da matriz gera um estado de tensão hidrostático na região da matriz próximo as partículas (Krock, 1967). A falha da interface resulta em uma mudança do estado de deformação plana para tensão plana. A matriz pode, então, escoar livremente. Assim, nas regiões próximas a interfaces rompidas observa-se a maior concentração de marcas de deformação plástica na

matriz (Fig. 7). Esta restrição imposta pelas partículas à deformabilidade da matriz resulta no aumento

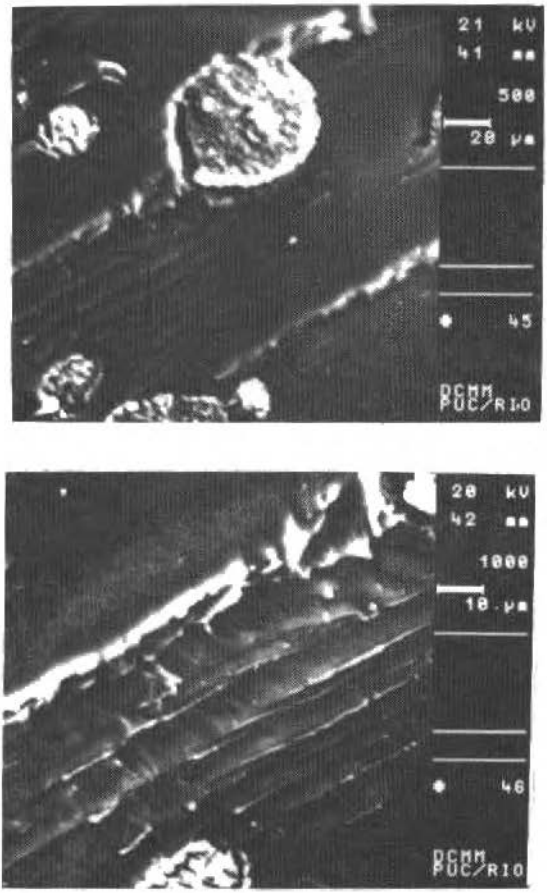

Fig. 7 Marcas de deformação plástica localizada na matriz epoxi, adjacentes a interfaces rompidas. a) Aspecto geral e b) Detalhe da área marcada na fig. 7a.

do limite de escoamento e da curva σ vs ε nominal do compósito em relação à matriz sem reforço, porém, implica em uma redução da deformação na tensão nominal máxima do compósito (cf., Fig. 2).

ii) exaurida a capacidade de deformação plástica na matriz, as trincas existentes e nucleadas preferencialmente nas interfaces são aceleradas, resultando na perda da capacidade do material suportar carga. Entretanto, a existência de interfaces abertas/íntegras atua no sentido de divergir/ancorar as trincas. A ancoragem de trinca pelas partículas de alumina ou o desvio da trinca nas interfaces rompidas representam mecanismos absorvedores de energia eficientes, que interferem no processo global de fratura, travando localmente a frente de trinca (Kinloch, Maxwell e Young, 1985; Nascimento, Abreu e d'Almeida, 1991) e reduzindo a velocidade de propagação (Kinloch, Maxwell e Young, 1985) devido a criação de múltiplas trincas secundárias (Bandyopadhay, 1990, Kinloch, Maxwell e Young, 1985). Deste modo, a falha do compósito ocorre de um modo controlado, sem ruptura catastrófica.

De fato, valores obtidos a partir de ensaios de tenacidade à fratura para o fator de intensidade de tensão, K_I, mostram que, para a velocidade de ensaio usada, a incorporação de alumina à matriz epoxi aumenta a tenacidade do compósito em relação a resina pura (d'Almeida, 1992).

Uma avaliação qualitativa da diferença descrita entre o processo de fratura em compressão do compósito e da resina sem carga, pode ser feita avaliando-se o valor da energia de deformação acumulada durante o ensaio (i.e., a área sob a curva P vs Δl). Na Tab. 3 estão listados os valores encontrados para a densidade de energia de deformação, sendo U a densidade de energia total, U_{cm} a densidade de energia até a carga máxima e U_p a densidade de energia de propagação. Pode-se ver que o aumento da energia de deformação total do compósito em relação ao polímero-matriz sem carga está associado, principalmente, ao termo de propagação (U_p). Esta parcela de energia é maior para o compósito e pode ser atribuída aos mecanismos de ancoragem e desvio de trinca pelos aglomerados de alumina.

Tabela 3 Densidade de energia de deformação ($J \times 10^{-6}/m^3$)

	U	U_{cm}	U_p
compósito	60,3	55,3	5,0
matriz	54,4	~54,0	<1

Conclusão

A introdução de partículas finas de alumina em uma resina epoxi bifuncional de cura a frio, altera o modo de falha em compressão do compósito em relação à matriz sem reforço. A diferença no comportamento à fratura foi associada a parcela de energia de propagação de trinca. Os mecanismos de ancoragem e desvio de trinca foram identificados como sendo os responsáveis pela maior resistência à propagação de trinca do compósito em relação à matriz.

Agradecimento

Os autores agradecem à Dow Química pelo fornecimento da resina epoxi e ao MCT pelo apoio financeiro.

Bibliografia

Atsuta, M. e Turner, D.T. (1982) "Fractography of Highly Crosslinked Polymers", Journal of Materials Science Letters, Vol. 1, pp. 167-169

Bandyopadhyay, S. (1990) "Rewiew of the Microscopic and Macroscopic Aspects of Fracture of Unmodified and Modified Epoxy Resins", Materials Science and Engineering, Vol. A125, pp. 157-184

Bandyopadhyay, S., Pearce, P.J. e Mestan, S.A. (1985) "Crack-Tip Micromechanics and Fracture Properties of Rubber Toughened Epoxy Resins", Proceeding of the 6th Churchill College Conference on Deformation, Yield and Fracture Polymers, paper 18, Cambridge, Inglaterra.

Bucknall, C.B. e Gilbert, A.H. (1989) "Toughening tetrafunctional epoxy resins using polyetherimide", Polymer, Vol. 30, pp. 213-217.

Cantwell, W.J., Roulin-Moloney, A.C. e Kaiser, T. (1988) "Fractography of Unfilled and Particulate-Filled Epoxy Resins", Journal of Materials Science, Vol. 23, pp. 1615-1631.

d'Almeida, J.R.M. (1992) "Epoxy and Alumina-Epoxy Composite Fracture Mechanisms Evaluation", Anais do Simpósio Íbero Americano de Polímeros, pp. 543-544, Vigo, Espanha.

d'Almeida, J.R.M. e Graça, M.L.A. (1990) "Influência do Estado de Tensão na Topografia de Fratura do Polimetilmetacrilato", Anais do II Micromat, pp. 213-216, São Paulo, Brasil.

da Silva, Jr, H.P., Paciornik, S., Galúcio, E.G. e d'Almeida, J.R.M. (1991) "Análise Metalográfica de Conjugado Epoxi-Microesferas Ocas de Vidro", Anais do XIII Colóquio da S.B.M.E., Vol. III, pp. 49-50, Caxambu, Brasil.

Kinloch, A.J., Maxwell, D.L. e Young, R.J. (1985) "The fracture of Hybrid-particulate composites", Journal of Materials Science , Vol. 20, pp. 4169-4184.

Krock, R.H. (1967) "Inorganic Particulate Composites", em Modern Composite Materials, Broutman, L.J. e Krock, R.H. eds., Addison-Wesley, Reading, Massachusetts, cap. 16.

Lange, F.F. e Radford, K.C. (1971) "Fracture Energy of an Epoxy Composite System", Journal of Materials Science, Vol. 6, pp. 1197-1203.

Low, I.M. e Mai, Y.W. (1988) "Micromechanisms of Crack Extension in Unmodified and Modified Epoxy Resins", Composites Science and Technology, Vol. 33, pp. 191-212.

Nascimento, R.S.V., Abreu, E.S.V. e d'Almeida, J.R.M. (1991) "Fractografia de Compósitos de Resina Epoxy e Microesferas de Cinzas de Carvão", Anais do XIII Colóquio da S.B.M.E., Vol. III, pp. 53-54, Caxambu, Brasil.

Ravi-Chandar, K. e Knauss, W.G. (1984) "An Experimental Investigation Into Dynamic Fracture: I. Crack Initiation and Arrest", International Journal of Fracture, Vol. 25, pp. 247-262.

Schoutens, J.E. (1984) "Simple and precise measurements of fibre volume and void fractions in metal matrix composite materials", Journal of Materials Science, Vol. 19, pp. 957-964.

Smith, J.W., Kaiser, T. e Roulin-Moloney, A.C. (1988) "Deformation-Induced Volume Damage in Particulate-Filled Epoxy Resins", Journal of Materials Science, Vol. 23, pp. 3833-3842.

RBCM - J. of the Braz. Soc. Mechanical Sciences
Vol. XV - nº 2 - 1993

ISSN 0100-7386
Printed in Brazil

Abstracts

Ferreira, J. R. and Cupini, N. L., 1993, "Choice of Tool in Turning of Carbon and Glass Fiber Reinforced Plastic" (In Portuguese), RBCM - J. of the Braz. Soc. Mechanical Sciences, Vol 15, n.2, pp. 112-123.

Experiments were carried out to study the performance of different tool materials. They were tested in turning of carbon and glass fiber reinforced fenolic resin composite. During the experiments, tool wear, surface roughness, and feed force behavior were observed. Experimental results showed that, due to the great influence of tool wear on workpiece surface roughness, only diamond tools are suitable for use in finish turning. In rough turning, the cemented carbide tools showed to be the best solution. Although it showed larger wear than diamond, the cost/benefit ratio is much lower and special precautions are not necessary.
Keywords: Machining - Tool - Composite Material

Melo, G. P. and Steffen Jr., V., 1993, "Mechanical Systems Identification Through Fourier Series Time Domain Technique", RBCM - J. of the Braz. Soc. Mechanical Sciences, Vol 15, n.2, pp. 124-135.

A time-domain technique based on Fourier series is used in this work for the parameters identification of mechanical systems with multi-degrees of freedom. The method is based on the orthogonality property of the Fourier series which enables the integration of the equations of motion. These equations are then converted to a linear algebraic model that is solved to obtain the unknown parameters. This way the method can be summarized as follows:
1. Expansion of the input and output signals in Fourier series;
2. Integration of the equations of motion using an operational matrix to integrate the series;
3. The parameters are calculated through a least-square estimation method.
Keywords: Parameter Identification - Modal Analysis - Time-Domain Technique - Fourier Series

Arruda, J. R. F. and Duarte, M. A. V., 1993, "Updating Rotor-Bearing Finite Element Models Using Experimental Frequency Response Functions", RBCM - J. of the Braz. Soc. Mechanical Sciences, Vol 15, n.2, pp. 136-149.

Most Finite Element model updating techniques require experimental modal parameters, which are obtained from modal tests. In the case of real rotor-bearing systems it is frequently unfeasible to perform complete modal tests due to difficulties such as exciting a rotating shaft and dealing with bearing nonlinearities. In this paper, the possibility of updating the Finite Element model of a rotor-bearing system by estimating the bearing stiffness and damping coefficients from a few measured Frequency Response Functions is investigated. The proposed model updating procedure consists of applying a nonlinear parameter estimation technique to correct a few FE model parameters chosen a priori. The parameter estimation problem is presented in its general form, from which the various methods can be derived, and then particularized to a nonlinear least squares problem where the objective function to be minimized is the sum of the square differences between the logarithm of the theoretical and experimental Frequency Response Function (FRF) magnitudes. The importance of using the logarithm of the magnitudes and its equivalence to the maximization of the correlation between the theoretical and experimental functions is pointed out. A closed form expression for the sensitivity matrix of the logarithm of the FRF magnitudes is derived, and it is shown that the finite differences approximation produces sufficiently accurate results at a much lower computational cost. The issues of identifiability and parameter estimation errors are addressed. A numerical example of a flexible rotor supported by two orthotropic bearings is presented to illustrate the proposed method.
Keywords: Rotor-Bearing - Finite Element Model - Frequency Response Functions

Almeida, C. A. and Pires Alves, J. A., 1993, "On Geometric Nonlinear FE Solution of Unidimensional Structure Dynamics", RBCM - J. of the Braz. Soc. Mechanical Sciences, Vol 15, n.2, pp. 150-164.

A numerical procedure for geometric nonlinear analysis of framed structures in presented. The finite element model employs 3-D linear to cubically varying space displacements and is capable of transmitting stress only in the direction normal to the cross-section. It is assumed that this normal stress is constant over the cross-sectional area, and that the area itself remains constant, allowing the element for large displacement analysis but under small strain condition. Two algorithms for the automatic incremental solution of the resulting nonlinear equilibrium equations in static analysis are accessed. These include the displacement control technique and the minimization of residual displacements, which allow to calculate the path response of general truss structures, even of those that exhibit unstable configurations. The formulation has been implemented and the results of various examples illustrate the element effectiveness in both static and dynamic analyses.
Keywords: Geometric Nonlinear Analysis - Automatic Incremental Solution - Displacement Control - Minimization of Residual Displacements

Estaleila, J. J. S., 1993, "Scientific Foundation of Mechanical Engineering" (in Spanish), RBCM - J. of the Braz. Soc. Mechanical Sciences, Vol 15, n.2, pp. 165-171.

The paper discusses the question of looking for the scientific foundations of technology in preference to the technological foundations of science.
Keywords: Science - Technology - Mechanical Engineering

Lyra, M. R. P., 1993, "Finite Element Analysis of Parabolic Problems: Combined Influence of Adaptive Mesh Refinement and Automatic Time Step Control", RBCM - J. of the Braz. Soc. Mechanical Sciences, Vol 15, n.2, pp. 172-198.

An adaptive finite element method with mesh refinement, by mesh enrichment, in time and space and an automatic time stepping control is described for a class of parabolic problems. The computational domain is represented by an assembly of 4-noded isoparametric elements. The mesh enrichment is achieved by locally subdividing each element into four new elements in those regions where further resolution is required during the analysis. The Euler backward time marching scheme is used and the time step sizes are gradually adapted. Both the space and the time discretization error estimation adopted involve only the computed approximate solution and those are use to dictate the adaptation. A discussion of the combined influence of time and spatial adaptation in the context of parabolic problems is also presented. Sample model applications are included to demonstrate the efficiency and accuracy, as well as the potentialities for engineering analysis, of the outlined procedure.
Keywords: Finite Element Analysis - Parabolic Problem - Adaptive Mesh Refinement - Automatic Time Step Control

Marques da Costa, F. H. M. and d'Almeida, J. R. M., 1993, "Uniaxial Compression Mechanical Behaviour of an Alumina-Epoxy Composite" (in Portuguese), RBCM - J. of the Braz. Soc. Mechanical Sciences, Vol 15, n.2, pp. 199-207.

The mechanical behaviour in uniaxial compression of an alumina-epoxy composite and its neat matrix epoxy resin was analysed. The incorporation of the alumina particles produced a marked change in the failure mode of the composite. The common neat resin burst failure was changed to a stable composite failure, even with the low volume fraction of alumina particles used in this work. The composite has a higher energy at fracture than the epoxy resin matrix and this difference was attributed to the propagation energy term. Crack anchoring and deflexion at the resin-alumina interfaces were identified as the main energy absorbing mechanisms.
Keywords: Composite - Particle Reinforcement - Crack Anchoring - Fracture Energy.

Journal of the Brazilian Society of Mechanical Sciences

Information for Authors

SCOPE AND POLICY

- The purpose of the Journal of the Brazilian Society of Mechanical Sciences is to publish papers of permanent interest dealing with research, development and design related to science and technology in Mechanical Engineering, encompassing interfaces with Civil, Electrical, Chemical, Naval, Nuclear, Agricultural, Materials, Petroleum, Aerospace, Food, System Engineering, etc., as well as with Physics and Applied Mathematics.
- The Journal publishes Full-Length Papers, Review Papers and Letters to the Editor. Authors must agree not publish elsewhere a paper submitted to and accepted by the Journal. Exception can be made for papers previously published in proceedings of conferences. In this case it should be cited as a footnote on the title page. Copies of the conference referees reviews should be also included. Review articles should constitute a critical appraisal of published information.
- The decision of acceptance for publication lies with the Editors and is based on the recommendations of at least two ad hoc reviewers, and of the Editorial Board, if necessary.

SUBMISSION

- Manuscripts and all the correspondence should be sent to the Editor or, alternatively, to the appropriate Associate Editor.
- Four (4) copies of the manuscript are required. The author should submit the original figures, which will be returned if the paper is not accepted after the review process.
- Manuscripts should be submitted in English or Portuguese. Spanish will also be considered.
- A manuscript submitted for publication should be accompanied by a cover letter containing the full name(s) of author(s), mailing adresses, the author for contact, including phone and fax number, and, if the authors so wish, the names of up to five persons who could act as referees.

FORMAT

- Manuscripts should begin with the title, including the english title, the abstract and up to five key words. If the paper's language is not English, an extended summary of about 500 words should be included. The manuscript should not contain the author(s) name(s).
- In research papers, sufficient information should be provided in the text or by refering to papers in generally available Journals to permit the work to be repeated.
- Manuscripts should be typed double-spaced, on one side of the page, using A-4 sized paper, with 2 cm margins. The pages should be numbered and not to excess 24 pages, including tables and figures. The lead author of a RBCM paper which exceeds the standard length of pages will be assessed a excess page charge.
- All symbols should be defined in the text. A separate nomenclature section should list, in alphabetical order, the symbols used in the text and their definitions. The greek symbols follow the English symbols, and are followed by the subscripts and superscripts. Each dimensional symbol must have SI (Metric) units mentioned at the end. In addition, English units may be included parenthetically. Dimensionless groups and coefficients must be so indicated as dimensionless after their definition.
- Uncertainties should be specified for experimental and numerical results.

ILLUSTRATIONS AND TABLES

- Figures and Tables should be referred in consecutive arabic numerals. They should have a caption and be placed as close as possible to the text first reference.
- Line drawings should be prepared on tracing paper or vellum, using India ink; line work must be even and black. Laser print output is acceptable. The drawings with technical data/results should have a boundary on all four sides with scale indicators (tick marks) on all four sides. The legend for the data symbols should be put in the figure as well as labels for each curve wherever possible.
- Illustrations should not be larger than 12 x 17 cm. Lettering should be large enough to be clearly legible (1.5-2.0 mm).
- Photographs must be glossy prints.

REFERENCES

- References should be cited in the text by giving the last name of the author(s) and the year of publication of the reference: either "Recent work (Smith and Jones, 1985) ... or "Recently Smith and Jones (1985) With four or more names, use the form "Smith et al.(1985)" in the text. When two or more references would have the same text identification, distinguish them by appending "a", "b", etc., to the year of publication.
- Acceptable references include: journal articles,dissertations, published conference proceedings, numbered paper preprints from conferences, books, submitted articles if the journal is identified, and private communications.
- References should be listed in alphabetical order, according to the last name of the first author, at the end of paper. Some sample references follow:

Bordalo, S.N., Ferziger, J.H. and Kline, S.J., 1989, "The Development of Zonal Models for Turbulence", Proceedings, 10th ABCM - Mechanical Engineering Conference, Vol. I, Rio de Janeiro, Brazil, pp. 41-44.

Clark, J.A., 1986, Private Communication, University of Michigan, Ann Arbor, MI.

Coimbra, A.L., 1978, "Lessons of Continuum Mechanics", Editora Edgard Blucher Ltda, São Paulo, Brazil.

Kandlikar, S.G. and Shah, R.K., 1989, "Asymptotic Effectiveness - NTU Formulas for Multiphase Plate Heat Exchangers", ASME Journal of Heat Transfer, Vol. 111, pp. 314-321.

McCormak, R.W., 1988, "On the Development of Efficient Algorithms for Three Dimensional Fluid Flow", Journal of The Brazilian Society of Mechanical Sciences, Vol. 10, pp. 323-346.

Silva, L.H.M., 1988. "New Integral Formulation for Problems in Mechanics", (in portuguese), Ph.D. Thesis, Federal University of Santa Catarina, Florianópolis, SC, Brazil.

Sparrow, E.M., 1980a, "Forced-Convection Heat Transfer in a Duct Having Spanwise-Periodic Rectangular Protuberances", Numerical Heat Transfer, Vol. 3, pp. 149-167.

Sparrow, E.M., 1980b, "Fluid-to-Fluid Conjugate Heat Transfer for a Vertical Pipe-Internal Forced Convection and External Natural Convection", ASME Journal of Heat Transfer, Vol. 102, pp. 402-407.

ISSN 0100 - 7386
REVISTA BRASILEIRA DE CIÊNCIAS MECÂNICAS
JOURNAL OF THE BRAZILIAN SOCIETY OF MECHANICAL SCIENCES

VOL. XV - Nº 2 - 1993